424
8841

The Distribution of Pressure on an Aerofoil, in a Stream with a Spanwise Velocity Gradient

W. A. MAIR, M.A., F.R.Ae.S.

(*University Engineering Laboratory, Cambridge*)

SUMMARY: Pressure measurements were made at one section of an aerofoil of constant chord spanning a wind tunnel. A flat plate was mounted in the tunnel upstream of the aerofoil, so that the wake from the plate produced a spanwise velocity gradient at the aerofoil. By traversing the plate across the tunnel the position of the wake could be altered relative to the pressure holes in the aerofoil, so that the complete pressure distribution over the aerofoil in the neighbourhood of the wake could be found. The results showed that, because of the secondary flow produced by the interaction between the aerofoil and the wake, the variation of pressure across the wake for a given chordwise position was very small, except close to the leading edge. Thus the lift coefficient, based on the velocity outside the wake, was nearly constant across the wake. The form drag coefficient, based on the same velocity, was considerably reduced in the wake. Even when the form drag coefficient was based on the *local* velocity of the stream, a considerable reduction was found in the wake.

1. Introduction

The experiments described in this paper were made to investigate the flow past an aerofoil, in a stream whose velocity varies in the spanwise direction. Such a flow occurs, for example, at the wing root of an aircraft, where a part of the wing is within the boundary layer on the fuselage, and in experiments on aerofoils spanning wind tunnels, where the flow at the ends of the wing is affected by the boundary layers on the tunnel walls.

There have been several attempts to investigate this problem theoretically, neglecting the effects of viscosity. In the earlier work, including that of Kármán and Tsien[1], the assumption was made that the velocity gradient in the spanwise direction was small compared with the chordwise velocity gradient over the aerofoil, so that the flow at each section of the aerofoil could be considered as two-dimensional. In the experiments described here the spanwise velocity gradient is comparatively large, so that in any theoretical analysis of the problem the foregoing simplifying assumption cannot be made.

In a theory developed by Hawthorne[2], a small perturbation velocity is superposed on a basic quasi two-dimensional flow to form the complete three-dimensional flow. The assumption of a *small* perturbation velocity means that the theory cannot be applied to an aerofoil with a rounded leading edge, having a stagnation point. (Hawthorne has used the theory to calculate the flow past an aerofoil with a cusped leading edge, at zero incidence.)

Received July 1954.

[The Aeronautical Quarterly, Vol. VI, February 1955]

Mendelsohn and Polhamus[3] have measured pressure distributions on a wing protruding from the wall of a wind tunnel, at various distances from the wall and at two angles of incidence. At the higher incidence the results were complicated by non-uniform stalling, but at the lower incidence a comparatively small change of chordwise pressure distribution was found as the wall was approached. The lift coefficient, based on the velocity outside the boundary layer, was only reduced by about 10 per cent. at a station very close to the wall. The drag of the aerofoil was not investigated.

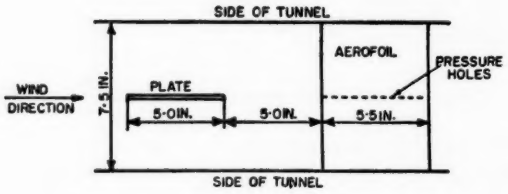

Fig. 1.

Plan of aerofoil and plate in tunnel.

The present experiments were made in order to extend the work of Mendelsohn and Polhamus. To simplify the experiments a wake, produced by a flat plate upstream of the aerofoil, was used instead of the tunnel-wall boundary layer. This enabled the aerofoil to be kept fixed in the tunnel, the wake being traversed along the span of the aerofoil by moving the upstream plate. The aerofoil was made with sufficient pressure holes at one chordwise station to enable the drag due to normal pressures to be determined, in addition to the lift.

Some measurements on an aerofoil in a wake have also been made by Ling[4] and the results have been reproduced by Hawthorne[2]. Ling's experiments were confined to measurements of drag on a balance, however, and no measurements of pressure distribution were made. The differences of drag observed by Ling were very small, so that any small errors in the measurements would have rather large effects on the conclusions.

Notation

c	chord of aerofoil
C_D	form drag coefficient, based on velocity outside wake
C_L	lift coefficient, based on velocity outside wake
C_p	pressure coefficient, based on velocity outside wake
C_D'	form drag coefficient, based on local velocity at half-chord position
C_L'	lift coefficient, based on local velocity at half-chord position
$\Delta C_D'$	difference between values of C_D' outside wake and at specified position within wake

ΔC_p difference between values of C_p on lower and upper surfaces of aerofoil, at specified position on chord

u local velocity in wake in absence of aerofoil

U velocity outside wake in absence of aerofoil

x distance along chord from leading edge of aerofoil

y distance from chord line of aerofoil, measured perpendicular to chord

$(y/c)_0$ value of (y/c) at point (near leading edge) where $C_p=0$

α angle of incidence of aerofoil

Δ change of $(y/c)_0$ associated with increase of incidence required to produce (in a uniform stream) observed increase of C_L'

δ difference between values of $(y/c)_0$ outside wake and at specified position within wake

δ_0 value of δ at $\alpha=0$

2. Experimental Details

The experiments were made in an open-return wind tunnel, with a working section 7½ in. wide by 20 in. high, at a wind speed of about 120 ft./sec. The aerofoil chord was 5·5 in., giving a Reynolds number of about $3{\cdot}5 \times 10^5$. Fig. 1 shows a plan view of the aerofoil in the tunnel. Following a suggestion of Mr. W. D. Armstrong, a perforated flat steel plate was used to produce the wake; this provided a simple method of making a plate with a rough surface that would produce a relatively thick wake. The plate was 0·07 in. thick, 5 in. long in the direction of the stream, and 13·8 in. high. The perforations were of 0·097 in. diameter, spaced about 0·14 in. apart.

Fig. 2.

Section of N.A.C.A. 0015-64 aerofoil, showing positions of pressure holes.

TABLE I

ORDINATES OF N.A.C.A. 0015-64 AEROFOIL SECTION

x/c	y/c	x/c	y/c	x/c	y/c
0·0125	0·0227	0·15	0·0607	0·60	0·0664
0·025	0·0307	0·20	0·0660	0·70	0·0560
0·05	0·0407	0·30	0·0727	0·80	0·0415
0·075	0·0476	0·40	0·0750	0·90	0·0233
0·10	0·0530	0·50	0·0727	0·95	0·0127

Leading edge radius $=0{\cdot}0247c$

Trailing edge thickness $=0{\cdot}0030c$.

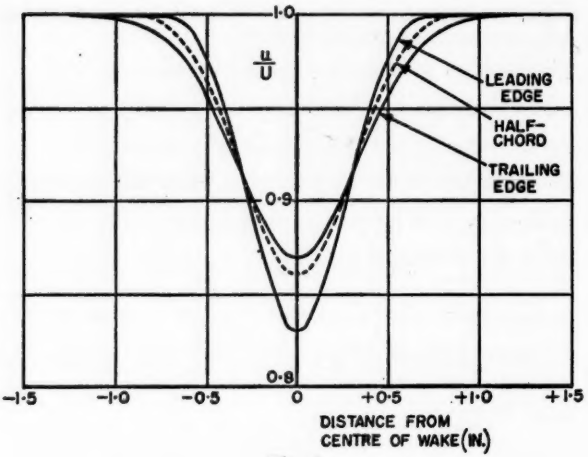

Fig. 3.
Velocity profiles in wake at position of aerofoil.

The aerofoil was of N.A.C.A. 0015-64 section (symmetrical) and was fitted with 30 pressure holes. The aerofoil section and the positions of the pressure holes are shown in Fig. 2 and the ordinates are given in Table I. The pressure holes were closely spaced near the leading edge and one was also fitted at the trailing edge, so that the lift and form drag coefficients could be determined accurately from the measured pressure distributions.

The wake produced by the plate was traversed with a pitot tube in the absence of the aerofoil at positions corresponding to the leading and trailing edges and at the half-chord position. The resulting velocity profiles are shown in Fig. 3. In all calculations involving the velocity in the wake at the position of the aerofoil, the velocity at the half-chord position has been used, except in considering the pressure at the front stagnation point, where the velocity at the position of the leading edge has been used.

3. Pressure Distributions

Chordwise pressure distributions were measured at incidences of 0°, 2°, 5° and 8°, on the wake centre line and at distances of $\frac{1}{4}$, $\frac{1}{2}$, 1 and $1\frac{1}{2}$ in. on either side of the centre line. For each of these distances from the wake centre line, mean values for the two sides of the wake were used in plotting the pressure distributions. Some further measurements at an incidence of 10·5° were rejected, because the pressure distributions showed that outside the wake there was a laminar separation near the leading edge on the upper surface, whereas in the more turbulent flow inside the wake this separation was suppressed. No separation of this kind near the leading edge was found at any of the lower incidences, but in some conditions there was evidence of a laminar separation on the lower surface near the trailing edge. This had only a small effect on the pressure distribution and is discussed later in considering the lift.

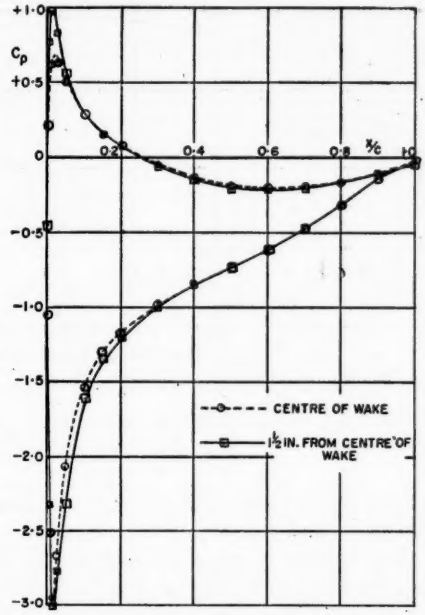

Fig. 4(*a*).
Pressure distributions at $\alpha = 8°$ plotted against x/c.

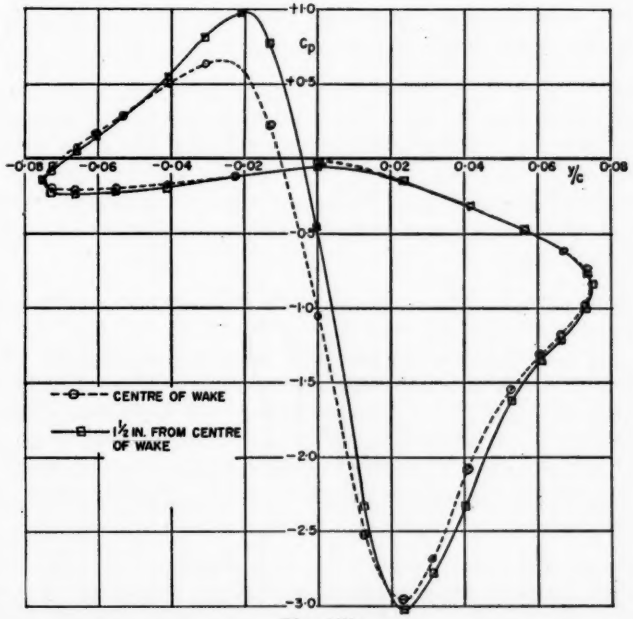

Fig. 4(*b*).
Pressure distributions at $\alpha = 8°$ plotted against y/c.

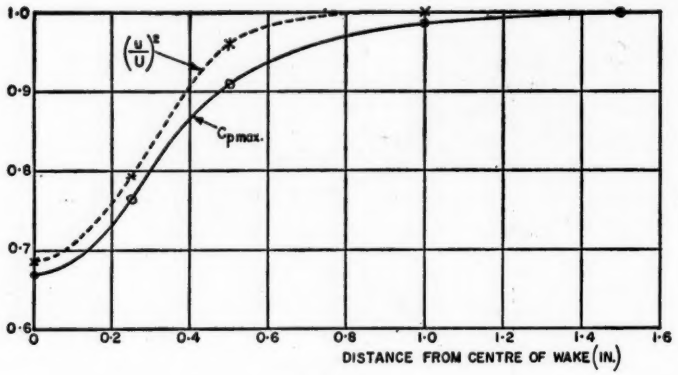

Fig. 5.

Maximum pressure coefficient on aerofoil.

For a given chordwise position on the aerofoil, it was found at all incidences that the pressure coefficient C_p, based on the velocity outside the wake, showed little variation across the wake, except at positions close to the leading edge of the aerofoil. This is shown, for example, in Figs. 4(*a*) and (*b*), where pressure distributions are plotted for $\alpha = 8°$ at the centre of the wake and outside the wake. Fig. 4(*a*) shows that the small variation of pressure distribution near the leading edge can have only a very small effect on the lift per unit span.

Figure 4(*b*), where C_p is plotted against y/c, shows more clearly the change of pressure distribution near the leading edge due to the presence of the wake. It can be seen that there are two main effects; in the wake the pressure at the stagnation point is reduced, as would be expected, and also the stagnation point is displaced along the lower surface away from the leading edge. Similar results were obtained at lower incidences, but of course at zero incidence there could be no displacement of the stagnation point.

For a given position in the wake the maximum value of C_p on the aerofoil was found to be independent of incidence between 0° and 8°. In Fig. 5 this maximum value ($C_{p\,max}$) is plotted against distance from the centre of the wake. The dotted curve shows $(u/U)^2$ in the absence of the aerofoil at the position of the leading edge. These curves show that $C_{p\,max}$ is slightly less than $(u/U)^2$ over the whole of the wake, suggesting that the secondary flow in the spanwise direction prevents the formation of a true stagnation point. The difference between the two curves at the centre of the wake is surprising, however, because by symmetry there cannot be any spanwise flow at the centre.

The pressure distribution curves (as in Figs. 4(*a*) and (*b*)) were integrated by means of a planimeter to derive coefficients of lift and form drag. The maximum possible errors in C_L and C_D were estimated to be about $\pm 0{\cdot}005$ and $\pm 0{\cdot}001$ respectively.

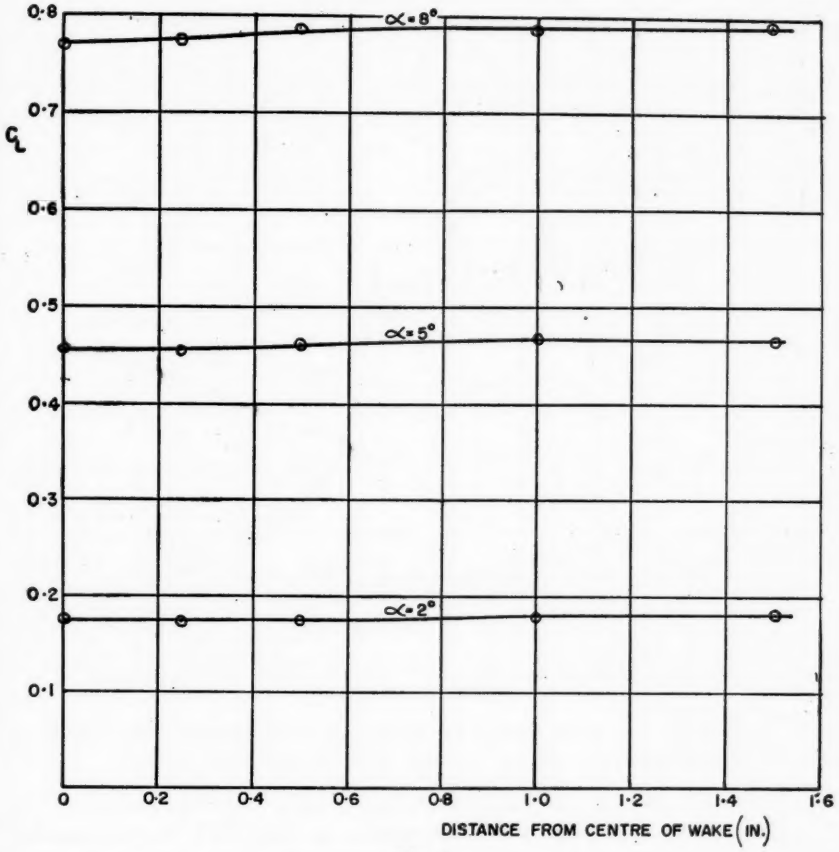

Fig. 6.
Variation of lift coefficient across wake.

4. Lift

Figure 6 shows the lift coefficient, based on velocity outside the wake, plotted against distance from the centre of the wake. At the centre of the wake the lift coefficient is only reduced by about 2 per cent., although the local velocity (at the half-chord position) is about 15 per cent. less than the velocity outside the wake. The change of lift coefficient is as small as this because the variation of pressure across the wake is confined to a small region near the leading edge, and this has only a very small effect on the lift coefficient (Fig. 4(*a*)).

Figure 7 shows the difference of pressure coefficient between the lower and upper surfaces, for an incidence of 8°. This provides a further illustration of the small spanwise variation of lift across the wake, and shows that the small variation

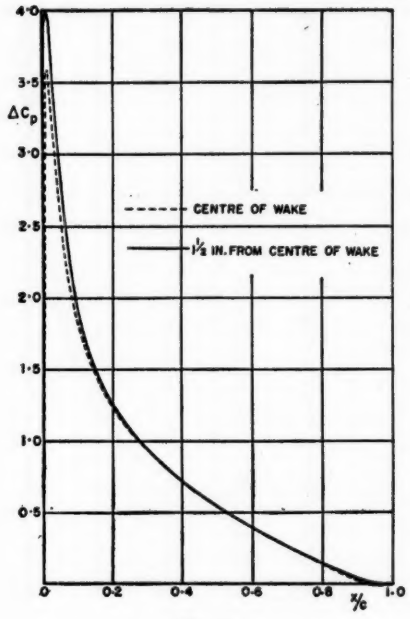

Fig. 7.
Chordwise load distribution at $\alpha = 8°$.

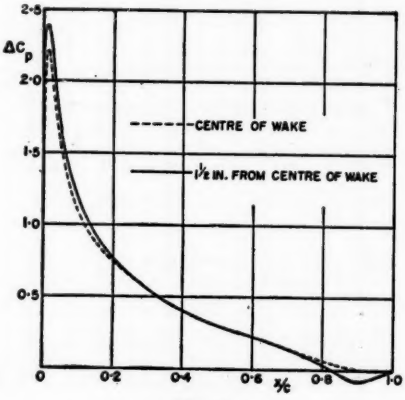

Fig. 8.
Chordwise load distribution at $\alpha = 5°$.

of pressure across the wake cannot be considered to be caused by a change of effective wind speed.

Figure 8 shows the chordwise load distribution at an incidence of 5°. A noticeable feature of this diagram is that outside the wake ΔC_p becomes negative near the trailing edge, whereas this does not occur at the centre of the wake. It is believed that the negative values of ΔC_p are associated with laminar separation on the lower surface at the rear part of the aerofoil, and that this separation is suppressed in the more turbulent flow in the wake. Similar effects have been observed previously on aerofoils with rather large trailing edge angles; for example, Preston, Sweeting and Cox[5] found negative values of ΔC_p near the trailing edge of a Piercy 1240 aerofoil, which were eliminated when transition wires were fitted at $0{\cdot}1c$.

Figure 8 shows that, if the laminar separation just discussed had not been present, the variation of C_L across the wake would have been slightly greater than that shown in Fig. 6.

5. Drag

Figure 9 shows the form drag coefficient, plotted against distance across the wake; the full lines refer to the coefficient C_D (based on velocity outside the wake),

KRESGE-HOOKER SCIENTIFIC LIBRARY
WAYNE UNIVERSITY

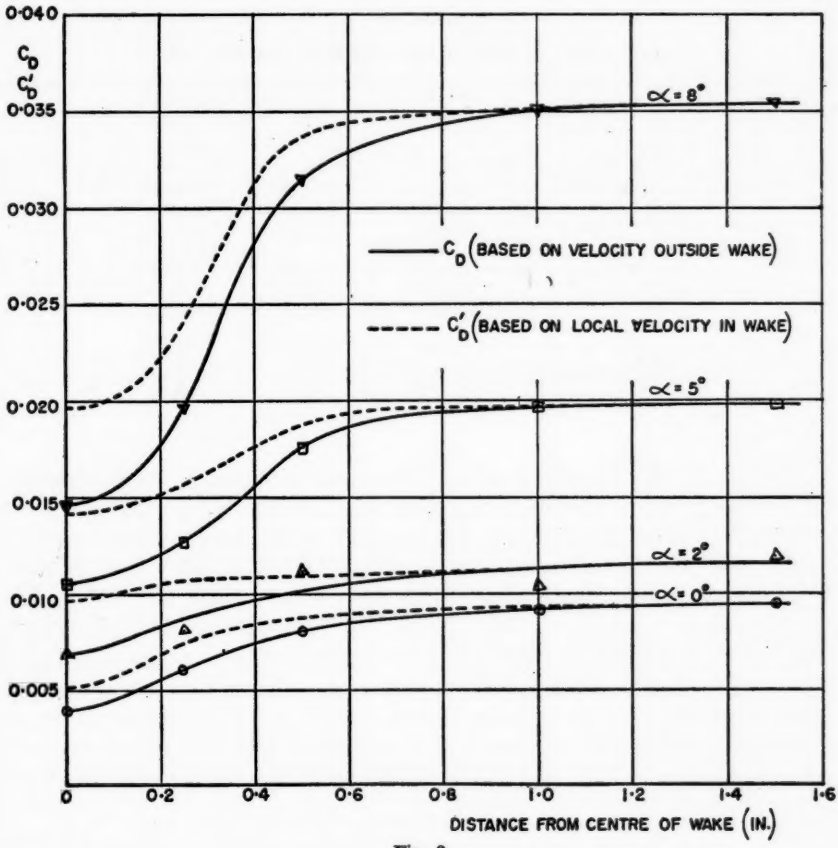

Fig. 9.

Variation of form drag coefficient across wake.

while the dotted lines refer to C_D' (based on local velocity in the wake). The values of C_D and C_D' are fairly high, because of the low Reynolds number. It is clear that both C_D and C_D' are considerably reduced in the wake, especially at the higher incidences. (If there were no secondary flow, and no induced upwash or downwash due to spanwise variation of circulation, C_D' would be constant across the wake.)

6. Discussion

The flow considered in these experiments is a complicated one, but some of the main features can be explained qualitatively, as follows.

Near the leading edge of the aerofoil the pressure is reduced inside the wake, because the total pressure of the stream is reduced, so that there is a spanwise

TABLE II

DISPLACEMENT OF POSITION ON AEROFOIL AT WHICH $C_p=0$

	Distance from centre of wake (in.)	0	0·25	0·5
$\alpha=2°$	Δ	0·0024	0·0013	0·0003
	δ	0·0030	0·0021	0·0008
	$\delta-\delta_0$	0·0017	0·0013	0·0005
$\alpha=5°$	Δ	0·0041	0·0026	0·0008
	δ	0·0035	0·0017	0·0003
	$\delta-\delta_0$	0·0022	0·0009	0·0000
$\alpha=8°$	Δ	0·0053	0·0036	0·0012
	δ	0·0067	0·0043	0·0013
	$\delta-\delta_0$	0·0054	0·0035	0·0010

pressure gradient causing a flow towards the centre of the wake. Slightly farther back on the aerofoil there are pressure gradients tending to cause a spanwise flow away from the centre of the wake, and in the resulting flow there is a component of vorticity in the direction of the undisturbed stream. The effect of the spanwise flow on the pressure distribution is to equalise the pressures along the span of the aerofoil, for a given chordwise position. Fig. 4(*a*) shows that this equalising process is very effective except at points close to the leading edge.

Since the pressure distribution is almost unaffected by the wake except near the leading edge, there cannot be much variation of lift coefficient across the wake. There is, however, a considerable reduction of form drag, because the reduction of pressure near the leading edge has a significant effect on the chordwise force component (Fig. 4(*b*)).

It has already been mentioned that in the wake the stagnation point is displaced along the lower surface away from the leading edge (Fig. 4(*b*)). In a uniform stream such a displacement of the stagnation point would be associated with an increase of circulation, and hence of lift coefficient, and it is of interest to compare the increase of lift coefficient, calculated from the displacement of the stagnation point, with the observed increases of the coefficient C_L', based on *local* velocity in the wake.

From diagrams of the kind shown in Fig. 4(*b*) the exact position of the stagnation point cannot be found, but it is possible to determine fairly accurately the value of y/c at the point on the aerofoil (near the leading edge) at which $C_p=0$. Denoting this value by $(y/c)_0$, let δ be the difference between the values of $(y/c)_0$ within the wake and outside it. Within the wake the lift coefficient C_L', based on local velocity, is increased. From the measurements made outside the wake it is possible to find the change of $(y/c)_0$ (say Δ) associated with the increase of incidence required to produce this increase of local lift coefficient. The quantities δ and Δ may then be compared.

TABLE III

NEGATIVE INDUCED DRAG

	Distance from centre of wake (in.)	0	0·25	0·5
$\alpha=0$	$C_L'\varepsilon$	0	0	0
	$\Delta C_D'$	0·0044	0·0021	0·0008
$\alpha=2°$	$C_L'\varepsilon$	0·0026	0·0013	0·0003
	$\Delta C_D'$	0·0027	0·0020	0·0012
$\alpha=5°$	$C_L'\varepsilon$	0·0156	0·0091	0·0025
	$\Delta C_D'$	0·0057	0·0041	0·0010
$\alpha=8°$	$C_L'\varepsilon$	0·0375	0·0237	0·0076
	$\Delta C_D'$	0·0158	0·0113	0·0018

The analysis is complicated, however, by the fact that δ is not zero even at zero incidence, because of the effect of the wake on the pressure distribution near the leading edge. If δ_0 is the value of δ at zero incidence, for a given position in the wake, it may perhaps be more appropriate to compare Δ with $(\delta-\delta_0)$.

Table II shows values of Δ, δ and $(\delta-\delta_0)$, calculated as just explained. The values given in the table show that Δ agrees in order of magnitude with either δ or $(\delta-\delta_0)$, suggesting that there is, in fact, an increase of circulation round the aerofoil in the wake, corresponding roughly with the observed increase of C_L'. This conclusion is consistent with observations of wing stalling made in other wind tunnels, where it has often been found that the part of the wing inside the tunnel boundary layer stalls at a lower incidence than the remainder of the wing.

The foregoing discussion of the variation of C_L' across the wake suggests that the observed reduction of form drag coefficient in the wake may be partly caused by an induced upwash due to the secondary flow, giving a " negative induced drag." Basing the coefficients of both lift and form drag on local velocity, the reduction of form drag coefficient due to this effect should be $C_L'\varepsilon$, where ε is the angle of induced upwash in radians. Values of $C_L'\varepsilon$ have been calculated from the measured lift distributions, assuming that the observed increase of C_L' in the wake is due entirely to the induced upwash ε, and that there is no variation of lift curve slope (based on local velocity) across the wake. In Table III these values are compared with the observed reduction of form drag coefficient $\Delta C_D'$. At high incidences the observed reduction of form drag coefficient is considerably less than the calculated " negative induced drag," *i.e.* there must be some other effect giving a substantial increase of drag. At zero incidence the negative induced drag is necessarily zero, although a reduction of C_D' is still observed. Thus in this case there must be some other effect causing a reduction of drag, independent of the negative induced drag.

Since form drag is entirely due to thickening or separation of the boundary layer at the rear of the aerofoil, it might be expected that a reduction of form drag

would result from the better mixing in the boundary layer, caused by the secondary streamwise vorticity, the mechanism being similar to that of vortex generators.

The suggestions just made, to account for the observed reduction of C_D', can only be regarded as tentative ones. It is clear that a complete explanation of the observed drag changes would be very complicated. Nevertheless, the fact that the observed reduction of C_D' in the wake is greater at the higher incidences suggests that negative induced drag may play some part.

7. Conclusions

It has been shown that, when an aerofoil of constant chord is placed in a stream with a spanwise velocity gradient, there is only a small spanwise variation of pressure coefficient for a given chordwise position. Basing coefficients of lift and drag on a constant velocity, it is found that there is little spanwise variation of lift coefficient, but there is a considerable reduction of form drag coefficient in a region of reduced stream velocity. The observed spanwise variation in the position of the stagnation point is roughly consistent with the variation of lift coefficient based on *local* velocity.

The foregoing results have some interesting practical applications. For example, when measurements are made on an aerofoil spanning the working section of a wind tunnel, the lift per unit span decreases only a little where the aerofoil enters the boundary layers on the walls of the tunnel. (This has already been shown by the work of Mendelsohn and Polhamus[3]). Again, at the junction between the wing and fuselage of an aeroplane, there should be a *reduction* of local drag coefficient of the wing due to the boundary layer on the fuselage. In practice a net reduction of drag has never been achieved, probably because there is a counteracting increase of drag due to the effect of the wing and its boundary layer on the fuselage boundary layer, but the results given here do at least suggest that the ideal to be aimed at in such cases is a *reduction* of drag.

References

1. von Kármán, Th. and Tsien, H. S. Lifting-Line Theory for a Wing in Non-Uniform Flow. *Quarterly of Applied Mathematics*, Vol. 3, pp. 1-11, 1945.

2. Hawthorne, W. R. The Secondary Flow about Struts and Aerofoils. *Journal of the Aeronautical Sciences*, Vol. 21, p. 588, September 1954.

3. Mendelsohn, R. A. and Polhamus, J. F. Effect of the Tunnel-Wall Boundary Layer on Test Results of a Wing Protruding from a Tunnel Wall. N.A.C.A. T.N. 1244, 1947.

4. Ling, A. T. Study of Secondary Flow Effect on Single Symmetrical Aerofoils. M.Sc. Thesis, Massachusetts Institute of Technology, 1952.

5. Preston, J. H., Sweeting, N. E. and Cox, D. K. The Experimental Determination of the Two-Dimensional Interference on a Large Chord Piercy 12/40 Aerofoil in a Closed Tunnel fitted with a Flexible Roof and Floor. R. & M. 2007, 1944.

Experiments with an Electrical Analogue for the Extension and Flexure of Flat Plates

P. J. PALMER, M.Sc., Ph.D., D.I.C., A.R.C.S., A.F.R.Ae.S., A.Inst.P.

and

S. C. REDSHAW, D.Sc., Ph.D., M.I.C.E., F.R.Ae.S.

(Department of Civil Engineering, University of Birmingham)

SUMMARY: Details of the design, construction and use of an electrical resistance network for solving certain of the problems encountered in the flexure and extension of flat plates are given. Some typical experiments have been carried out with the aid of this network and the method of operation of the analogy is described. The results of these experiments are presented and they are compared with the corresponding theoretical values. The comparison is as good as could be expected in view of the limitations imposed by the very coarse mesh which was used; essentially the same results would have been obtained by the exercise of a relaxation computation, using the same size of net. No practical difficulties would be encountered in building a large network having a very fine mesh.

1. Introduction

An earlier report[1] considered the feasibility of constructing various electrical networks for the solution of the partial differential equations concerning the extension and flexure of flat plates. The most promising of these networks was considered to be a pure resistance network, and it was recommended in the report that such an analogue should be constructed and tested.

The purpose of the present report is to give details of the construction of a small pure resistance network, to show how it can be used to solve the relevant differential equations and to give the results obtained with it.

It must be emphasised that the network constructed and reported here was only a small one, so that all the results are necessarily those obtained by a solution appropriate to a coarse grid. If the results obtained with this small network are regarded as indicating the analogy to be satisfactory, then a larger network can be built without any difficulty.

Received September 1954.

NOTATION

a	distance between mesh points
D	flexural rigidity of plate
E	electrical potential in high potential grid
f	a continuous function
f_A, f_B, f_C	neighbouring ordinates in the finite difference representation of f
H, H'	resistances in the gradient measurement circuit (Fig. 7)
$M = (M_x + M_y)/\{D(1+\nu)\} = -\nabla^2 w$	
M_x, M_y	bending moments in plate in x and y directions
n	direction normal to plate boundary; integer
q	intensity of distributed load normal to plate
R	value of resistances connecting low potential grid to medium potential grid
R'	value of resistances connecting medium potential grid to high potential grid
r	value of resistances in low potential grid
v	electrical potential in low potential grid
V	electrical potential in medium potential grid
w	normal deflection of plate
x, y	axes in plate
ϕ	stress function
$\psi = -(\sigma_x + \sigma_y) = -\nabla^2 \phi$	
ν	Poisson's ratio
ρ	value of resistances in medium potential grid
$\eta_{AC}, \eta_B, \eta_S$	potentials in the gradient measurement circuit (Fig. 7)
$\sigma_x, \sigma_y, \tau_{xy}$	stress components in plate

$$\nabla^2 = \frac{\partial^2}{\partial x^2} + \frac{\partial^2}{\partial y^2}$$

$$\nabla^4 = \frac{\partial^4}{\partial x^4} + \frac{2\partial^4}{\partial x^2 \partial y^2} + \frac{\partial^4}{\partial y^4}$$

Suffixes

0	position in grids corresponding to a typical point in the plate
1, 2, 3, 4	neighbouring points to that defined by suffix 0 (Fig. 1)

2. The Mathematical Background

2.1. Various Cases

Extension and flexure problems of flat elastic plates are of very great importance in applied elasticity and, as shown by Southwell[2], there is a definite interconnection between the two classes of problems. Details of the mathematical analogies which exist between the flexural and extensional problems have been admirably presented by Fox and Southwell[3], who considered the problem of a flat elastic plate which is either bent or stretched. In all, four cases were presented since the edge conditions may specify either traction or displacements, both in the flexural and in the extensional problems.

The four cases may be defined as follows:—

(A) The flexural problem in which displacements are specified at the boundary.

(B) The flexural problem in which forces are specified at the boundary.

(C) The extensional problem in which displacements are specified at the boundary and the only body forces are gravitational.

(D) The extensional problem in which forces are specified at the boundary and the only body forces are gravitational.

Normally Cases A and D are solved by one mathematical method and Cases B and C by another, although Southwell has shown that all four cases are, in fact, mathematically identical. To attempt to solve all four cases by means of one solution, either mathematically or electrically, leads in some cases to boundary conditions which are intractable.

It is for this reason that the pure resistance network was used to solve problems of Cases A and D alone. Case A entails the solution of the equation

$$\nabla^4 w = \frac{q}{D} \quad . \quad . \quad . \quad . \quad . \quad . \quad . \quad (1)$$

such that usually w and its first normal derivative take specified values at the boundary; w is the normal deflection of the plate, q the intensity of the distributed load, and D the flexural rigidity of the plate. Case D entails the solution of the equation

$$\nabla^4 \phi = 0 \quad . \quad . \quad . \quad . \quad . \quad . \quad (2)$$

such that usually ϕ and its first normal derivative take specified values at the boundary, ϕ being a stress function.

If derivatives higher than the first are specified at the boundary then it may still be possible to obtain a solution by means of the network, and further comments will be made about this later.

2.2. Particular Flexural Case

Equation (1), which was first derived and considered by Lagrange, may be written as

$$\left(\frac{\partial^2}{\partial x^2}+\frac{\partial^2}{\partial y^2}\right)\left(\frac{\partial^2 w}{\partial x^2}+\frac{\partial^2 w}{\partial y^2}\right)=\frac{q}{D} \quad . \quad . \quad . \quad . \quad . \quad (3)$$

Now the bending moments, in a flat plate, when expressed in terms of the normal deflection have the form

$$\left.\begin{aligned} M_x &= -D\left(\frac{\partial^2 w}{\partial x^2}+\nu\frac{\partial^2 w}{\partial y^2}\right) \\ \text{and} \quad M_y &= -D\left(\frac{\partial^2 w}{\partial y^2}+\nu\frac{\partial^2 w}{\partial x^2}\right) \end{aligned}\right\} . \quad . \quad . \quad . \quad . \quad . \quad (4)$$

Hence $$\left(\frac{\partial^2 w}{\partial x^2}+\frac{\partial^2 w}{\partial y^2}\right)=\frac{-(M_x+M_y)}{D(1+\nu)}=-M \quad . \quad . \quad . \quad (5)$$

the last equality being by definition.

Thus the solution of equation (3) reduces to the solution of the two interrelated second-order partial differential equations given by

$$\left.\begin{aligned} &\frac{\partial^2 M}{\partial x^2}+\frac{\partial^2 M}{\partial y^2}=-\frac{q}{D} \\ \text{and} \quad &\frac{\partial^2 w}{\partial x^2}+\frac{\partial^2 w}{\partial y^2}=-M \end{aligned}\right\} . \quad . \quad . \quad . \quad . \quad . \quad (6)$$

Any solution using an electrical resistance network is really analogous to the corresponding finite difference solution and not to the differential solution, although the difference between the two theoretical solutions can be as small as desired provided that the chosen ordinates are sufficiently close together. However, from the point of view of comparing the electrical network with theory, the finite difference forms of equation (6) are required. If the suffix 0 represents a typical ordinate defined by some value of x and y, and if the suffixes 1, 2, 3 and 4 represent neighbouring points on a square grid of side a, then the finite difference form of equations (6) becomes

$$\left.\begin{aligned} &M_1+M_2+M_3+M_4-4M_0+\frac{q_0 a^2}{D}=0 \\ \text{and} \quad &w_1+w_2+w_3+w_4-4w_0+M_0 a^2=0 \end{aligned}\right\} . \quad . \quad . \quad . \quad . \quad (7)$$

the expression q_0 representing the intensity of loading at the chosen position.

2.3. Particular Extensional Case

Equation (2), which is normally known as the biharmonic equation, may be written as

$$\left(\frac{\partial^2}{\partial x^2}+\frac{\partial^2}{\partial y^2}\right)\left(\frac{\partial^2\phi}{\partial x^2}+\frac{\partial^2\phi}{\partial y^2}\right)=0. \quad . \quad . \quad . \quad . \quad . \quad (8)$$

The stress components, expressed in terms of a stress function, have the form

$$\left.\begin{aligned}\sigma_x &= \frac{\partial^2\phi}{\partial y^2}\\ \sigma_y &= \frac{\partial^2\phi}{\partial x^2}\\ \tau_{xy} &= -\frac{\partial^2\phi}{\partial x\partial y}\end{aligned}\right\}. \quad . \quad . \quad . \quad . \quad . \quad . \quad (9)$$

Hence if, by definition,

$$\psi=-(\sigma_x+\sigma_y) \quad . \quad . \quad . \quad . \quad . \quad (10)$$

then the solution of equation (8) reduces to the solution of the following equations:—

$$\left.\begin{aligned}&\frac{\partial^2\psi}{\partial x^2}+\frac{\partial^2\psi}{\partial y^2}=0\\ \text{and}\quad &\frac{\partial^2\phi}{\partial x^2}+\frac{\partial^2\phi}{\partial y^2}=-\psi\end{aligned}\right\}. \quad . \quad . \quad . \quad . \quad . \quad (11)$$

The finite difference form of these equations is given by

$$\left.\begin{aligned}&\psi_1+\psi_2+\psi_3+\psi_4-4\psi_0=0\\ \text{and}\quad &\phi_1+\phi_2+\phi_3+\phi_4-4\phi_0+a^2\psi_0=0\end{aligned}\right\}. \quad . \quad . \quad . \quad (12)$$

3. The Electrical Network

3.1. Analogy

The complete electrical resistance network is shown diagrammatically in Fig. 1. The low potential network consists of a square grid of side a, of equal resistances of value r. A network of this type alone would be suitable for solving the Laplace equation[4]. A similar network, but with resistances of value ρ, forms the medium potential grid. Corresponding points on each of these two grids are connected by large resistances of value R. In addition the high potential grid, which contains no resistances, has its nodal points connected to corresponding points on the medium potential grid by large resistances of value R'. The type of network formed by the R and r resistances alone, or alternatively the R' and ρ resistances, would form a suitable analogy for the Poisson equation[5].

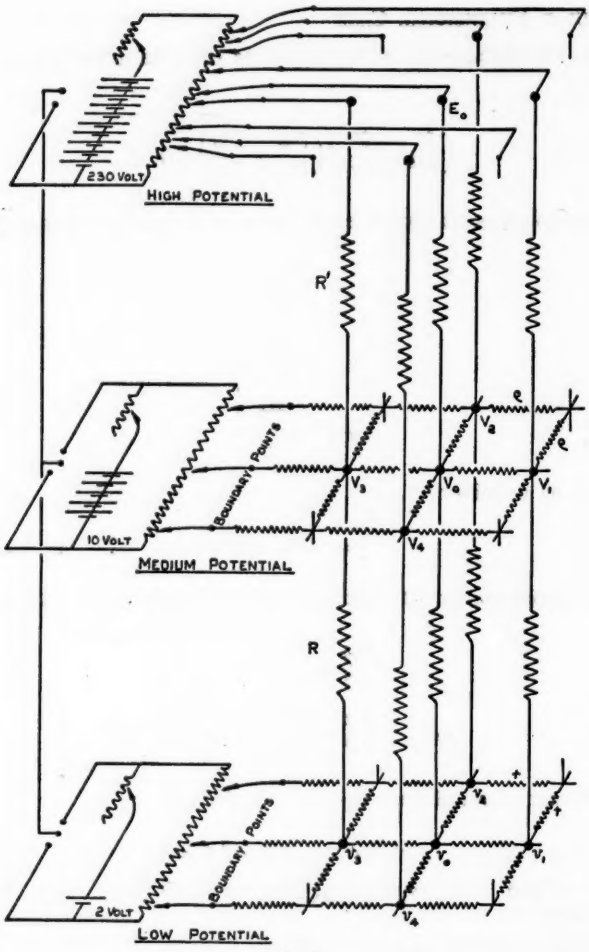

Fig. 1.
The electrical network.

The complete network also makes provision for applying any desired electrical potential to the boundary points on both the low and medium potential nets, together with facilities for applying potentials to the nodes of the high potential grid.

To show that this network does provide an analogy to problems of elasticity, it is only necessary to apply Kirchhoff's law to two points in the network.

Consider the total current flow into the node marked with potential V_0, in the medium potential grid; then

$$\sum_{n=1}^{4}\left(\frac{V_n-V_0}{\rho}\right)+\frac{E_0-V_0}{R'}+\frac{v_0-V_0}{R}=0 \quad . \quad . \quad . \quad (13)$$

from which

$$V_1+V_2+V_3+V_4-4V_0+\frac{\rho E_0}{R'}+\left(\frac{-\rho V_0}{R'}+\frac{\rho v_0}{R}-\frac{\rho V_0}{R}\right)=0. \quad . \quad (14)$$

It can now be seen that provided the three terms in brackets are small and can be neglected, then

$$V_1+V_2+V_3+V_4-4V_0+\frac{\rho E_0}{R'}=0 \quad . \quad . \quad . \quad (15)$$

and it will be realised that this equation is analogous to the first of equations (7) and, if $E_0=0$, it is also analogous to the first of equations (12).

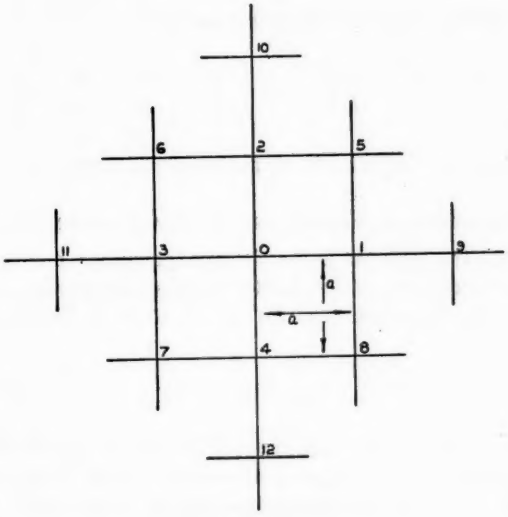

Fig. 2.
Network pattern.

Further, consider the total current flow into the node marked with potential v_0 in the low potential grid; then

$$\sum_{n=1}^{4}\left(\frac{v_n-v_0}{r}\right)+\frac{V_0-v_0}{R}=0 \quad . \quad . \quad . \quad . \quad (16)$$

from which

$$v_1+v_2+v_3+v_4-4v_0+\frac{V_0 r}{R}+\left(\frac{-v_0 r}{R}\right)=0. \quad . \quad . \quad . \quad (17)$$

Here again, if the last term is negligible compared with the others,

$$v_1+v_2+v_3+v_4-4v_0+\frac{V_0 r}{R}=0 \quad . \quad . \quad . \quad . \quad (18)$$

which provides an equation analogous to the second of equations (7) and the second of equations (12).

The precise physical functions which were taken to correspond to the electrical potentials are given in Table I together with the exact relationship between the physical and electrical parameters.

If equation (3) is considered as it stands, instead of splitting it up into a pair of interrelated differential equations, then the finite difference form is

$$20w_0 - 8\sum_{n=1}^{4} w_n + 2\sum_{n=5}^{8} w_n + \sum_{n=9}^{12} w_n - \frac{q_0 a^4}{D} = 0 \quad . \quad . \quad . \quad (19)$$

where the suffixes 1 to 12 refer to the value of w at points on a square grid of side a as shown in Fig. 2.

The corresponding expression for v is given by

$$20v_0 - 8\sum_{n=1}^{4} v_n + 2\sum_{n=5}^{8} v_n + \sum_{n=9}^{12} v_n - \frac{r\rho E_0}{RR'} + \frac{r}{R}\left\{\frac{\rho V_0}{R'} - \frac{\rho v_0}{R} + \frac{rV_0}{R} - \frac{rv_0}{R} + \frac{\rho V_0}{R}\right\} = 0. \quad . \quad . \quad . \quad . \quad (20)$$

where the error is given immediately by the bracketed terms.

3.2. Choice of Resistance Values and Accuracy of Analogy

The terms that are neglected in the electrical equations, numbers (15) and (18), can be made small provided that the resistance values are suitably chosen. Regarding equation (14), the fractional error can be seen to be of the order

$$-\frac{\rho}{R'} + \frac{\rho v}{RV} - \frac{\rho}{R}. \quad . \quad . \quad . \quad . \quad . \quad (21)$$

This can be made small provided that R and R' are much greater than ρ. Since this condition also ensures that v is much smaller than V, then the second term will be particularly small, so that the fractional error will be of the order

$$-\frac{\rho}{R'} - \frac{\rho}{R}. \quad . \quad . \quad . \quad . \quad . \quad (22)$$

As regards equation (17), the fractional error is of the order

$$-\frac{r}{R} \quad . \quad . \quad . \quad . \quad . \quad . \quad . \quad . \quad (23)$$

so that, provided that R is much greater than r, the error is truly negligible.

For the present network the following values of the resistances were taken,

$$\left.\begin{array}{ll} r = 100 \text{ ohms}, & R = 200{,}000 \text{ ohms} \\ \rho = 100 \text{ ohms}, & R' = 100{,}000 \text{ ohms and} \\ & \quad 50{,}000 \text{ ohms} \end{array}\right\}.$$

These values ensured that the errors were negligible so that the analogies were truly justified. R' was initially taken as 200,000 ohms but it was necessary to

TABLE I

RELATIONSHIP BETWEEN PHYSICAL AND ELECTRICAL FUNCTIONS

Network	*Voltage Symbol*	*Flexure of Plate*			*Extension of Plate*		
		Order of Voltage used	*Corresponding Plate Function*	*Relationship*	*Order of Voltage used*	*Corresponding Plate Function*	*Relationship*
High Potential Grid	E	230 volts	q	$E \rightarrow \frac{qa^3RR'}{D\rho r}$	—	—	—
Medium Potential Grid	V	0→3·0 volt	M	$V \rightarrow \frac{MaR}{r}$	0→6·0 volt	ψ	$V \rightarrow \frac{\psi a^2 R}{r}$
Low Potential Grid	v	0→0·005 volt	w	$v \rightarrow \frac{w}{a}$	0→0·015 volt	ϕ	$v \rightarrow \phi$

reduce this value, since the maximum potential available for the high potential net was 230 volts (E), and if R and R' were too large, then v was too small to be accurately measured.

It should be noted that the final effect of the resistances chosen for the network is to make the three potentials E, V and v to be all of different orders of magnitude.

Table I gives the orders of the electrical potentials which were used in the experiments.

3.3. Construction of Electrical Network

That part of the network comprising the R, ρ and r resistances was built into a self-contained unit, a rear view of which is shown in Fig. 3. The mesh separation is one eighth so that there are 9×9 nodal points. The terminals corresponding to the nodal points in the low and medium potential nets can be seen on the front of the unit in Fig. 4. This unit also contained some rheostats wired to the boundary points of the medium potential net to assist with the setting up of the boundary conditions.

The R' resistances comprised a separate unit which could be attached to the main unit when required. Potential dividers were also available for applying any required potential to the boundary points. All potential measurements were made with the usual potentiometer and galvanometer arrangement. The complete apparatus is shown in Fig. 4. High stability carbon resistors were used throughout, these being specially selected to give a tolerance of $\pm\frac{1}{2}$ per cent. about the mean values

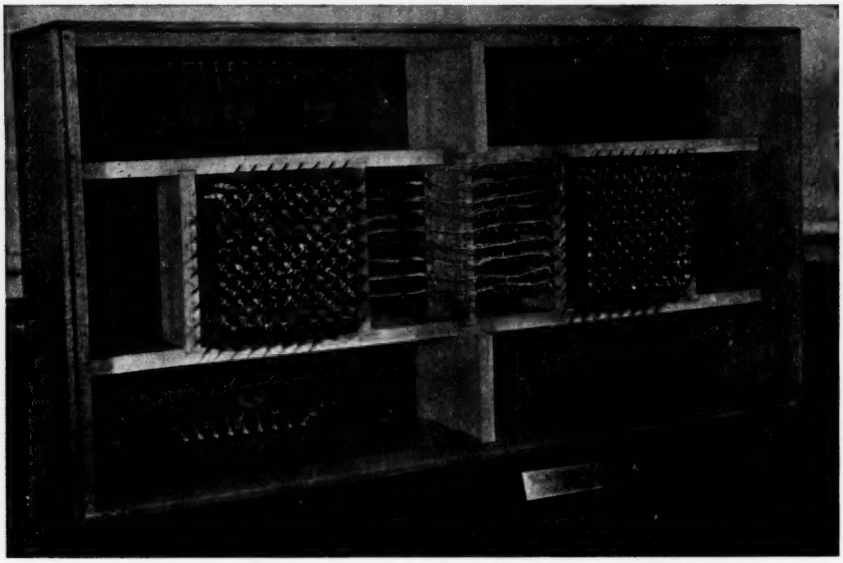

Fig. 3.
The electrical analogue. Rear view of main unit comprising the two principal nets and the interconnecting resistances.

3.4. Operation of Electrical Network

The operation of the network is simple and the procedure is as follows.

If the problem is of flexure, then the potentials E must first be applied to the high potential grid by means of a potential divider; these potentials will be determined from the intensity of loading by reference to Table I. If the problem is one of extension, the high potential grid is disconnected together with the R' resistances.

As regards the low and medium potential grids, it is necessary to set the potentials v and V, at the boundary points, to the appropriate boundary conditions. This involves a difficulty since it is not common for the boundary conditions of the problem to be in this convenient form. For example, instead of knowing v and V at the boundary, it is more likely that v and $\partial v/\partial n$, the normal derivative of v, will be specified. In this case, the procedure is to set the appropriate values of v on the boundary of the low potential net and then to adjust the values of V on the boundary of the medium potential net, until $\partial v/\partial n$ assumes the desired values round the low potential boundary. This involves a type of electrical iteration process, but with a little care and experience the desired conditions can rapidly be achieved.

It is of interest to note that a similar electrical analogy has been proposed by Boscher and Malavard[6] and Liebmann[7], but in both cases the method for setting up the boundary conditions was different. Liebmann fed currents into the low potential boundary points to set up the required slopes and then adjusted the

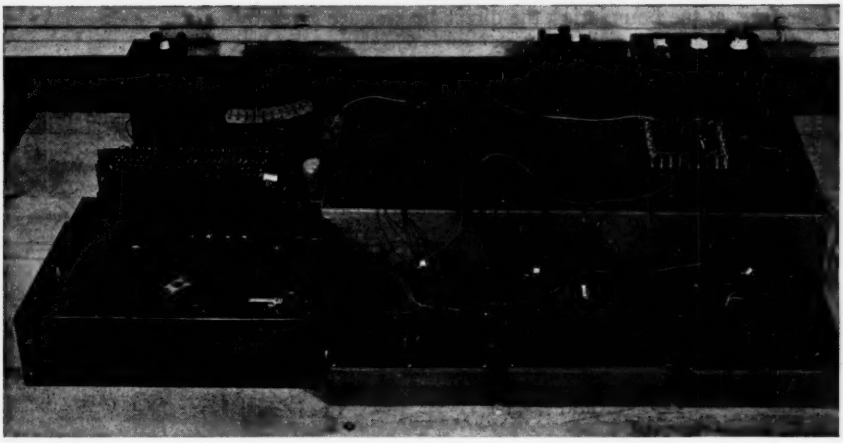

Fig. 4.

The electrical analogue, showing all equipment (square plate with uniform normal pressure and built-in edges).

medium potential boundary values to produce the required low potential boundary values; this method has also been tried by the present authors and is described later. Boscher and Malavard worked with zero boundary potential on the low potential grid, this being achieved by first producing a Laplace solution to an auxiliary problem.

Although all problems investigated had two axes of symmetry, the board was not adapted for axes of symmetry as it was felt desirable to verify that identical results were obtained in each quadrant.

4. The Experimental Results

4.1. Extension of a Plate by a Parabolic Distribution of Stress

The particular problem of the extension of a flat plate, which was chosen to be investigated by means of the network, was that of a square flat plate subjected to a parabolic tensile stress distribution on each of two opposite edges. This problem, to which a theoretical solution exists, has been investigated analytically by strain energy by Timoshenko and Goodier[8], and by relaxation by Longman[9].

If the square plate is of side d, with axes x and y from an origin at the centre of the plate, so that the loaded edges are at $x=\pm d/2$ and the unloaded edges are at $y=\pm d/2$, then the value of the stress function at the boundary is

$$\phi_{\text{boundary}}=K\left(\frac{y^2}{2d^2}-\frac{y^4}{3d^4}\right). \quad . \quad . \quad . \quad . \quad . \quad (24)$$

Therefore, at the boundaries, the direct stresses are given by

$$\left.\begin{aligned}(\sigma_x)_{x=\pm d/2} &= \frac{K}{d^2}\left(1-\frac{4y^2}{d^2}\right)\\ (\sigma_y)_{y=\pm d/2} &= 0\\ (\tau_{xy})_{y=\pm d/2} &= (\tau_{xy})_{x=\pm d/2} = 0\end{aligned}\right\} \quad . \quad . \quad . \quad . \quad (25)$$

The gradient of ϕ normal to the boundary is

$$\left.\begin{aligned}\left(\frac{\partial\phi}{\partial x}\right)_{x=\pm d/2} &= 0\\ \text{and}\quad \left(\frac{\partial\phi}{\partial y}\right)_{y=\pm d/2} &= \frac{K}{3d}\end{aligned}\right\} \quad . \quad . \quad . \quad . \quad . \quad (26)$$

Thus for the purpose of the tests, where v represents ϕ, the constant K was taken to be equal to 0·12 volts, so that the maximum value of v on the boundary became 0·01250 volts, and the slope normal to the boundary was zero on two edges and had the value $0{\cdot}04/d = 0{\cdot}00500/a$ on the other two edges.

To apply these conditions to the network, the high potential grid and the R' resistances were removed, since they are not required in an extensional problem. The values of v on the boundary were then obtained from equation (24) together with Table I and applied, by means of the potential divider, to the low potential net. Finally, the values of V on the boundary of the medium potential net were adjusted until the corresponding values of $\partial v/\partial n$, on the low potential net, were as required.

The setting of the boundary conditions was actually carried out in three different ways detailed as follows, the first two being similar to that already described and the third method similar to that proposed by Liebmann.

(*i*) The first approximation to the gradient is given by

$$\left(\frac{\partial v}{\partial n}\right)_A = \frac{v_B - v_A}{a} \quad . \quad . \quad . \quad . \quad . \quad . \quad (27)$$

where v_A is the value of v on the boundary and v_B is the value of v at the next node, a distance a from the boundary. This means that if v_A and $(\partial v/\partial n)_A$ are known, then v_B is also known. Thus using this method v_A can be set up on the low potential net boundary and the boundary potential on the medium potential net can be adjusted until v_B assumes its prescribed value.

The results of using this method are given in Fig. 5.

(*ii*) A better approximation to the gradient $\partial v/\partial n$ is given by

$$\left(\frac{\partial v}{\partial n}\right)_A = \frac{4v_B - 3v_A - v_C}{2a} \quad . \quad . \quad . \quad . \quad (28)$$

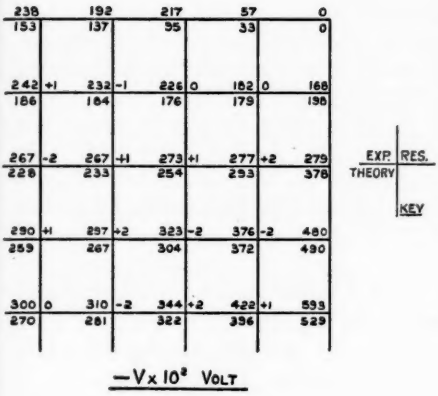

Fig. 5.
Flate plate with parabolic stress distribution on two opposite edges. (Gradient based on two ordinates.)

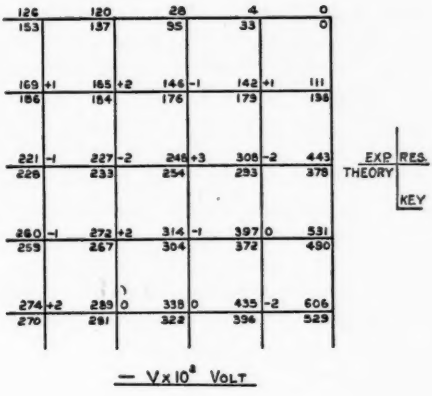

Fig. 6.
Flat plate with parabolic stress distribution on two opposite edges. (Gradient based on three ordinates.)

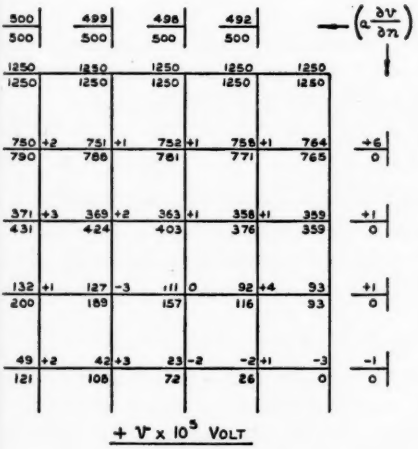

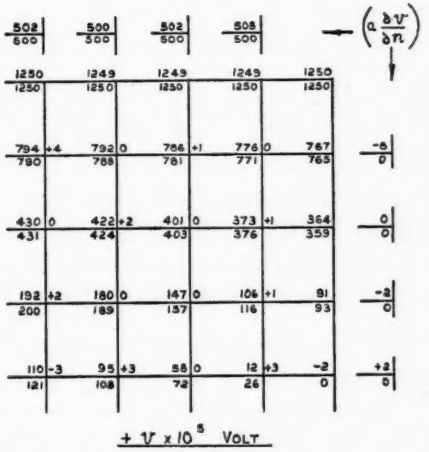

where v_0 is the value of the node at a distance $2a$ from the boundary. Using this method, v_A is set up as before, and then the boundary values on the medium potential net are adjusted until the relationship (28) is satisfied. This is rendered simple by means of an electrical circuit devised for the purpose and shown in Fig. 7. The slope, based on three ordinates, is given immediately by the potentiometer.

The results of using this method are given in Fig. 6.

(*iii*) A third possible method of applying the boundary conditions is to set the gradient of the potential at the boundary of the low potential net, before setting the

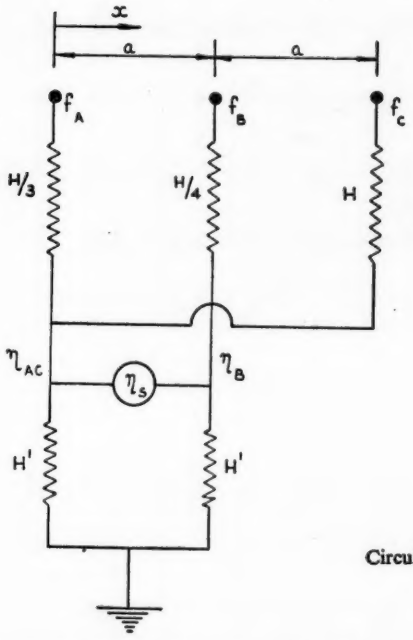

$$\left(\frac{\partial f}{\partial x}\right)_A = \frac{1}{2a}\left(4f_B - 3f_A - f_C\right)$$

$$= \frac{1}{2a}\left(4 + \frac{H}{H'}\right)\left(\eta_B - \eta_{AC}\right)$$

$$= \frac{1}{2a}\left(4 + \frac{H}{H'}\right)\eta_S$$

Fig. 7.
Circuit for gradient based on three ordinates.

boundary potential itself. This is achieved by feeding currents into the boundary points of the low potential net until they produce the desired gradient of potential. The boundary potentials on the low potential net are then obtained by adjusting the boundary potentials on the medium potential net.

4.2. Discussion of Results of Extension Experiments

The results of the experiments with the flat plate in extension are shown in Figs. 5 and 6, together with the corresponding theoretical values. Since the plate had two axes of symmetry the results corresponding to only one quarter of the plate were recorded, the other quadrants yielding almost identical values. The potentials on both nets were recorded, the actual voltages being given; the theoretical elasticity parameters being converted into corresponding electrical voltages for comparison. Also shown in the figures are the remainders or residuals obtained when the relaxation formula is applied to the experimental values.

The expressions for the relaxation residuals are

$$\text{RES.} = \sum_{n=1}^{4} V_n - 4V_0 \qquad (29)$$

for the medium potential net, and

$$\text{RES.} = \sum_{n=1}^{4} v_n - 4v_0 - \frac{r}{R}V_0 \qquad (30)$$

for the low potential net.

In all three experiments, the relaxation residual is small, indicating that the analogy is accurate subject to the coarseness of the mesh used. In Fig. 5, where the gradient is based on two ordinates, the comparison between experiment and theory is not good, but in Fig. 6 where the gradient is based on three ordinates, the agreement is quite good in view of the small number of points used. In the case where the boundary conditions were applied in a different manner, similar to that used by Liebmann, the results were reasonable, but considerable practical difficulty was encountered since there was a large degree of cross-coupling on the boundary conditions, such that when the boundary potential was adjusted the slope was also affected and *vice versa*. Also, it was noted that the potentials were less steady, due to the boundary circuit arrangement, and this caused the finite difference formulae residuals to be higher. This method of setting the boundary conditions was not proceeded with.

4.3. Flexure of a Plate by a Uniform Distributed Load

The particular problem of the flexure of a plate which was investigated was that of a square flat plate subjected to a uniform normal loading, the edges of the plate being either simply-supported or built-in. Again, the theoretical solution of this problem is known and is given by Timoshenko[10].

In these experiments the high potential grid was required, together with the R' resistances. A uniform distributed load required all the nodes in this grid to be connected together and a large potential applied to them, since E is to be constant.

Dealing first with the case of simply-supported edges, the relevant boundary conditions are

$$\left.\begin{aligned} & M_x = M_y = 0 \\ \text{and} \quad & w = 0 \end{aligned}\right\} \quad . \quad . \quad . \quad . \quad . \quad . \quad (31)$$

so that as regards the electrical network, the conditions become

$$\left.\begin{aligned} & V = 0 \\ \text{and} \quad & v = 0 \end{aligned}\right\} \quad . \quad . \quad . \quad . \quad . \quad . \quad . \quad (32)$$

These conditions are particularly simple to apply as they imply that the boundaries of both the medium and low potential nets are shorted and earthed.

This experiment was carried out twice, once with $R' = 100{,}000$ ohms and once with $R' = 50{,}000$ ohms, so as to increase the values of the potentials v. The results of the latter experiment are given in Fig. 8.

For built-in edges, the boundary conditions are

$$\left.\begin{aligned} & \frac{\partial w}{\partial n} = 0 \\ \text{and} \quad & w = 0 \end{aligned}\right\} \quad . \quad . \quad . \quad . \quad . \quad . \quad (33)$$

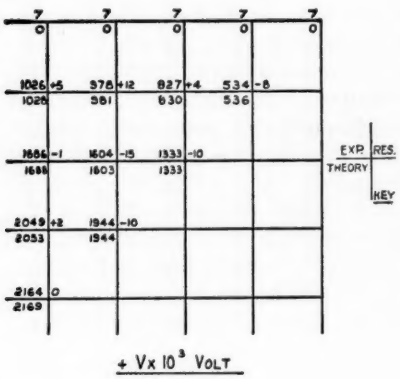

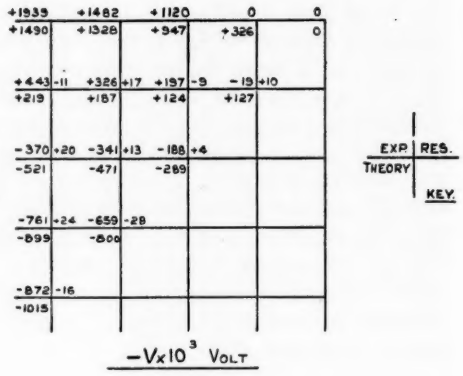

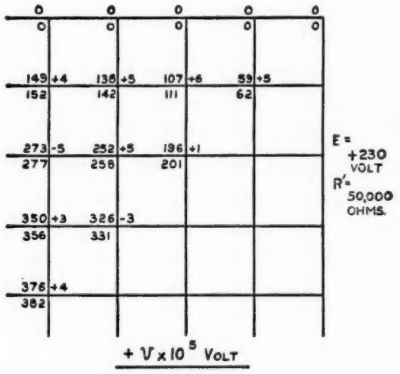

Fig. 8.
Square plate with uniform normal pressure.
Simply-supported edges.

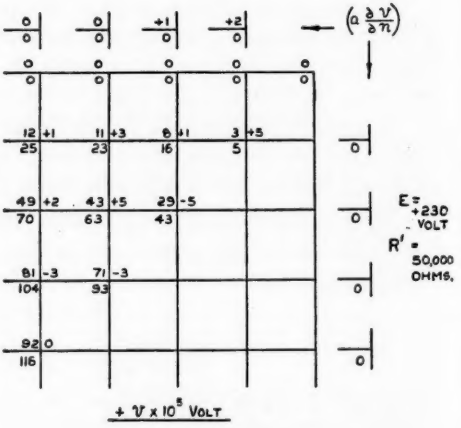

Fig. 9.
Square plate with uniform normal pressure.
Built-in edges. (Gradient based on three ordinates.)

so that for the electrical network the conditions become

$$\left.\begin{aligned} \frac{\partial v}{\partial n}&=0 \\ \text{and}\quad v&=0 \end{aligned}\right\}. \qquad \ldots\ldots \quad (34)$$

These conditions were applied in the same way as were the boundary conditions for the case of a plate in extension; Fig. 9 gives the results of the experiment when the boundary gradient is based on three ordinates, with $R'=50{,}000$ ohms.

4.4. Discussion of Results of Flexural Experiments

The results of the experiments with a flat plate in flexure are given in Figs. 8 and 9. Here, owing to symmetry, only one eighth part of the nets were recorded, the other sectors yielding almost identical results. The finite difference formulae residuals, together with the theoretical results, are also given, all in terms of electrical voltages.

For simply-supported edges the results are extremely good, but in this case it was not necessary to perform any electrical iteration, since it was possible to apply directly the boundary conditions.

The results for built-in edges were not so good, even when the gradient was based on three ordinates. However, this is thought to be mainly due to the coarse net used, since only nine ordinates are available to define a curve with two points of contraflexure.

It was also noted that the high potential E, which was a mains voltage, tended to drift and so make the recording a little tedious; this voltage should, for preference, be stabilised.

It should be noted that if the boundary conditions specified involve a differential higher than the first, then a procedure similar to that employed for setting a gradient based on three ordinates could be used. This condition would apply if the plate had a free edge, but this experiment was not tried as it was felt that the network available was too small to be likely to yield accurate results.

5. Conclusions

The work detailed in this report shows that the use of a pure resistance network, to solve some of the problems of extension and flexure of flat plates, is quite practicable.

The results obtained are quite satisfactory, bearing in mind the size of the network used. The fact that the finite difference formulae residuals are small shows that the solutions obtained with the network will be practically identical with those obtained by a relaxation solution on a grid of the same size.

The network is simple to construct and, since it only consists of resistances, it is very reliable. The operation of the network is a simple matter.

If a large network were to be built it would be desirable to have voltage stabilisation for the high potential net. Also, if the number of boundary points were increased it might be necessary to have a display of the boundary potentials, possibly by means of a battery of millivoltmeters.

Acknowledgment

The work described in this paper was financed by the Ministry of Supply and carried out in the Department of Civil Engineering in the University of Birmingham. The authors wish to thank the Chief Scientist, Ministry of Supply, for permission to publish the paper.

REFERENCES

1. REDSHAW, S. C. Electrical Analogues for the Solution of Problems Concerning the Extension and Flexure of Flat Elastic Plates. A.R.C. 15,335, May 1952.

2. SOUTHWELL, R. V. On the Analogues Relating Flexure and Extension of Flat Plates. *Quarterly Journal of Mechanics and Applied Mathematics*, Vol. III, Part 3, pp. 257-270, September 1950.

3. FOX, L. and SOUTHWELL, R. V. Relaxation Methods Applied to Engineering Problems. VIIA, Biharmonic Analysis as Applied to the Flexure and Extension of Flat Elastic Plates. *Phil. Trans. Roy. Soc.*, C., No. 2, Vol. I, pp. 15-56, October 1941.

4. REDSHAW, S. C. An Electrical Potential Analyser. *Proceedings of the Institution of Mechanical Engineers*, 159, pp. 55-62, 1948.

5. PALMER, P. J. The Determination of Torsion Constants for Bulbs and Fillets by Means of an Electrical Potential Analyser. Aluminium Development Association, Research Report No. 22, December 1953.

6. BOSCHER, J. and MALAVARD, L. Détermination Analogique des Fonctions Biharmoniques. Bulletin No. 8. Société Française des Mécaniciens, 1953.

7. LIEBMANN, G. A Resistance-Network Analogue Method for Solving Plane Stress Problems. Associated Electrical Industries, Research Report No. A. 271, March 1953.

8. TIMOSHENKO, S. and GOODIER, J. N. *Theory of Elasticity*. McGraw-Hill, 1951.

9. LONGMAN, I. M. A Method of Stress Analysis for an Elastic Solid Under Conditions of Plane Strain or Stress. The British Iron and Steel Research Association, March 1951 (Unpublished).

10. TIMOSHENKO, S. *Theory of Plates and Shells*. McGraw-Hill, 1940.

On an Approximate Method of Calculating Pressures on Non-lifting Head Shapes at Supersonic Speeds

H. K. ZIENKIEWICZ
(*Fluid Motion Laboratory, University of Manchester*)

SUMMARY: Slender-body theory is used to derive the ogive of curvature approximation for very slender, pointed, convex head shapes at supersonic speeds. Results of application of this approximation, together with the λ-method for circular arc ogives, to a variety of non-slender head shapes show very good agreement with the method of characteristics, van Dyke's second-order theory and experiment. Good agreement with the method of characteristics and with experiment is obtained even in cases when the stagnation pressure losses across the nose shock wave are not negligible.

1. Introduction

In Ref. 1 a number of approximate methods of calculating pressures on non-lifting, pointed, convex head shapes at supersonic speeds have been put forward. The present paper summarises some recent developments of the most promising of these methods, the so-called "ogive of curvature method." In particular, the basic assumption underlying this method is justified by showing that it leads to the exact result in the limit of vanishingly small supersonic similarity parameter βt, the error in the pressure coefficient at any point on the head relative to the pressure coefficient at the nose vanishing as $(\log \beta t)^{-1}$. This result, obtained by using the slender-body theory, is rather more satisfactory than the original justification of the assumption, which was based on purely empirical grounds[1].

The ogive of curvature approximation is then used together with the λ-method for circular arc ogives[2] to calculate pressures on a number of non-slender head shapes at Mach numbers such that the supersonic similarity parameter βt varies between about 0·4 and 1·0. Comparison with the corresponding pressure distributions calculated by the method of characteristics (taking account of flow rotation) and by van Dyke's second-order theory and with some experimental pressure distributions shows very good agreement and leads to the conclusion that the ogive of curvature method effectively bridges the gap between the linearised and the conical-shock-expansion theories[3].

NOTATION

A, B, ... , H	designation of head profiles (*see* Table I)
C_p	pressure coefficient, $=(p-p_0)/q$
C_{pc}	ogive of curvature pressure coefficient

Received October 1954.

$K = 2\beta \tan(\chi/2)$, supersonic similarity parameter for circular arc ogives

$K_h = 2M \tan(\chi/2)$, hypersonic similarity parameter for circular arc ogives

L length of ogive of curvature

M free stream Mach number

p, p_0 local and free stream static pressures, respectively

q dynamic head, $= \frac{1}{2}\gamma p_0 M^2$

$r(x)$ equation of head profile

s, S cross-sectional areas of head and ogive of curvature, respectively

t, T thickness ratios (maximum diameter/length) of head and ogive of curvature, respectively

x, r and X, R cylindrical co-ordinates (*see* Fig. 1)

y, Y x- and X-like variables of integration

$\beta = \sqrt{(M^2 - 1)}$

γ ratio of specific heats

$\theta = \tan^{-1} r'(x)$, profile slope

λ factor of proportionality defined by equation (9)

χ ogive of curvature nose semi-angle

Dashes denote differentiation with respect to x or X.

Suffixes

t two-dimensional simple-wave flow

n conditions at the nose

2. The Ogive of Curvature Approximation in the Slender-Body Theory

Referring to Fig. 1 consider a slender, pointed, convex head profile at zero incidence in a supersonic air stream of Mach number M. The length of the body is taken as unity and its maximum diameter is t. The equation of the head profile is $r = r(x)$, such that r' and r'' are $O(t)$ and it is assumed that r' and r'' are everywhere continuous but $r'(1)$ is not necessarily zero. Then, under the usual assumptions of the slender-body theory, the pressure coefficient at a point $P(x, r)$ on the body surface is given by[4]

$$C_p = \frac{1}{\pi}\left\{[s''(0) - s''(x)]\log x + s''(x)\log\frac{2x}{\beta r} + \int_0^x \log(x-y)\,d[s''(y)]\right\} - \\ - r'^2(x) + O(t^3 \log t) \quad . \quad . \quad (1)$$

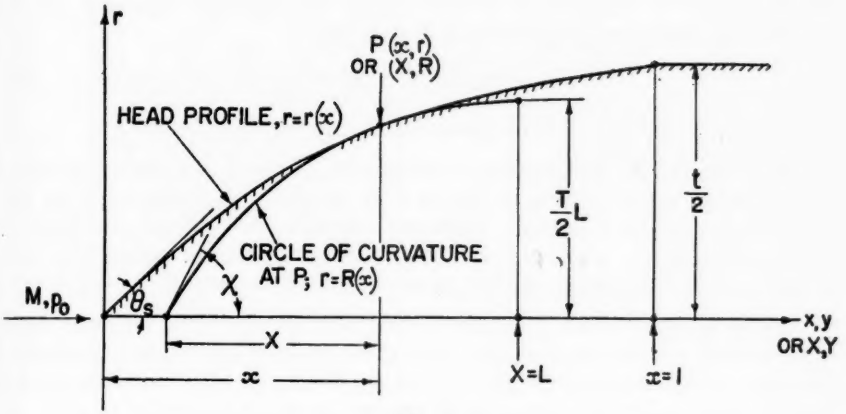

Fig. 1.
Co-ordinates and notation.

where $s=\pi r^2$ is the cross-sectional area of the head shape and $\beta=\sqrt{(M^2-1)}$. In equation (1) the dominant term is the second, being $O(t^2 \log t)$, while the remaining terms are $O(t^2)$. Hence, we can rewrite equation (1) as

$$C_p=\frac{s''(x)}{\pi}\log\frac{2x}{\beta r}+O(t^2). \quad . \quad . \quad . \quad . \quad . \quad (2)$$

Consider next the flow about the ogive of curvature of the head profile at P (Fig. 1). This ogive is obtained by revolving about the axis of symmetry an arc of the circle of curvature of the profile at P. The length of the ogive up to the point of zero slope is L and its maximum diameter is TL. Approximating the ogive of curvature by the corresponding parabolic arc body (differences in ordinate, slope and curvature between the two profiles are $O(T^3)$ and therefore are negligible in the present application), it can be shown that

$$\left.\begin{aligned} T&=\tfrac{1}{2}(r'^2-2rr'')^{\frac{1}{2}}=O(t)\\ \frac{x}{X}&=\tfrac{1}{2}\frac{xr'}{r}\left[\left(1-\frac{2rr''}{r'^2}\right)^{\frac{1}{2}}+1\right]=O(1)\end{aligned}\right\} \quad . \quad . \quad . \quad (3)$$

where the orders of magnitude follow from the assumption that r, r', and r'' are all $O(t)$. Thus, the ogive of curvature is also a slender body so that, with the origin of the X, R co-ordinates at the nose of the ogive and approximating as in equation (2), the pressure coefficient at the point $P(X, R)$ on the ogive of curvature at P is

$$C_{pc}=\frac{S''(X)}{\pi}\log\frac{2X}{\beta R}+O(T^2). \quad . \quad . \quad . \quad . \quad (4)$$

But, by the definition of the ogive of curvature, $R(X)=r(x)$, $R'(X)=r'(x)$ and

$R''(X)=r''(x)$, so that $S''(X)=s''(x)$. Hence, by virtue of equations (3) it immediately follows from equations (2) and (4) that

$$C_p=C_{pc}+O(t^2) \quad . \quad . \quad . \quad . \quad . \quad (5)$$

provided that r' and r'' do not vanish simultaneously, for then $X=\infty$.

Thus, to order $t^2 \log t$ the pressure coefficient at a point P on a slender, pointed, convex head shape is the same as that at P on the ogive of curvature at P at the same free stream Mach number. The error relative to the pressure coefficient at the nose of the body, which is proportional to $t^2 \log \beta t$, vanishes as $(\log \beta t)^{-1}$ and the ogive of curvature approximation becomes exact in the limit of $\beta t \longrightarrow 0$.

At the nose, the actual profile and its circle of curvature have the same slope and curvature, and near the nose they coincide to first order in x. Hence, obviously, the ogive of curvature approximation gives the correct pressure coefficient at the nose. Further, since for a given Mach number the pressure gradient at the nose depends only on $r'(0)$ and $r''(0)$, provided that the flow is everywhere supersonic (*see, e.g.*, Ref. 5 for a full discussion), the ogive of curvature approximation gives also the correct value of this gradient. Hence equation (5) can be written more precisely as

$$C_p=C_{pc}+O[x^2 f(x) t^2] \quad . \quad . \quad . \quad . \quad . \quad (6)$$

where $f(x)=O(1)$ and depends on the profile shape.

In fact, the ogive of curvature approximation in the slender-body theory gives better accuracy than might be expected from the estimate of the order of error, because some of the $O(t^2)$ terms cancel out (*e.g.*, the $r'^2(x)$ term in equation (1), although of $O(t^2)$, is given correctly by the ogive of curvature approximation, because $r'=R'$). It appears difficult to obtain an estimate of the error for an arbitrary profile better than that in equation (6), due to the awkward form of equation (1) and of the relation between x and X (equations (3)). However, the following example may serve as an indication of the accuracy of the ogive of curvature approximation in the slender-body theory.

Take the equation of the head profile to be given by $r=\frac{1}{2}tx(3-2x)^{\frac{1}{2}}$. Then, from equation (1)

$$C_p=\frac{3}{2}t^2\left[(1-2x)\log\frac{4}{\beta t(3-2x)^{\frac{1}{2}}}+2x-\frac{3(1-x)^2}{2(3-2x)}\right] \quad . \quad . \quad (7)$$

while, applying the ogive of curvature approximation, it is found that

$$C_{pc}=C_p+\Delta C_p$$

where C_p is as in equation (7), and

$$\frac{\Delta C_p}{t^2}=\frac{3(1-x)[3(3-2x+x^2)]^{\frac{1}{2}}-(3-2x)^2}{2(3-2x)}-(1-2x)\log\frac{3(1-x)+[3(3-2x+x^2)]^{\frac{1}{2}}}{2(3-2x)}. \quad . \quad . \quad . \quad . \quad (8)$$

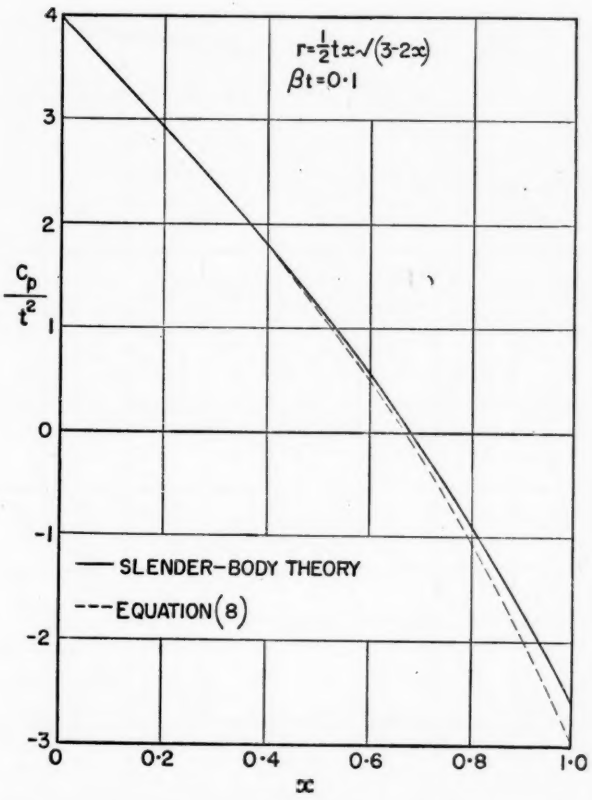

Fig. 2.
Comparison of pressure distributions as given by the slender-body theory and the ogive of curvature approximation.

C_p and C_{pc} for $\beta t = 0{\cdot}1$ are plotted against x in Fig. 2. It can be seen that over the forward 80 per cent. of the head length ΔC_p is less than 5 per cent. of C_p at the nose; the relative differences between C_p and C_{pc} can, of course, be made arbitrarily small by decreasing βt.

3. Application of the Ogive of Curvature Method to Non-Slender Head Shapes

The ogive of curvature approximation is of little practical value in the slender-body theory, except perhaps for head shapes with s'' such that the integral in equation (1) cannot be evaluated in a closed form. What merit the method possesses lies largely in the fact that it can be applied to non-slender head shapes for which no other equally rapid and accurate method exists at present. The application of this method to such head shapes is made possible by the availability

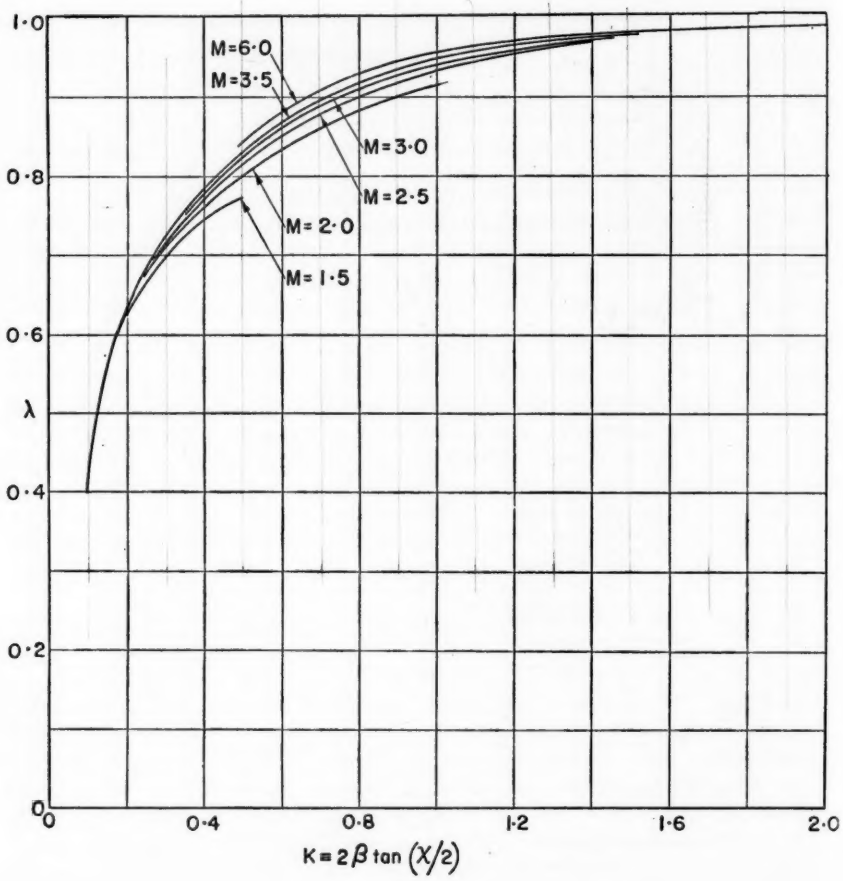

Fig. 3.
Circular arc ogives. Variation of λ with supersonic similarity parameter and free stream Mach number.

of accurate pressure distributions on non-slender circular arc ogives. One could use directly the characteristics pressure distributions, generalised on the basis of the hypersonic similarity law, which are given in Refs. 6 and 7. However, since the similarity generalisation involves a certain loss of accuracy, particularly at Mach numbers between 1·5 and 2, it is more accurate to use the so-called λ-method put forward by the author[2]. For convenience of readers unfamiliar with this method a brief summary is given in what follows.

On analysing the characteristics pressure distributions of Ref. 6, the author discovered[2] a remarkably simple relationship between the axi-symmetric flow over a circular arc ogive and the two-dimensional simple-wave flow over the same profile. Let p_n and M_n be the static pressure and the local Mach number,

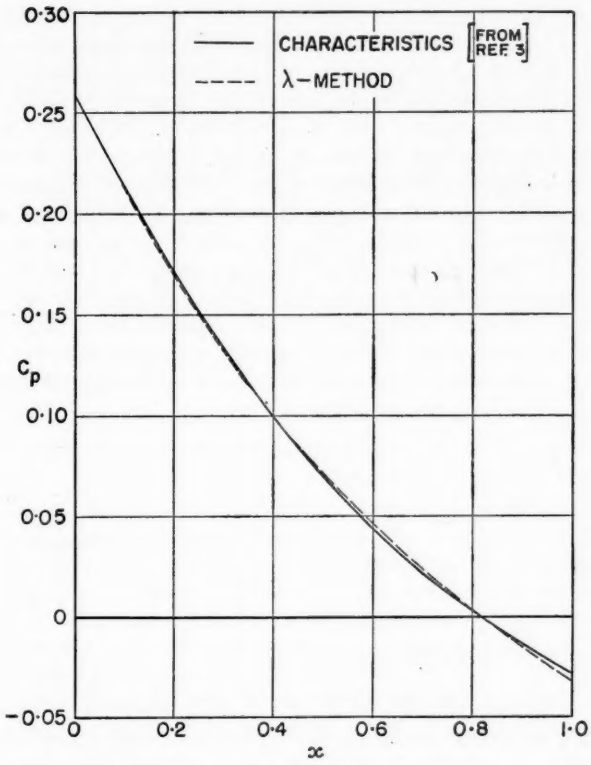

Fig. 4.
Circular arc ogives. Typical comparison of λ-method with method of characteristics. $\chi = 18{\cdot}9°$, $M = 3$.

respectively, at the nose of a circular arc ogive, p be the static pressure at a point P on the ogive in axi-symmetric flow and p_t be the static pressure that would obtain at the point P if the flow expanded two-dimensionally over the same profile from the given conditions at the nose. Then, it turns out that

$$\left.\begin{aligned} p_n - p &= \lambda\,(p_n - p_t) \\ \text{or}\quad C_{pn} - C_p &= \lambda\,(C_{pn} - C_{pt}) \end{aligned}\right\} \quad . \quad . \quad . \quad . \quad . \quad (9)$$

where the factor of proportionality λ is constant over the profile and a function only of the free stream Mach number M and of χ, the nose semi-angle of the ogive.

In Ref. 2, λ was calculated from the irrotational characteristics results[6] and a chart was given showing the variation of λ with χ and M for $1{\cdot}5 \leqslant M \leqslant 3{\cdot}5$, $0{\cdot}5 \leqslant 2M \tan(\chi/2) \equiv K_h \leqslant 1{\cdot}0$. This chart has since been revised and extended to $K_h = 2$ by using the characteristics results of Ref. 7, which included the effects of flow rotation, and to values of $K_h < 0{\cdot}5$ by using a number of unpublished characteristics and second-order theory solutions. The revised and extended λ chart is

shown in Fig. 3; the supersonic similarity parameter K, rather than the hypersonic parameter K_h is used as the abscissa to reduce the dependence of λ on M. The value of λ for $K=0{\cdot}1$ was obtained using the slender-body theory. Above this value of K the slender-body theory is generally considered to be unreliable, at least as regards pressure distributions. For K much below $0{\cdot}1$ this theory indicates that λ ceases to be approximately constant along the profile. Thus $K=0{\cdot}1$ appears to be the lower limit of the applicability of the λ-method. In addition, the method is at present limited to $M \geqslant 1{\cdot}5$ owing to the lack of data required for evaluating λ at $M < 1{\cdot}5$. However, it is believed that equation (9) would still apply at Mach numbers below $1{\cdot}5$ provided that χ is small enough for the flow over the ogive to be everywhere supersonic and large enough for $K \geqslant 0{\cdot}1$. At the other end of the range of K for which λ has been determined, it is of interest to note that as K increases above about $1{\cdot}5$, λ very closely approaches unity, indicating that the flow is then practically two-dimensional; this is in agreement with Eggers's conical-shock-expansion theory for high Mach number flows[8].

As an indication of the accuracy of the λ-method, a typical comparison with the method of characteristics is shown in Fig. 4.

The procedure for applying the λ-method, together with the ogive of curvature approximation, to calculation of pressures on non-slender head shapes is very simple. Once the distributions of the profile slope

$$\theta = \tan^{-1} r'(x)$$

and of the ogive of curvature nose semi-angle

$$\chi = \cos^{-1} [\cos\theta\,(1 + rr'' \cos^2\theta)]$$

are known along the profile, the corresponding values of λ for a given Mach number are found from Fig. 3. Then, using the tables of flow about cones[9] to find $C_{pn}(\chi, M)$ and a standard Prandtl-Meyer expansion table to find C_{pt} by the usual methods, C_p, the pressure coefficient at any point on the profile follows from equation (9) and the ogive of curvature approximation. Computing details, suitable *pro formae* and worked examples are given in Ref. 1.

When applying the ogive of curvature method to head shapes such that the loss of stagnation pressure across the nose shock is not negligible (greater than, say, 5 per cent. of the free stream stagnation pressure) one of two alternative procedures can be followed. The first is to take the stagnation pressure on the local ogive of curvature as equal to that at the nose of the actual body, which requires different free stream stagnation pressures for the actual body and the ogive of curvature; the second is to take the free stream stagnation pressures as equal, which violates the condition of constant stagnation pressure along the body surface. At first sight the first alternative appears more plausible and was in fact adopted in Ref. 1, since for all the head shapes considered at the time stagnation pressure losses were negligible and there was no evidence as to which procedure would lead to better accuracy. However, since then investigation of pressure distributions on head shapes with large nose angles (and at Mach numbers such that losses of stagnation pressure across the nose shock were up to 30 per cent. of the free stream stagnation

TABLE I

PROFILES OF HEAD SHAPES

Designation	*Equation*	*Fineness Ratio* $(1/t)$
A	$r=\frac{1}{6}\left[1-(1-x)^{1\cdot5}\right]$	3
B	$\frac{1}{6}\left[1-(1-0\cdot6x)^{3}\right]$	3
C	$0\cdot03968\,(\pi x+\sin \pi x)$	4
D	$\frac{1}{6}\left[\frac{1}{\pi}\,(\psi-\frac{1}{2}\sin 2\psi)\right]^{\frac{1}{2}}, \quad \psi=\cos^{-1}(1-2x)$	3
E	$\frac{1}{6}\left[x\,(2-x)\right]^{3/4}$	3
F	$\frac{1}{6}\,x^{3/4}$	3
G	$0\cdot0655\,x+0\cdot02782\log_{10}(1+42\cdot37x)$	4·5
H	$0\cdot0636\,x+0\cdot03286\log_{10}(1+26\cdot74x)$	4·5

pressure) have revealed that the first procedure consistently underestimated pressures on such heads and that the second procedure yielded much better accuracy. Consequently, the second procedure has been adopted as standard and in fact is implicit in the ogive of curvature approximation as stated in the present paper, namely, that "*the pressure coefficient* at a point P on a convex head shape is the same as that at P on the ogive of curvature at P at the same free stream Mach number". This modification of the original method requires an obvious modification of the computing procedure given in Ref. 1. If velocity or Mach number distributions along the head are required, these should be obtained from the pressure distributions using the *correct* value of the (constant) stagnation pressure along the body surface and not the fictitious values on the local ogives of curvature used in the computation of pressure coefficients.

A difficulty arises in applying the ogive of curvature method to head shapes such that curvature of the profile becomes infinite or zero at the end of the head*. In the former case, $-r''(1)=\infty$, as $x\longrightarrow 1$ a point is reached where χ is so large that it falls outside the range of the λ-χ chart (Fig. 3) and even if this were not so, curvature would eventually increase sufficiently for the whole concept of the ogive of curvature to become meaningless. When $r''(1)=r'(1)=0$, $\chi\longrightarrow 0$ as the end of the head is approached and a point is reached where $K<0\cdot1$, which is outside the limit of applicability of the λ-method. In the Appendix, a procedure for dealing with such cases is suggested which, though perhaps somewhat artificial, appears to give acceptable results. In any case, the region of a head affected by $-r''(1)=0$ or ∞ is usually small and it would not matter very much how one extrapolated there

*Cases when this occurs elsewhere on the head need not be considered here. For, profiles with infinite curvature at $0<x<1$ are unlikely to be of practical interest, the possibility of $r''(0)=-\infty$ is excluded by the assumption of a sharp nose, while the case of zero curvature presents no difficulty unless the slope is also zero (*cf.* equations (5) and (3)), which on a convex profile with continuous slope can only occur at $x=1$.

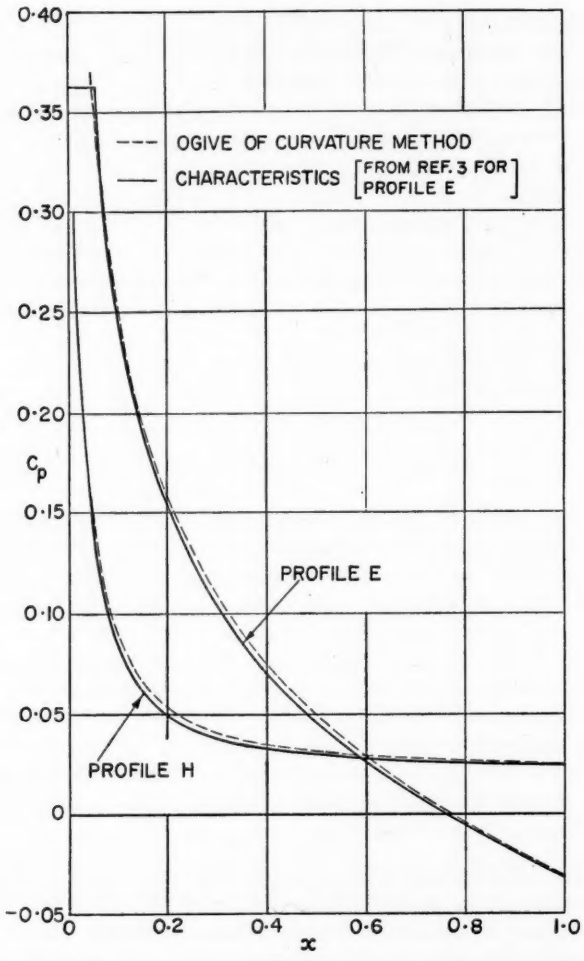

Fig. 5.
Comparison of ogive of curvature method with method of characteristics.
Profile E at $M=3{\cdot}0$ and profile H at $M=2{\cdot}3$.

the pressure distribution, particularly from the point of view of wave drag calculations (the profile slope near the end of the head being necessarily small, especially when $r''(1)=r'(1)=0$).

4. Comparison with More Exact Theories and Experiment

Since it was first put forward, the ogive of curvature method has been extensively tested by comparison with results of other theories and with experimental results on several head shapes. Since in the ogive of curvature method the pressure distribution is closely connected with the profile slope and curvature, profiles with

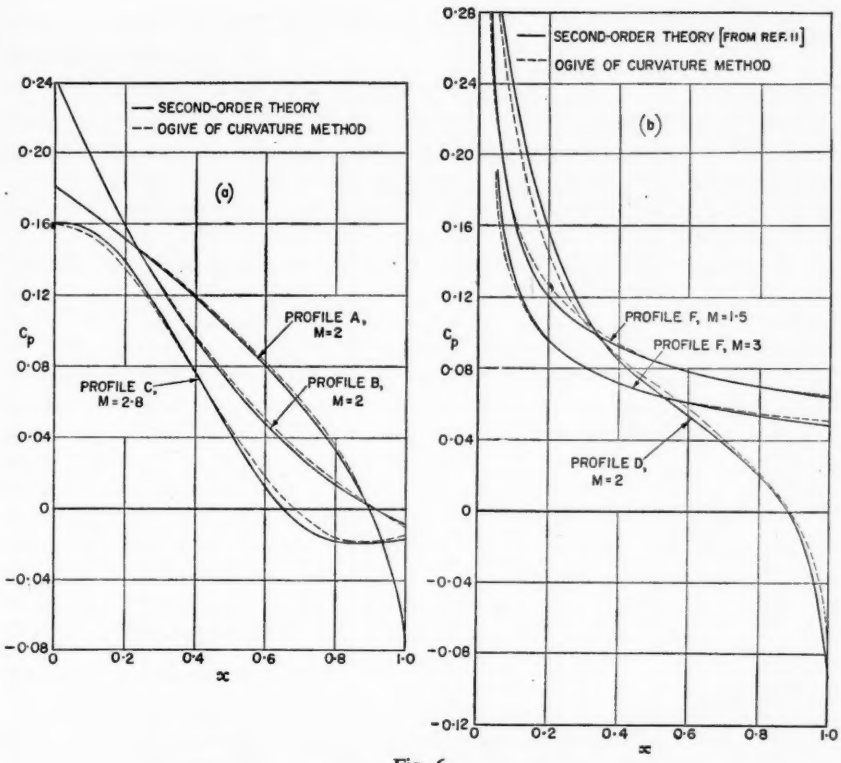

Fig. 6.
Comparison of ogive of curvature method with second-order theory.
(*a*) Profiles A, B and C. (*b*) Profiles D and F.

a wide variety of slope and curvature distributions were chosen for comparison. For obvious reasons it is possible to include here only a representative selection of the results. Profile geometry of the head shapes considered is summarised in Table I.

4.1. Method of Characteristics

Figure 5 shows pressure distributions obtained by the ogive of curvature method on profiles E and H compared with the corresponding pressure distributions calculated by the method of characteristics, including the effects of flow rotation. The profile E has a blunt nose and, to make it possible to apply the method of characteristics, a cone tangent to the profile at $x=0{\cdot}05$ was used in Ref. 3 to replace the blunt nose. When applying the ogive of curvature method it is, of course, more convenient to replace the blunt nose by a circular arc ogive rather than a cone; this was not done in the case of the profile E, since the pressure distribution for $x<0{\cdot}05$ is of no interest for the present purpose.

Particularly gratifying is the good agreement obtained for the profile H. This profile has a large nose semi-angle (24°) followed by a very rapid change of curvature near the nose, while the curvature and slope near the end of the head are so small

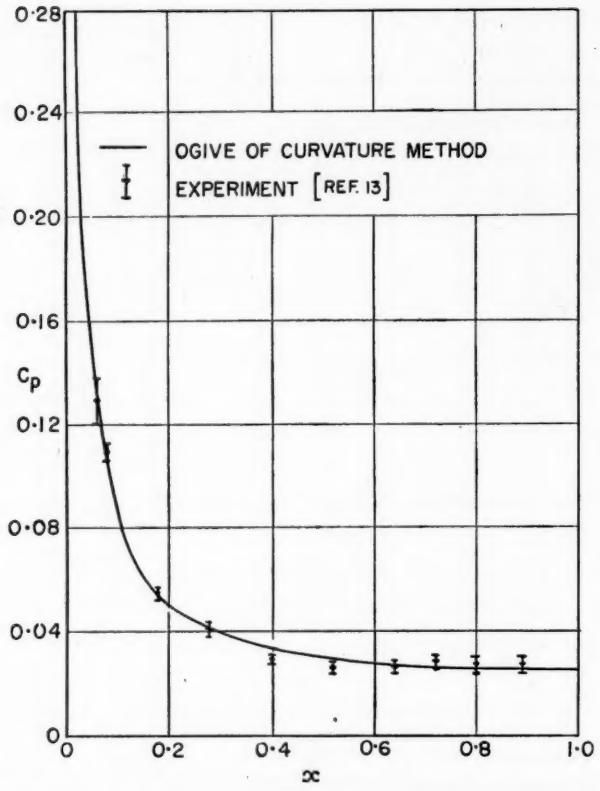

Fig. 7.

Comparison of ogive of curvature method with experiment. Profile G at $M=2{\cdot}45$.

that the limit of applicability of the λ-method is approached there. Hence, comparison of pressure distributions on this profile is a severe test of the ogive of curvature method. Comparison of the computing labour required by the two methods is also of interest. Calculations by the ogive of curvature method took approximately 1 hour. In the characteristics solution* a very small mesh size had to be used near the nose, which resulted in some 280 mesh points and a computing time of over 300 hours.

4.2. Second-Order Theory

By now, van Dyke's second-order theory[10] has been widely applied by several investigators and, in the case of head shapes, has been shown to give very good accuracy for $\beta t < 1$. Although much more rapid than the method of characteristics,

*Carried out at the Mathematics Division, National Physical Laboratory, under the direction of A. R. Curtis.

it still requires a considerable computing effort, of the order of 10–20 hours for one pressure distribution.

Good agreement between the ogive of curvature method and the second-order theory has been obtained in all the several cases investigated, some of which are shown in Fig. 6(*a*) (profiles A, B and C) and Fig. 6(*b*) (profiles D and F). Of special interest are regions near the end of the heads A and D, which terminate with infinite curvature of the profile, and of the head C, which terminates with zero profile slope and curvature. In these regions the procedure referred to in the last paragraph of Section 3 and described in the Appendix was used with apparent success.

4.3. Experiment

The accuracy of the ogive of curvature method has also been explored by comparison with wind tunnel experiments on a number of head shapes. The results, published in Refs. 12 and 13, show good agreement. A representative comparison (profile G at $M=2{\cdot}45$) is shown in Fig. 7. The profile G is similar to the profile H (*cf.* Table I), but has an even larger nose semi-angle (30°) and the free stream Mach number is such that the stagnation pressure loss across the nose shock is about 14 per cent. of the free stream stagnation pressure. As can be seen from Fig. 7, the theory predicts correctly the enormous expansion from the pressure at the nose ($C_{pn}=0{\cdot}600$) and over most of the head agreement with experiment is within the experimental scatter*. Similar agreement was obtained for other head shapes and Mach numbers[13].

5. Conclusions

Slender-body theory shows that the ogive of curvature approximation becomes exact in the limiting case of head shapes with vanishingly small supersonic similarity parameter βt. When this approximation is used together with the λ-method for circular arc ogives, comparisons with the method of characteristics, van Dyke's second-order theory and experiment show that its range of applicability is much wider than might be expected from the assumptions made in its derivation and that in fact it gives very good accuracy for non-slender head shapes with βt as high as 1·0–1·5. Since for $\beta t > 1{\cdot}5$ Eggers's conical-shock-expansion theory becomes accurate[3, 8], the ogive of curvature method bridges the gap between Eggers's theory and the linearised and slender-body theories.

Interpreted as an extension of the familiar concept of two-dimensional simple-wave flow, the ogive of curvature method implies that the pressure coefficient on a convex axi-symmetric head shape depends only on the free stream Mach number, the local profile slope and the local ratio of the radius of curvature of the profile to the profile ordinate.

In spite of its accuracy the method is very rapid, requiring only about a tenth or a hundredth of the computing effort necessary for the application of the second-order theory or the method of characteristics, respectively.

*Four pressure measurements were obtained at each station as the model was rotated through four angular positions[13]. In Fig. 7 the average of these readings is indicated by a dot and their scatter by a vertical stroke.

There is nothing in the slender-body theory derivation of the ogive of curvature approximation to suggest that it should not apply to complete bodies of revolution as well as head shapes, provided that profile slope and curvature are everywhere continuous. However, owing to the lack of accurate pressure distributions beyond the point of maximum thickness on circular arc ogives, it is not possible to say at the moment whether this would also hold for non-slender bodies.

ACKNOWLEDGMENT

The work reported here was done while the author was at the Guided Weapons Division, The English Electric Company, and the author is indebted to the Company for permission to publish this paper.

REFERENCES

1. BOLTON SHAW, B. W. and ZIENKIEWICZ, H. K. The Rapid, Accurate Prediction of Pressure on Non-lifting Ogival Heads of Arbitrary Shape, at Supersonic Speeds. A.R.C. Current Paper 154 (The English Electric Co. Report LA.t.034, June 1952).
2. ZIENKIEWICZ, H. K. A Method for Calculating Pressure Distributions on Circular Arc Ogives at Zero Incidence at Supersonic Speeds, Using the Prandtl-Meyer Flow Relations. A.R.C. Current Paper 114 (The English Electric Co. Report LA.t.024, January 1952).
3. EHRET, D. M. Accuracy of Approximate Methods for Predicting Pressures on Pointed Non-lifting Bodies of Revolution in Supersonic Flow. N.A.C.A. T.N. 2764, August 1952.
4. LIGHTHILL, M. J. Supersonic Flow Past Bodies of Revolution. R. & M. 2003, January 1945.
5. VAN DYKE, M. D. A Study of Hypersonic Small Disturbance Theory. *Journal of the Aeronautical Sciences*, Vol. 21, No. 3, March 1954, pp. 179-186; also N.A.C.A. T.N. 3173, May 1954.
6. EHRET, D. M., ROSSOW, V. J. and STEVENS, V. I. An Analysis of the Applicability of the Hypersonic Similarity Law to the Study of Flow About Bodies of Revolution at Zero Angle of Attack. N.A.C.A. T.N. 2250, December 1950.
7. ROSSOW, V. J. Applicability of the Hypersonic Similarity Rule to Pressure Distributions which include the Effects of Rotation for Bodies of Revolution at Zero Angle of Attack. N.A.C.A. T.N. 2399, June 1951.
8. EGGERS, A. J. and SAVIN, R. C. Approximate Methods for Calculating the Flow About Non-lifting Bodies of Revolution at High Supersonic Airspeeds. N.A.C.A. T.N. 2579, December 1951.
9. Tables of Supersonic Flow Around Cones. Technical Report No. 1. Department of Electrical Engineering, Massachusetts Institute of Technology, 1947.
10. VAN DYKE, M. D. First- and Second-order Theory of Supersonic Flow Past Bodies of Revolution. *Journal of the Aeronautical Sciences*, pp. 161-178, March 1951.
11. JORGENSEN, L. H. Nose Shapes for Minimum Pressure Drag at Supersonic Mach Numbers. *Journal of the Aeronautical Sciences*, pp. 276-279, April 1954.
12. ZIENKIEWICZ, H. K., CHINNECK, A., BERRY, C. J. and PEGGS, P. J. Experiments at $M=1{\cdot}8$ on Bodies of Revolution Having Ogival Heads. A.R.C. Current Paper 148, January 1953.
13. MARSON, G. B., KEATES, R. E. and SOCHA, W. An Experimental Investigation of the Pressure Distribution on Five Bodies of Revolution at Mach Numbers of 2·45 and 3·19. College of Aeronautics Report No. 79, April 1954.

Appendix

Treatment of Profiles with Zero or Infinite Curvature at the End of the Head

Referring to Fig. 1, let the point P now denote the last point on the head for which λ can be determined from Fig. 3; at $x=1$ we have either $r''=-\infty$, or $r''=r'=0$.

Differentiating equation (9) with respect to θ yields

$$\frac{dp}{d\theta}=\lambda\frac{dp_t}{d\theta}\ .$$

Using the well-known Prandtl-Meyer relation this can be written as

$$\frac{dp}{d\theta}=\lambda'\left(\frac{dp}{d\theta}\right)_t \qquad . \quad . \quad . \quad . \quad . \quad (10)$$

where

$$\lambda'=\left(\frac{M_t}{M_1}\right)^2\left(\frac{M_1^2-1}{M_t^2-1}\right)^{\frac{1}{2}}\left(\frac{p_t}{p}\right)\lambda,$$

M_t and M_1 are the Mach numbers corresponding to p_t and p, respectively, and

$$\left(\frac{dp}{d\theta}\right)_t=\frac{\gamma pM_1^2}{\sqrt{(M_1^2-1)}}$$

is the local pressure gradient, with respect to flow direction, which would exist in the two-dimensional simple-wave flow with local static pressure p and Mach number M_1.

Thus, equation (10) gives the axi-symmetric pressure gradient at the point P as a fraction, λ', of the corresponding two-dimensional pressure gradient.

When $r''(1)=-\infty$, the flow is locally two-dimensional at $x=1$ (this follows from the characteristics equations) and $\lambda'=1$ there. Since λ' is known at P and can be similarly found for any point upstream of P, λ' can be plotted against θ and its average value, λ'_a, between θ_P and $(\theta)_{x=1}$ found, *e.g.* by graphical integration. Then the change of pressure between the point P and the end of the head is given approximately by λ'_a times the corresponding two-dimensional change of pressure.

When $r''(1)=r'(1)=0$, $\chi\longrightarrow 0$ as $x\longrightarrow 1$ and for values of χ such that $2\beta\tan(\chi/2)<0{\cdot}1$, λ is no longer constant along local ogives of curvature (*cf.* Section 3). However, the average value of λ tends to zero as $\chi\longrightarrow 0$. This follows simply from the fact that for small χ the axi-symmetric change of pressure between the nose and the end of a circular arc ogive is proportional to $\chi^2\log\beta\chi$, while the corresponding two-dimensional change of pressure is proportional to χ; hence the ratio of the two changes of pressure, which is a measure of the average λ, varies as $\chi\log\beta\chi$. Therefore, we can proceed as in the case of $r''(1)=-\infty$, but now we take $\lambda'=\lambda=0$ at $x=1$.

Some Properties of Nodes in Vibrating Systems

R. E. D. BISHOP, M.A., M.Sc.(Eng.), Ph.D. and D. C. JOHNSON, M.A.

(University Engineering Laboratory, Cambridge)

SUMMARY: Special forms of the receptance functions of mechanical systems are shown to indicate the existence of nodes. These are associated with horizontal straight lines in receptance diagrams. The effects of this nodal condition are explained in terms of simple torsional and translational systems for the sake of simplicity; but the theory may be extended to any type of system and any set of generalised co-ordinates. A particular instance arises if principal co-ordinates are used. The paper is a sequel to an earlier paper[2].

1. Introduction

Receptance* functions have been used by several writers[3, 4, 2]. They have been shown to lead to great simplification of vibration analysis when complicated systems are concerned. The purpose of this paper is to explain the special, degenerate analytical forms that receptance functions may take and to show how their existence is manifested in receptance diagrams. The technical importance of this is explained in Section 3.

It is possible to develop the theory, which is given here, in terms of any set of generalised co-ordinates; a case of special interest arises if principal co-ordinates are used. In fact, this has been done by the authors in a book which will appear in due course. This plan is not followed here, partly for the sake of simplicity and partly because the main features of the theory can be given with reference to simple torsional oscillations of conservative systems with finite freedom. For this purpose, results can conveniently be taken from Bishop's paper[2] of which the present paper can be regarded as a sequel.

NOTATION

$A, B, C \ldots$	vibrating systems
${}_kA_{rs}$	constant defined in equation (6)
F_s	amplitude of torque applied to s^{th} disc
$f(\omega^2), F(\omega^2)$, etc.	polynomial functions of ω^2 defined as required
I	polar moment of inertia

*The word "receptance" is used instead of "mechanical admittance" in accordance with a suggestion which has been published; *e.g. see Journal of the Royal Aeronautical Society*, April 1954.

Received June 1954.

k	spring stiffness (*see* Figs. 4 and 5)
M	mass of particle (*see* Figs. 4 and 5)
p_r	r^{th} principal co-ordinate
t	time
x_s	displacement of s^{th} disc (also *see* Fig. 4)
$\alpha, \beta, \gamma, \ldots$	receptances of $A, B, C \ldots$.
Δ	polynomial in ω^2 defined by equation (3)
λ	spring stiffness (*see* Figs. 4 and 5)
ω	excitation frequency

2. The Series Form of Receptances

If rigid discs are attached to a light elastic shaft so as to form a simple torsional system which is free from damping, that system may be thrown into oscillation by a harmonic torque $F_s \sin \omega t$ which is applied to the s^{th} disc. If attention is confined to the steady harmonic oscillation having the applied frequency ω, then the motion of the r^{th} disc is found to be proportional to $F_s \sin \omega t$ and may therefore be expressed by the equation

$$x_r = \alpha_{rs} F_s \sin \omega t \quad . \quad . \quad . \quad . \quad . \quad (1)$$

where α_{rs} is a constant called the "cross-receptance" between x_r and x_s. Its value is found to depend upon the constants of the system concerned and upon ω. If the motion is measured at the same disc as that to which the torque is applied (the r^{th} disc, say) then

$$x_r = \alpha_{rr} F_r \sin \omega t \quad . \quad . \quad . \quad . \quad . \quad (2)$$

where α_{rr} is now the "direct-receptance" at x_r.

Table I of Ref. 2 contains the receptance functions of several simple torsional systems. It is seen that all are of the form

$$\alpha_{rs} = \frac{f(\omega^2)}{\Delta} \quad . \quad . \quad . \quad . \quad . \quad . \quad (3)$$

where $f(\omega^2)$ and Δ are polynomials in ω^2. It is also seen that all the receptances of any given system have the same denominator Δ. The frequency equation of the system is given by

$$\Delta = 0 \quad . \quad . \quad . \quad . \quad . \quad . \quad (4)$$

and it will be supposed to have roots $\omega^2 = \omega_1^2, \omega_2^2, \ldots \omega_n^2$; there are as many of these as there are degrees of freedom—that is, there are n of them—and they are all real and positive. It follows that equation (3) may be written

$$\alpha_{rs} = \frac{f(\omega^2)}{(\omega_1^2 - \omega^2)(\omega_2^2 - \omega^2) \ldots (\omega_n^2 - \omega^2)} \cdot \quad . \quad . \quad . \quad (5)$$

Finally, it is found that, as any receptance of a system can be written in this form, it can be expanded into a series of partial fractions such that

$$\alpha_{rs} = \frac{{}_1A_{rs}}{\omega_1^2 - \omega^2} + \frac{{}_2A_{rs}}{\omega_2^2 - \omega^2} + \ldots + \frac{{}_nA_{rs}}{\omega_n^2 - \omega^2} \quad . \quad . \quad . \quad (6)$$

where the numerators are all constants. The quantities $\omega_1, \omega_2, \ldots \omega_n$ are the natural frequencies of the system in order of ascending magnitudes.

These observations can, of course, be generalised. This can be done by means of Lagrangean theory (*see* Ref. 4) but, for the purposes of this paper, the results can conveniently be quoted.

Suppose that a system of n discs mounted on a light elastic shaft is brought into steady harmonic oscillation by a harmonic torque $F_s \sin \omega t$ applied at the s^{th} disc. The angular motions $x_1, x_2, \ldots x_n$ of the discs are given by

$$\left.\begin{aligned} x_1 &= \alpha_{1s} F_s \sin \omega t \\ x_2 &= \alpha_{2s} F_s \sin \omega t \\ &\ldots\ldots\ldots\ldots \\ x_n &= \alpha_{ns} F_s \sin \omega t \end{aligned}\right\} \quad . \quad . \quad . \quad . \quad . \quad (7)$$

By the series form of the receptances, therefore

$$\left.\begin{aligned} x_1 &= \left[\frac{{}_1A_{1s}}{\omega_1^2 - \omega^2} + \frac{{}_2A_{1s}}{\omega_2^2 - \omega^2} + \ldots + \frac{{}_nA_{1s}}{\omega_n^2 - \omega^2}\right] F_s \sin \omega t \\ x_2 &= \left[\frac{{}_1A_{2s}}{\omega_1^2 - \omega^2} + \frac{{}_2A_{2s}}{\omega_2^2 - \omega^2} + \ldots + \frac{{}_nA_{2s}}{\omega_n^2 - \omega^2}\right] F_s \sin \omega t \\ &\ldots\ldots\ldots\ldots\ldots\ldots\ldots\ldots\ldots\ldots\ldots\ldots\ldots\ldots\ldots\ldots \\ x_n &= \left[\frac{{}_1A_{ns}}{\omega_1^2 - \omega^2} + \frac{{}_2A_{ns}}{\omega_2^2 - \omega^2} + \ldots + \frac{{}_nA_{ns}}{\omega_n^2 - \omega^2}\right] F_s \sin \omega t \end{aligned}\right\} \quad . \quad . \quad (8)$$

If, now, ω approaches the k^{th} natural frequency ω_k, the k^{th} column of fractions will account for more and more of the motion and, in order that the motion shall remain finite, the amplitude F_s of the applied torque must be diminished. By this limiting process, a state of free oscillation with frequency ω_k is approached such that

$$x_1 : x_2 : \ldots : x_n :: {}_kA_{1s} : {}_kA_{2s} : \ldots {}_kA_{ns}. \quad . \quad . \quad . \quad (9)$$

That is to say the *relative* magnitudes of ${}_kA_{1s}, {}_kA_{2s}, \ldots {}_kA_{ns}$ define the shape of the k^{th} principal mode. It may be mentioned that the same modal shape is reached no matter which disc is acted on by the harmonic applied torque. That is, the subscript s of equation (9) plays no part in defining the modal shape.

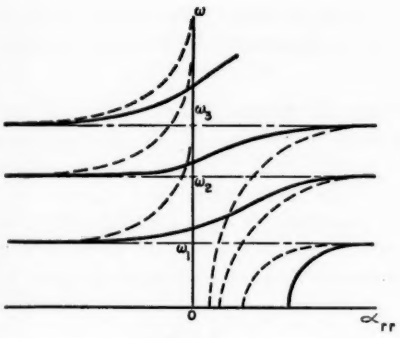

Fig. 1.

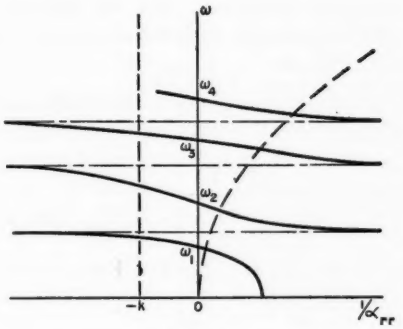

Fig. 2.

3. Receptance Diagrams

It is convenient to discuss two types of graphical representation of direct receptances. The first is a plot of α_{rr} against ω and the second is a plot of $1/\alpha_{rr}$ against ω.

A typical curve of the first kind is shown in Fig. 1 in which ω is plotted vertically. The full-line branches of this curve are found by adding the dotted curves in accordance with equation (6) when the equation is that of a *direct* receptance α_{rr}; each dotted curve represents one of the partial fractions and thus has the form of the resonance curve of a simple oscillator. Fig. 1 illustrates the fact that the constants ${}_1A_{rr}, {}_2A_{rr}, \ldots {}_nA_{rr}$ all have the same sign. The reason for this is that, were it not so, loops would appear in the diagram which would mean that one or more branches was multi-valued in α_{rr} or ω; this cannot be so for a reason which will be explained later.

The second important type of receptance diagram is that of $1/\alpha_{rr}$ against ω, and a typical curve is shown in Fig. 2. This curve is found by plotting horizontally the reciprocals of the abscissae of the curve of Fig. 1. The natural frequencies of the system are given by the n intersections of the branches of this curve with the ω-axis, where α_{rr} is infinite. On the other hand, the $n-1$ intermediate frequencies at which there are horizontal asymptotes are "anti-resonance frequencies"; at these values of ω, $\alpha_{rr}=0$, so that a harmonic torque applied to the r^{th} disc (with one of these frequencies) will produce no motion of that disc.

This second type of diagram has been used extensively (*e.g. see* Refs. 1, 4 and 2). It has also found application in certain numerical techniques. The reason for the importance of diagrams of $1/\alpha_{rr}$ is that they are helpful in the discussion of complex systems. Thus, if a system A can be considered as made up of two sub-systems B and C which are linked at a single co-ordinate x_r (say), then

$$\frac{1}{\alpha_{rr}} = \frac{1}{\beta_{rr}} + \frac{1}{\gamma_{rr}} \quad . \quad . \quad . \quad . \quad . \quad (10)$$

where the receptances of A are denoted by α, those of B by β and those of C by γ. Therefore, the abscissae of the $1/\beta_{rr}$ and $1/\gamma_{rr}$ diagrams may be added to give the $1/\alpha_{rr}$ diagram*.

Of particular interest are those cases where B is some given system and C is a particle, an anchored spring or a simple oscillator. For instance, by contemplating the effects of making such modifications as these to any vibrating system B, it is easily found that the branches of Fig. 2 cannot be multi-valued in $1/\alpha_{rr}$ or ω (β_{rr} being identified with α_{rr} in this case); this is therefore true also of the branches of Fig. 1. Again, if the free end of an anchored massless spring of stiffness k is attached to B at x_r, $\gamma_{rr}=1/k$ and the frequencies of the modified system are given by the equation

$$\frac{1}{\beta_{rr}} = -k. \quad . \quad . \quad . \quad . \quad . \quad . \quad (11)$$

The full lines in Fig. 2 now represent branches of the $(1/\beta_{rr}, \omega)$ curve and the curve for $1/\gamma_{rr}$ is the vertical dotted line. It is seen that all the natural frequencies of the original system are raised by the presence of the spring. The addition of this spring will be referred to as the "addition of stiffness" at the co-ordinate concerned.

The shapes of the receptance curves for a given system are determined by the constants of the system and may vary within the limits mentioned. Now it is often useful to know the shapes of these curves as may be seen from the following simple example. Suppose that the full-line curve of Fig. 2 represents $1/\beta_{rr}$, the reciprocal of the direct receptance at the r^{th} disc of a torsional system B, and it is required to estimate the effect upon the natural frequencies of B of increasing the polar moment of inertia of the r^{th} disc, by an amount I. This increase of inertia can be regarded as a system C such that

$$\gamma_{rr} = -\frac{1}{I\omega^2} \quad \text{or} \quad \frac{1}{\gamma_{rr}} = -I\omega^2. \quad . \quad . \quad . \quad . \quad (12)$$

According to equation (10), the natural frequencies of the modified system are given by

$$\frac{1}{\beta_{rr}} = I\omega^2 \quad . \quad . \quad . \quad . \quad . \quad . \quad (13)$$

That is, the intersections of the full-line curves and the dotted parabola in Fig. 2 determine the new natural frequencies. Now, if a particular full-line branch is sensibly flat for positive values of $1/\beta_{rr}$ and only curves upwards to the left of the axis†, then the natural frequency appropriate to the intersection of that branch with the vertical axis is not altered materially by the attachment of the extra inertia (that is, by system C).

*This feature is dealt with at length in Ref. 2.

†This is the case with the upper branches of Fig. 11 of Ref. 2.

It is natural to enquire to what extreme shapes practical receptance curves can tend. The rest of this paper is devoted to a discussion of these special forms of the curves and to the implications of the underlying theory.

The diagrams mentioned are concerned only with direct receptances. It is sometimes profitable to use diagrams of α_{rs} and $1/\alpha_{rs}$ plotted against ω; but they will not be required here.

4. The Horizontal Line in Receptance Diagrams

A node will be said to exist at a particular disc (the r^{th}, say) of a torsional system when that disc does not move during motion in a particular principal mode (the k^{th}, say)*. In discussing this nodal condition, it is convenient to approach the state by a form of limiting process.

Suppose that a torsional system is undergoing forced oscillation in all its principal modes according to equation (8), and the system is such that x_r does vary during motion in the k^{th} mode. To discuss the condition when there is a node at x_r (in this mode), a series of systems will be contemplated such that each differs slightly from its predecessor and such that the physical constants become so adjusted that the required nodal form is approached. This (ultimate) system is the one whose receptance functions will be examined. If exciting torques are applied at the co-ordinates $x_1, x_2, \ldots x_n$ in turn and, in each case the response at x_r is to become smaller in the k^{th} mode, it follows that the limiting process consists of letting ${}_kA_{r1}$, ${}_kA_{r2}, \ldots {}_kA_{rn}$ all tend to zero (*see* equation (8))†.

Equation (6) may be written in the form

$$\alpha_{rs} = \frac{{}_kA_{rs}}{\omega_k^2 - \omega^2} + \frac{F(\omega^2)}{g(\omega^2)}$$

$$= \frac{{}_kA_{rs}\, g(\omega^2) + (\omega_k^2 - \omega^2) F(\omega^2)}{(\omega_k^2 - \omega^2) g(\omega^2)} \quad . \quad . \quad . \quad . \quad . \quad (14)$$

where $F(\omega^2)$ and $g(\omega^2)$ are functions of ω^2. On applying the limiting process to obtain a node at x_r, so that ${}_kA_{rs}$ tends to zero, it is seen that

$$\alpha_{rs} \longrightarrow \frac{(\omega_k^2 - \omega^2)}{(\omega_k^2 - \omega^2)} \frac{F(\omega^2)}{g(\omega^2)}. \quad . \quad . \quad . \quad . \quad . \quad (15)$$

It follows, then, that all the functions $f(\omega^2)$ of equation (3) contain, as a factor, the k^{th} factor of Δ. These common factors do not affect the general shape of the receptance diagrams except where $\omega = \omega_k$. For this special value their ratio becomes indeterminate, as may be seen from equation (14), requiring a horizontal straight line to be drawn in all α_{rs} and $1/\alpha_{rs}$ diagrams at the ordinate ω_k.

*This conforms with the usual usage of the word "node." Mathematically, this means that $\partial x_r / \partial p_k = 0$, where p_k is the k^{th} principal co-ordinate. The reader will perceive that this leads to an extension of the usual meaning of "node" if x_r is the r^{th} *generalised* co-ordinate.

†The shape of the k^{th} principal mode of the limiting system is determined by the ratios between these constants that are approached as they all become small.

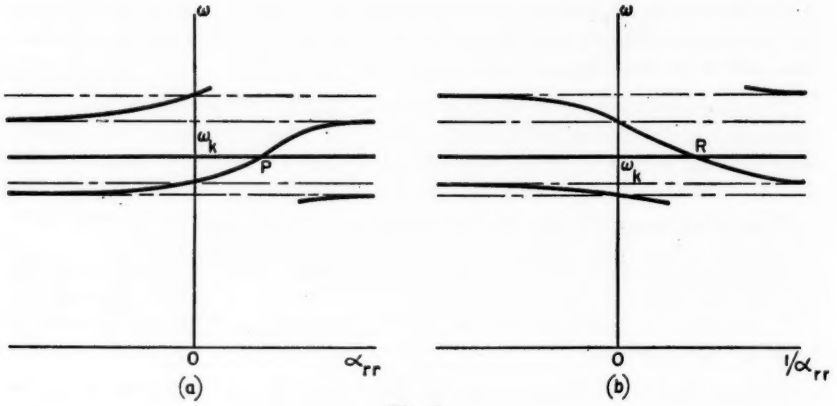

Fig. 3.

This result may be arrived at graphically. Taking the case of the direct receptance α_{rr}, the effect of the limiting process may be traced in Fig. 1. The k^{th} (dotted) resonance curve becomes very narrow at all points except those in the immediate neighbourhood of ω_k, since the numerator of the k^{th} partial fraction in the equation (6) for α_{rr} becomes very small. In the limit, the curve is replaced by a straight horizontal line as shown in Fig. 3(*a*). The counterpart of this on the $1/\alpha_{rr}$ diagram is shown in Fig. 3(*b*).

The presence of the horizontal line in Fig. 3(*b*) means that the natural frequency of the k^{th} principal mode will not be altered if any sub-system is attached at the co-ordinate x_r.

Figure 4 shows a conveniently simple system which may be used to illustrate the result given in equation (15). If any of the receptances at x_2 are set up by the usual methods (*e.g. see* Ref. 3) it is found that the numerator has a factor in common with the denominator; this should be expected, since there is obviously a principal mode of oscillation in which the central mass remains stationary. It is found that

$$\alpha_{12}=\alpha_{23}=\frac{-k(k+2\lambda-2M\omega^2)}{M\omega^2(k+2\lambda-2M\omega^2)(5k-2M\omega^2)} \quad . \quad . \quad . \quad (16)$$

$$\alpha_{22}=\frac{-(k-2M\omega^2)(k+2\lambda-2M\omega^2)}{M\omega^2(k+2\lambda-2M\omega^2)(5k-2M\omega^2)} \quad . \quad . \quad . \quad (17)$$

The height, ω_k, of the straight line in Fig. 3(*b*) depends upon the system concerned. The line may occupy any position relative to the remaining branches and the rest of this paper deals with the two special cases that may exist. These are (I) where ω_k coincides with an anti-resonance frequency of the remaining branches and so lies on an asymptote and (II) where ω_k is a resonance frequency of the remaining branches so that the line intersects another branch at the ω-axis.

5. Case I: ω_k an Anti-Resonance Frequency of the Remaining Branches

If the point P in Fig. 3(a) lies on the vertical axis, no motion occurs at x_r due to all the principal modes combined when the system is excited at x_r with the frequency ω_k. This may be given an analytical interpretation as will now be shown.

The series (6) for α_{rr} may now be written in the form

$$\alpha_{rr} = \frac{{}_kA_{rr}}{(\omega_k^2 - \omega^2)} + \frac{h(\omega^2)(\omega_k^2 - \omega^2)}{g(\omega^2)} \quad \text{(say)} \quad . \quad . \quad (18)$$

since it is required that the contributions of *all* the modes to the motion x_r shall vanish as $\omega \longrightarrow \omega_k$. It follows that

$$\alpha_{rr} = \frac{{}_kA_{rr}\, g(\omega^2) + h(\omega^2)(\omega_k^2 - \omega^2)^2}{\Delta} \quad . \quad . \quad . \quad . \quad (19)$$

and, if the limiting process is now used to obtain a node at x_r in the k^{th} principal mode (*i.e.* if ${}_kA_{rr} \longrightarrow 0$), then

$$\alpha_{rr} \longrightarrow \frac{(\omega_k^2 - \omega^2)}{(\omega_k^2 - \omega^2)} \cdot \frac{(\omega_k^2 - \omega^2)\, h(\omega^2)}{g(\omega^2)} \quad . \quad . \quad . \quad . \quad (20)$$

That is, in the expression (3) for α_{rr}, not only does $f(\omega^2)$ contain a factor that appears in Δ, but now that factor is repeated.

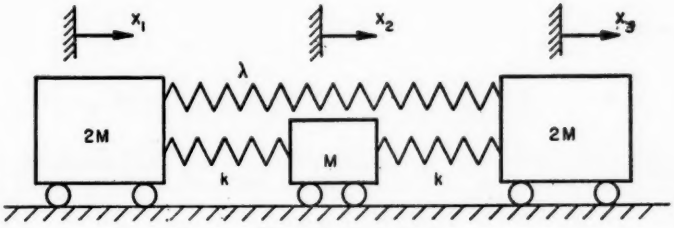

Fig. 4.

The system of Fig. 4 can be made to illustrate this result in an elementary way. By setting $\lambda = 0$, it is seen that (*i*) the cross-receptances of equation (16) retain the form of equation (15) whereas (*ii*) the direct receptance assumes the form of equation (20).

The type of receptance function which is given by equation (20) can arise in a particular way. Suppose that a system may be divided into two sub-systems B and C such that x_r is the only linking co-ordinate. It has been shown that the reciprocal receptance at x_r for a system of this kind can be formed by adding those for each sub-system separately in accordance with equation (10). If this addition is performed

in a diagram like Fig. 2 when the two reciprocal receptances $1/\beta_{rr}$ and $1/\gamma_{rr}$ become infinite at nearly the same frequency, a branch is found which is nearly flat; as equality of these anti-resonance frequencies is approached, the horizontal line emerges at the ordinate ω_k. The composite system A will be capable of performing free oscillations with frequency ω_k, the relative amplitudes of B and C determining the modal shape, since the forces at x_r due to the two sub-systems must balance. It is also evident that if ω_k is an anti-resonance frequency at x_r for B and C, no motion will be caused at x_r by a harmonic force or torque $F_r \sin \omega t$ with this frequency. Since there is no motion in the k^{th} mode due to the existence of the node, it may be asserted that the contribution of the remaining principal modes collectively is also zero.

6. Case II: ω_k a Resonance Frequency of the Remaining Branches

The case will now be examined where the intersection R of Fig. 3(b) lies on the vertical axis. This evidently implies that the natural frequency ω_k (corresponding to the k^{th} principal mode in which a node exists at x_r) coincides with an adjacent natural frequency ω_l. That is, Δ now has two equal roots.

The direct receptance at x_r may be written

$$\alpha_{rr} = \frac{{}_1A_{rr}}{\omega_1^2-\omega^2} + \ldots + \frac{{}_kA_{rr}}{\omega_k^2-\omega^2} + \frac{{}_lA_{rr}}{\omega_l^2-\omega^2} + \ldots + \frac{{}_nA_{rr}}{\omega_n^2-\omega^2}$$

$$= \frac{(\omega_k^2-\omega^2)(\omega_l^2-\omega^2)f_1(\omega^2) + [{}_kA_{rr}(\omega_l^2-\omega^2) + {}_lA_{rr}(\omega_k^2-\omega^2)]f_2(\omega^2)}{\Delta}.$$

If now $\omega_l \longrightarrow \omega_k$,

$$\alpha_{rr} \longrightarrow \frac{(\omega_k^2-\omega^2)}{(\omega_k^2-\omega^2)}\left[\frac{f_3(\omega^2)}{(\omega_1^2-\omega^2)\ldots(\omega_k^2-\omega^2)\ldots(\omega_n^2-\omega^2)}\right]. \quad (21)$$

The line appears in this expression together with the contents of the square brackets. The latter have the form of a direct receptance *without* a repeated factor and give rise to $n-1$ principal modes in the usual way.

It is significant that, in the derivation of equation (21), use was not made of the limiting process ${}_kA_{rs} \longrightarrow 0$ by means of which equation (15) was arrived at. The line which has been associated with a node has been arrived at apparently without the requirement that a node shall exist. Another new feature is that (21) is valid for all the co-ordinates; *i.e.* there is nothing in the derivation which refers to a *particular* co-ordinate x_r. The line appears in all the diagrams of reciprocal receptance and is always at the height of an intersection of the remaining branches with the ω-axis. It is also seen that there is nothing which limits this argument to direct receptances; it is equally true for cross-receptances.

These features can be illustrated by reference, once again, to the system of Fig. 4. If $\lambda = 2k$, the denominator of equations (16) and (17) is given the repeated

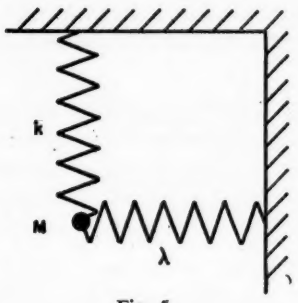

Fig. 5.

root $(5k-2M\omega^2)$ and, when the receptance functions are found by the method of Ref. 3, the following results are reached:—

$$\left.\begin{aligned}
\alpha_{11}=\alpha_{33}&=\frac{(5k-2M\omega^2)}{(5k-2M\omega^2)}\left[\frac{-1/5}{M\omega^2}+\frac{3/5}{5k-2M\omega^2}\right]\\
\alpha_{12}=\alpha_{23}&=\frac{(5k-2M\omega^2)}{(5k-2M\omega^2)}\left[\frac{-1/5}{M\omega^2}+\frac{-2/5}{5k-2M\omega^2}\right]\\
\alpha_{13}=\alpha_{31}&=\frac{(5k-2M\omega^2)}{(5k-2M\omega^2)}\left[\frac{-1/5}{M\omega^2}+\frac{-2/5}{5k-2M\omega^2}\right]
\end{aligned}\right\} \quad . \quad . \quad (22)$$

whereas

$$\left.\begin{aligned}
\alpha_{21}&=\frac{(5k-2M\omega^2)}{(5k-2M\omega^2)}\left[\frac{-1/5}{M\omega^2}+\frac{-2/5}{5k-2M\omega^2}\right]\\
\alpha_{22}&=\frac{(5k-2M\omega^2)}{(5k-2M\omega^2)}\left[\frac{-1/5}{M\omega^2}+\frac{8/5}{5k-2M\omega^2}\right]\\
\alpha_{23}&=\frac{(5k-2M\omega^2)}{(5k-2M\omega^2)}\left[\frac{-1/5}{M\omega^2}+\frac{-2/5}{5k-2M\omega^2}\right]
\end{aligned}\right\} \quad . \quad . \quad . \quad (23)$$

If attention is now confined to the partial fractions within the square brackets of equations (22) and (23) and principal modes are sought as in the derivation of equation (9), then those modes have the forms

$$\left.\begin{aligned}
x_1 : x_2 : x_3 &:: \quad 3 : -2 : -2 \quad \text{by equation (22)}\\
x_1 : x_2 : x_3 &:: -1 : \quad 4 : -1 \quad \text{by equation (23)}
\end{aligned}\right\} \quad . \quad . \quad . \quad (24)$$

Thus, the principal modes of the system of Fig. 4 (with $\lambda=2k$) are no longer unique.

In seeking an explanation of these new properties it is necessary to note the effect upon the principal modes of a repeated factor of Δ. If two principal modes have the same frequency, they lose their identities and one of them may be defined arbitrarily to be such as to provide a node at any selected co-ordinate. This follows because the system can then vibrate freely in any form which is a linear combination

of the two modes. Any such form can, alternatively, be taken as a principal mode and, in particular, one such form may be chosen which has a node at some specified co-ordinate.

This may be illustrated simply by means of the system shown in Fig. 5, in which a particle performs small vibrations in the plane of the light springs. So long as the spring stiffnesses k and λ differ, the system has natural frequencies given by

$$\omega_1^2 = \frac{k}{M}; \qquad \omega_2^2 = \frac{\lambda}{M} \quad . \quad . \quad . \quad . \quad . \quad (25)$$

(for conformity with the notation, this implies that $k < \lambda$). Each principal mode is obviously to be identified with motion parallel to the axis of one of the springs. However, if k is equal to λ, the two natural frequencies are equal and the modes may be selected arbitrarily. Thus, they may be taken as distortions by which the particle moves along the lines at 45° to the axes of the springs; indeed, they can even be taken as motions by which the body describes circles in each direction about its mean position.

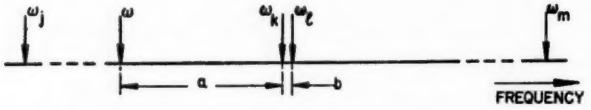

Fig. 6.

This lack of uniqueness of the principal modes may be shown to exist by an analytical approach. It has been seen that counterparts of equation (21) may readily be found for all the α_{rs} and it was demonstrated in equation (24) that, after the extraction of the factors $(\omega_k^2 - \omega^2)$ from the top and bottom of this expression, $n-1$ principal modes may be found in the manner of equation (9). But it was found that the one having the frequency ω_k is no longer unique since the ratios (9) now depend upon s. Let it be supposed that ω_k and ω_l are close, but distinct, roots of equation (4). If the excitation frequency is much closer to ω_k than to any other natural frequency (apart from ω_l) as shown in Fig. 6, the receptances take the form

$$\alpha_{rs} \doteq \frac{{}_kA_{rs}}{\omega_k^2 - \omega^2} + \frac{{}_lA_{rs}}{\omega_l^2 - \omega^2} \quad (r = 1, 2, \ldots n). \quad . \quad . \quad (26)$$

A limiting process is now contemplated in which the ratio $a/b = C$ is preserved (where $a = \omega_k - \omega$, $b = \omega_l - \omega_k$ and C is some large fixed number) as $a \longrightarrow 0$. Evidently the modal shape

$$x_1 : x_2 : \ldots . : x_n :: ({}_kA_{1s} + {}_lA_{1s}) : ({}_kA_{2s} + {}_lA_{2s}) : \ldots . : ({}_kA_{ns} + {}_lA_{ns}) \quad . \quad (27)$$

is obtained in this way. This has been found from a harmonic excitation applied at x_s which must become vanishingly small as $a \longrightarrow 0$ in order to retain a finite motion.

Had this excitation been applied at some other co-ordinate x_t in this process a different shape would have been found because, in general,

$$\frac{{}_kA_{us}+{}_lA_{us}}{{}_kA_{vs}+{}_lA_{vs}} \neq \frac{{}_kA_{ut}+{}_lA_{ut}}{{}_kA_{vt}+{}_lA_{vt}}. \quad . \quad . \quad . \quad (28)$$

Thus the modal shape depends upon the choice of the point of excitation x_s. As has already been shown, this lack of uniqueness is to be expected on physical grounds.

It has been shown that, if a node is connected to a fixed point through a spring, that is to say if stiffness is added at this co-ordinate, the frequency of the appropriate principal mode is left unaltered. Suppose that a system has a repeated factor $(\omega_k^2-\omega^2)$ of Δ. The effect of adding stiffness at such a point is to render determinate the principal modes that were previously indeterminate; the one has a node at the point of attachment and has frequency ω_k, while the other has a higher frequency. As shown in Fig. 2, the effect of the spring is to shift the vertical axis of the $(1/\alpha_{rr}, \omega)$ diagrams to the left, so that, here, the point R (Fig. 3(*b*)) is shifted thereby from the ω-axis to a position such as is shown in Fig. 3(*b*). In this way the type of system is reduced to a less specialised form*. It is seen that, of the pair of frequencies which were originally equal, that one which is raised does not reach the adjacent anti-resonance frequency of the original system unless the anchoring spring is infinitely stiff.

The converse of this process arises if one attempts to convert a non-specialised system to one having repeated factors of Δ. Suppose that one point only of the system is accessible and that this point is not a node for any principal mode. Then the diagram of the reciprocal of the direct receptance at this co-ordinate will not contain a horizontal line and the addition of mass or stiffness at this accessible point cannot create one (*see* Fig. 2). It may be deduced then, that the system cannot be modified in these ways so as to give its frequency equation repeated roots. On the other hand, if the accessible point is a node in one of the principal modes, it has been seen that the attachment of a spring at this point simply shifts the diagram of reciprocal receptance bodily to the right, so that an equal frequency system can be obtained in this way if the intersection R (Fig. 3) is to the left of the axis of ω. If R is to the right of the axis, it may be brought into coincidence with it by the addition of mass at the accessible point; this second process distorts the receptance diagram as well as moving it.

If two points are accessible, x_1 and x_2 say, then it may be possible to make x_2 a node by adding mass or stiffness at x_1. After this, the system can be given equal frequencies by a modification at x_2 as before. Alternatively, a rigid, massless linkage may be made to join x_1 and x_2 such that some point within it is a node in one principal mode; now, by the previous argument, the equal-frequency system may be arrived at by a suitable modification at this point.

*This may be illustrated by taking $\lambda=2k$ in the system of Fig. 4 (so that Δ has a repeated root) and then anchoring one of the end masses through a spring.

7. Conclusions

The relation $\alpha_{rs}=f(\omega^2)/\Delta$ gives rise to certain special cases. These obtain when the numerator and denominator have a common factor, and it has been shown that they imply the existence of a node at one of the co-ordinates. The node is associated with a horizontal line in receptance diagrams. The consequences of repetition of this common factor, either in $f(\omega^2)$ or in Δ, have been examined.

It has been assumed that, when a factor is repeated, it does not appear more than twice. This is not an essential requirement and its removal introduces no new concepts; it leads to the possibility of superimposing horizontal lines in receptance diagrams. Again, two different common factors of $f(\omega^2)$ and Δ may be repeated and so on.

The methods of this paper can be applied to generalised co-ordinates and, in particular, principal co-ordinates. In the latter event a node is said to exist at the r^{th} principal co-ordinate p_r for all the remaining principal modes. This would imply that diagrams of the receptances at $p_1, p_2, \ldots p_n$ should each contain $n-1$ horizontal lines in addition to the single curve given by $\alpha=A/(\omega_k^2-\omega^2)$; the horizontal axis itself will be one of the straight lines if the system is not anchored.

References

1. Biot, M. A. Coupled Oscillations of Aircraft Engine-Propeller Systems. *Journal of the Aeronautical Sciences*, Vol. 7, pp. 376-382, July 1940.

2. Bishop, R. E. D. The Analysis and Synthesis of Vibrating Systems. *Journal of the Royal Aeronautical Society*, October 1954.

3. Duncan, W. J. Mechanical Admittances and their Applications to Oscillation Problems. R. & M. 2000, 1947.

4. Johnson, D. C. The Application of Admittance Methods to the Classical Theory of Small Oscillations. *Engineering*, Vol. 171, 4453, pp. 650-652, June 1951.

On the Unsteady Motion of a Slender Body through a Compressible Fluid

L. E. FRAENKEL

*(Department of Aeronautics, Imperial College)**

SUMMARY: Ward's slender-body theory is extended to examine the unsteady motion of a slender body through a fluid at rest. The cross-sectional area and shape of the body, its forward velocity and its lateral motion are all arbitrary functions of time, but are subject to the restrictions of small disturbances. The length of the body is fixed. An approximate velocity potential is obtained by the joint use of two integral transforms, and the accuracy of this potential is discussed in some detail. General expressions for the aerodynamic forces acting on the body are derived in terms of a co-ordinate system which moves forward with the body in the mean direction of motion, but is fixed laterally. These expressions are then transformed, for the particular case of an oscillating rigid body moving forward with variable velocity, to expressions in terms of co-ordinates referred to the body axes. (The former co-ordinate system makes possible a fairly compact general treatment, whereas the latter is more convenient if the solution of a particular rigid-body problem is required.) Finally, arguments are advanced to justify the application of the slender-body theory to wings of slender plan form whose trailing edges are perpendicular to the direction of motion, and results are given for an oscillating wing moving forward with variable velocity.

1. Introduction

Since Ward's slender-body theory[1] has already been extended to problems of unsteady flow by Miles[2] and Phythian[3], the appearance of a third paper on this subject requires some justification. Miles considered very general unsteady motions of a slender body, but confined his analysis to supersonic speeds. Phythian considered both subsonic and supersonic speeds, but dealt only with particular types of motion. Miles worked principally with "wind axes," whereas Phythian used "body axes"; the transformation from one to the other is not always simple.

In the present paper general motions at subsonic and supersonic speeds are considered and results referred to wind and body axes are correlated. The analysis is based on the joint use of two integral transforms and of the Stieltjes integral. This leads to what is believed to be a fresh discussion of the effect, on the accuracy of the slender-body solution, of discontinuities in the source and multi-source strengths and their derivatives. Correct general expressions for the drag are also derived for

Received June 1954.

*The work reported here was done while the author was in the Department of Aeronautics, University of Glasgow.

the first time: Miles's result for drag is restricted to motions in which the body surface is fixed laterally*, while Phythian's formulation of the momentum equation is incorrect for motions with rotary oscillations.

It is extremely difficult to introduce this new matter without sketching in a suitable background, and accordingly the complete theory of the unsteady motion of slender bodies is briefly derived *ab initio*.

NOTATION†

a_n, α_n	coefficients in expansion of slender-body potential
b_0, β_0	functions in slender-body potential
$b,\ b_a, b_b$	functions defining wing span (Section 8)
B, B_a, B_b	maximum values of b, b_a, b_b
c	velocity of sound
C, C_B	body contours in plane $s=$constant, $s=l$
$f = f_a + if_b$	
f_a, f_b	*see* equation (39)
F	*see* equation (53)
g, γ	functions defining body surface
$h = [\omega^2 + (p^2/c_0^2)]^{\frac{1}{2}}$	
$I(t)$	distance travelled (*see* equation (9))
$J(s,t)$	*see* equation (34)
k, κ	doublet strength
K_n	modified Bessel function of the second kind
l	body length
m	circumferential variable
n	normal outward from body in plane $s=$constant
$\mathbf{n}$	unit normal inward to volume of fluid
p	index of Laplace transform (Sections 3, 4, 8); static pressure (Section 5)
$\mathbf{q}$	fluid velocity
(r, θ, s)	cylindrical co-ordinates of frame moving longitudinally with body but fixed laterally

*Professor Miles has explained in a private communication to the author that he calculated the drag under this restriction, but forgot to state it when summarising his results in Ref. 2.

†Certain Greek symbols directly related to Latin ones, like $\alpha_n(\sigma, \tau) = a_n(s, t)$, are defined in the *first* part of this list.

$\mathscr{R}$	real part of
R	value of r on body surface
S	cross-sectional area of body
S_b	body surface
t	time
$U(t)$	velocity of body in negative σ-direction
$\mathbf{v}$	*see* after equation (47)
V	volume of fluid
V_m	*see* equation (59)
w	complex function such that $\mathscr{R}w=\phi$
(x, y, s)	Cartesian co-ordinates corresponding to (r, θ, s)
z	complex variable $re^{i\theta}$
α, β	body incidence in xs, ys-plane
ε	maximum value of R
ρ	density
σ	longitudinal co-ordinate from fixed origin, $s-l(t)$
τ	time
ϕ, φ	slender-body velocity potential
ϕ_a, ϕ_b, ϕ_I	errors of ϕ, *see* Appendix
Φ	exact velocity potential
ω	index of Fourier transform
$\boldsymbol{\Omega}$	angular velocity of rotating frame
$(\ )_0$	conditions at infinity
$(\ )_1$	quantities referred to body axes

2. Formulation of the Problem

Let (x, y, σ) be a right-handed system of Cartesian co-ordinates fixed in a fluid at rest at infinity, let (r, θ, σ) be the corresponding system of cylindrical polar co-ordinates, and let τ denote the time. A slender body, whose nose and base rest at $\sigma=0$ and $\sigma=l$, respectively, until time $\tau=0$, begins to move at this instant in the direction of the negative σ-axis with velocity $U(\tau)$, small lateral departures from the σ-axis being permitted.

Let ε denote the upper limit of r for points on the body; we specify that the length of the body be $O(1)$ and that the Mach number of the forward motion and all time rates of change be bounded (the forward and lateral velocities of the body may, however, be discontinuous): the case $\varepsilon \longrightarrow 0$ is then examined.

The words "cross section" and "body contour" are used to describe sections and the body boundary in planes normal to the longitudinal body axis, and "axial section" and "profile" are used to describe sections and the body boundary in planes through this axis. The body is subject to the restrictions specified by Ward, except that its cross-sectional area and shape may vary with time and that, initially, bodies are considered which fail to satisfy, in regions whose total length is at most $O(\varepsilon)$, the requirement of small profile slope and curvature: that is, the effects of rounded and open noses and tails and of discontinuities in profile slope are considered initially. Rounded noses and tails are assumed to be such that the cross-sectional area and its derivatives are everywhere $O(\varepsilon^2)$, (this requirement is satisfied, for example, by a slender ellipsoid).

Consider the irrotational flow of a perfect, inviscid fluid. Let $\Phi(x, y, \sigma, \tau)$ be the velocity potential, c the speed of sound at any point and time, c_0 the speed of sound in the undisturbed fluid, and let Γ be the ratio of the specific heats. The governing differential equation is

$$\left.\begin{aligned} \nabla^2\Phi &= \frac{1}{c^2}\left[\frac{\partial^2}{\partial\tau^2} + 2\nabla\Phi\,.\,\nabla\frac{\partial}{\partial\tau} + \nabla\Phi\,.\,(\nabla\Phi\,.\,\nabla)\nabla\right]\Phi, \\ \text{where} \qquad c^2 &= c_0{}^2 - \frac{\Gamma-1}{2}\left[2\frac{\partial\Phi}{\partial\tau} + (\nabla\Phi)^2\right]. \end{aligned}\right\} \quad . \quad . \quad (1)$$

If Φ and its derivatives are small, equation (1) may be linearised to give the wave equation

$$\nabla^2\Phi = \frac{1}{c_0{}^2}\frac{\partial^2\Phi}{\partial\tau^2}. \quad . \quad . \quad . \quad (2)$$

3. The Slender-Body Solution

We introduce Fourier and Laplace transforms:—

$$\bar{F}(x, y, \omega, \tau) = \int_{-\infty}^{\infty} e^{i\omega\sigma} F(x, y, \sigma, \tau)\, d\sigma, \quad . \quad . \quad (3)$$

which we also write $\bar{F}(x, y, \omega, \tau) \rightleftharpoons F(x, y, \sigma, \tau)$,

$$\text{and} \quad \bar{\bar{F}}(x, y, \omega, p) = \int_{0}^{\infty} p e^{-p\tau} \bar{F}(x, y, \omega, \tau)\, d\tau, \quad . \quad . \quad . \quad (4)$$

$$\text{or} \quad \bar{\bar{F}}(x, y, \omega, p) \rightleftharpoons F(x, y, \sigma, \tau).$$

To obtain the subsidiary equation of (2), we multiply it by the kernels of the integrals and integrate. If there are points $(x_s, y_s, \sigma_s, \tau_s)$ where the solution will prove singular and (2) itself is not satisfied, the subsidiary equation cannot be

justified on lines $x=x_s$, $y=y_s$; but if elsewhere (*i*) Φ and its first partial derivatives are continuous with respect to space and time, and (*ii*) Φ and its first and second partial derivatives $\longrightarrow 0$ as $\sigma \longrightarrow \infty$ in such a manner that integrals of the type (3) converge, it is found, upon integrating by parts, that the subsidiary equation is

$$\left.\begin{aligned} &\frac{\partial^2 \bar{\Phi}}{\partial x^2}+\frac{\partial^2 \bar{\Phi}}{\partial y^2}=h^2(\omega,p)\,\bar{\Phi}, \\ \text{where}\qquad &h^2(\omega,p)=\omega^2+p^2/c_0^2. \end{aligned}\right\} \quad . \quad . \quad . \quad . \quad . \quad (5)$$

If the first partial derivatives of Φ are discontinuous across spherical surfaces of the form

$$c_0^2(\tau-\tau_0)^2=(x-x_0)^2+(y-y_0)^2+(\sigma-\sigma_0)^2,$$

or across surfaces which consist of an envelope of such spheres, (Φ itself being continuous), $\bar{\Phi}$ still satisfies (5); for it may be shown by the method of Ref. 4 that the sum of the additional terms which each discontinuity contributes to the subsidiary equation is zero.

A general solution of (5), representing disturbances on the σ-axis, is

$$\bar{\Phi}(r,\theta,\omega,p)=\bar{A}_0(\omega,p)\,K_0(hr)+\sum_{n=1}^{\infty} K_n(hr)\,[\bar{A}_n(\omega,p)\cos n\theta+\bar{B}_n(\omega,p)\sin n\theta], \quad (6)$$

where the K_n are modified Bessel functions of the second kind[5], and the $\bar{A}_n$, $\bar{B}_n$ are arbitrary functions. It is assumed for the moment that ω and p may be treated as $O(1)$; then since r is $O(\varepsilon)$ on and near the body only the dominant term in the series expansion of each Bessel function is retained, the apparent error being a factor $1+O(\varepsilon^2)$. There results the approximate potential

$$\varphi(r,\theta,\sigma,\tau)=\mathscr{R}\{\alpha_0(\sigma,\tau)\log z+\beta_0(\sigma,\tau)+\sum_{n=1}^{\infty}\alpha_n(\sigma,\tau)\,z^{-n}\} \quad . \quad . \quad (7)$$

$$\left.\begin{aligned} \text{where}\qquad &z=re^{i\theta},\quad \bar{\alpha}_0=-\bar{A}_0,\quad \bar{\beta}_0=\bar{\alpha}_0(E+\log h/2), \\ &\bar{\alpha}_n=2^{n-1}(n-1)!\;h^{-n}(\bar{A}_n+i\bar{B}_n), \end{aligned}\right\} \quad . \quad . \quad (8)$$

and E is Euler's constant. Like Ward's solution for the steady supersonic case, this potential is harmonic in (r,θ); the coefficients α_n are determined by finding the harmonic function which satisfies the boundary condition and expanding it in series. The series converges outside a circular cylinder enclosing the body.

We now introduce variables s, t such that s is measured along the σ-axis from the plane of the nose of the body. We write

$$\int_0^{\tau} U(\tau')\,d\tau'=I(\tau)=I(t), \quad . \quad . \quad . \quad (9)$$

$$s=\sigma+I(\tau),\quad t=\tau, \quad . \quad . \quad . \quad . \quad . \quad (10)$$

and let $\partial/\partial t$ imply r, θ, s held constant, whereas $\partial/\partial\tau$ implies r, θ, σ held constant. Equation (7) may now be written

$$\phi(r,\theta,s,t)=\mathscr{R}\{a_0(s,t)\log z+b_0(s,t)+\sum_{n=1}^{\infty}a_n(s,t)\,z^{-n}\} \quad . \quad . \quad (11)$$

where $a_0(s,t)=\alpha_0(\sigma,\tau)$, etc.

4. The Evaluation of a_0 and b_0

If the surface of the body is defined by

$$\gamma(x,y,\sigma,\tau)=g(x,y,s,t)=0,$$

the boundary condition is $\nabla\gamma\,.\,\nabla\varphi=-\dfrac{\partial\gamma}{\partial\tau}$ on the body,

$$\text{or} \qquad \nabla g\,.\,\nabla\phi=-\left[U(t)\frac{\partial}{\partial s}+\frac{\partial}{\partial t}\right]g. \quad . \quad . \quad . \quad (12)$$

This boundary condition, together with our restrictions on the shape of the body and a knowledge of two-dimensional incompressible flows, ensures that $\partial\phi/\partial x$ and $\partial\phi/\partial y$ are $O(\varepsilon)$ everywhere except in the immediate neighbourhood of a rounded nose or tail, (where $\partial g/\partial s$ is larger than $O(\varepsilon)$). Hence the a_n are $O(\varepsilon^{n+2})$, except in these regions; ϕ, $\partial\phi/\partial s$, $\partial\phi/\partial t$, etc., are $O(\varepsilon^2\log\varepsilon)$; and $\partial^2\phi/\partial x^2$, $\partial^2\phi/\partial y^2$, etc., are $O(1)$. Accordingly, equation (12) becomes

$$\frac{\partial g}{\partial x}\frac{\partial\phi}{\partial x}+\frac{\partial g}{\partial y}\frac{\partial\phi}{\partial y}=-\left[U(t)\frac{\partial}{\partial s}+\frac{\partial}{\partial t}\right]g+O(\varepsilon^3\log\varepsilon),$$

$$\text{or} \qquad \frac{\partial\phi}{\partial n}=U(t)\frac{\partial n}{\partial s}+\frac{\partial n}{\partial t}+O(\varepsilon^3\log\varepsilon), \quad . \quad . \quad . \quad (13)$$

where n is the normal outward from the body contour in a plane $s=$constant, and, by a special notation,

$$\frac{\partial n}{\partial s}=-\frac{\partial g/\partial s}{\sqrt{\{(\partial g/\partial x)^2+(\partial g/\partial y)^2\}}}, \qquad \frac{\partial n}{\partial t}=-\frac{\partial g/\partial t}{\sqrt{\{(\partial g/\partial x)^2+(\partial g/\partial y)^2\}}} \quad . \quad (14)$$

($\partial n/\partial s$ and $\partial n/\partial t$ are defined as positive when the boundary moves outwards with increasing s or t).

By integrating $\partial\phi/\partial n$ around the body contour in a plane $s=$constant, using first (11) and then (13), we find that

$$a_0(s,t)=\frac{1}{2\pi}\left[U(t)\frac{\partial}{\partial s}+\frac{\partial}{\partial t}\right]S(s,t), \quad . \quad . \quad . \quad (15)$$

where $S(s,t)$ is the cross-sectional area of the body. In the regions $s<0$, $s>l$, or $t<0$, a_0 and all the a_n vanish.

$\bar{\beta}_0(\omega, p)$ is now inverted by recalling that

$$\bar{\beta}_0 + \bar{\alpha}_0 \log r = \bar{\alpha}_0 \left(E + \log \frac{hr}{2}\right) = \lim_{r \to 0+} - \bar{\alpha}_0 K_0(hr). \quad . \quad (16)$$

$K_0(hr)$ may readily be inverted by using the identity[5]

$$K_0(z) = \frac{1}{2} \int_0^\infty \exp\left(-u - \frac{z^2}{4u}\right) \frac{du}{u},$$

and inverting with respect to ω first. It is found that

$$K_0(hr) \rightleftharpoons \frac{1}{2} \frac{1}{\sqrt{(\sigma^2 + r^2)}} H[c_0 \tau - \sqrt{(\sigma^2 + r^2)}], \quad . \quad . \quad . \quad (17)$$

where H is the Heaviside unit function. This is the well-known acoustic source potential. The double Faltung integral appropriate to our integral transforms is

$$\bar{F}(\omega, p) \bar{G}(\omega, p) \rightleftharpoons \int_{-\infty}^{\infty} d\sigma' \int_{\tau'=0-}^{\tau} F(\sigma - \sigma', \tau - \tau')\, dG(\sigma', \tau'), \quad . \quad . \quad (18)$$

where the integral with respect to τ' is a Stieltjes integral; so that in the present case

$$-K_0(hr)\, \bar{\alpha}_0 \rightleftharpoons -\frac{1}{2} \int_{-\infty}^{\infty} d\sigma' \int_{\tau'=0-}^{\tau - \frac{1}{c_0}\sqrt{\{(\sigma-\sigma')^2 + r^2\}}} \frac{1}{\sqrt{\{(\sigma-\sigma')^2 + r^2\}}}\, d\alpha_0(\sigma', \tau')$$

$$= -\frac{1}{2} \int_{-\infty}^{\infty} \frac{\alpha_0\left(\sigma', \tau - \frac{1}{c_0}\sqrt{\{(\sigma-\sigma')^2 + r^2\}}\right)}{\sqrt{\{(\sigma-\sigma')^2 + r^2\}}}\, d\tau'. \quad . \quad (19)$$

By means of the rule for integration by parts based on the Stieltjes integral, this becomes

$$-K_0(hr)\, \bar{\alpha}_0 \rightleftharpoons \frac{1}{2} \int_{\sigma'=-\infty}^{\infty} \sinh^{-1} \frac{\sigma' - \sigma}{r}\, d\alpha_0\left(\sigma', \tau - \frac{1}{c_0}\sqrt{\{(\sigma-\sigma')^2 + r^2\}}\right), \quad . \quad (20)$$

where we now have a Stieltjes integral with respect to σ'. The relation $\alpha_0(A, B) = a_0(A + I(B), B)$ is used, and the variable of integration is changed from σ' to τ', where

$$c_0 \tau' = c_0 \tau - \sqrt{\{(\sigma-\sigma')^2 + r^2\}}, \quad \sigma' - \sigma = \mp \sqrt{\{c_0^2 (\tau - \tau')^2 - r^2\}}. \quad . \quad (21)$$

Hence

$$-K_0(hr)\,\bar{a}_0 \underset{\text{as}}{=} -\frac{1}{2}\int_{r'=-\infty}^{\tau-\frac{r}{c_0}} \sinh^{-1}\frac{\sqrt{\{c_0^2(\tau-\tau')^2-r^2\}}}{r}\,da\left(\sigma-\sqrt{\{c_0^2(\tau-\tau')^2-r^2\}}+I(\tau'),\tau'\right)+$$

$$+\frac{1}{2}\int_{r'=\tau-\frac{r}{c_0}}^{-\infty} \sinh^{-1}\frac{\sqrt{\{c_0^2(\tau-\tau')^2-r^2\}}}{r}\,da_0\left(+\sqrt{\{c_0^2(\tau-\tau')^2-r^2\}}+I(\tau'),\tau'\right)$$

$$=-\frac{1}{2}\int_{t'=0-}^{t-\frac{r}{c_0}} \cosh^{-1}\frac{c_0(t-t')}{r}\left[da_0\left(s-\sqrt{\{c_0^2(t-t')^2-r^2\}}-I(t)+I(t'),t'\right)+\right.$$

$$\left.+da_0\left(s+\sqrt{\{c_0^2(t-t')^2-r^2\}}-I(t)+I(t'),t'\right)\right]. \qquad (22)$$

Hence $\bar{\beta}_0+\bar{a}_0\log r=\lim_{r\to 0+}-K_0(hr)\,\bar{a}_0$

$$\underset{\text{as}}{=}-\frac{1}{2}\int_{t'=0-}^{t}\log\frac{2c_0(t-t')}{r}\left[da\left(s-c_0(t-t')-I(t)+I(t'),t'\right)+\right.$$

$$\left.+da_0\left(s+c_0(t-t')-I(t)+I(t'),t'\right)\right], \qquad (23)$$

$$\text{and } b_0(s,t)=-a_0(s,t)\log 2c_0-\frac{1}{2}\int_{t'=0-}^{t}\log(t-t')\left[da_0\left(s-c_0(t-t')-I(t)+I(t'),t'\right)+\right.$$

$$\left.+da_0\left(s+c_0(t-t')-I(t)+I(t'),t'\right)\right]. \qquad (24)$$

Some physical significance may be attached to the foregoing expressions by considering an (r,σ,τ)-space (Fig. 1). A disturbance at a point $(0,\sigma',\tau')$, which lies between the trajectories of the nose and tail of the body, affects only points (r,σ,τ) on its "aftercone," $c_0(\tau-\tau')=\sqrt{\{(\sigma-\sigma')^2+r^2\}}$. Conversely, in an (r',σ',τ')-space the flow at a point (r,σ,τ) is affected only by disturbances $(0,\sigma',\tau')$ lying on the hyperbola $c_0(\tau'-\tau)=-\sqrt{\{(\sigma'-\sigma)^2+r^2\}}$, which is formed by the intersection of the "forecone" of (r,s,t) with the plane $r'=0$. If all the aftercones of disturbances were drawn in Fig. 1, a section by a plane $\tau=$constant would indicate the disturbed field at that instant in a physical, $r\sigma$-plane. The slender-body approximation assumes $r\to 0+$, and replaces the cones by planes tangent to them and parallel to the r-axis.

If $U(t)=c_0$, the function $b_0(s,t)$ tends logarithmically to infinity as $t\to\infty$, that is, as the steady state is approached. The other terms in the slender-body solution remain bounded and $O(\varepsilon^2\log\varepsilon)$.

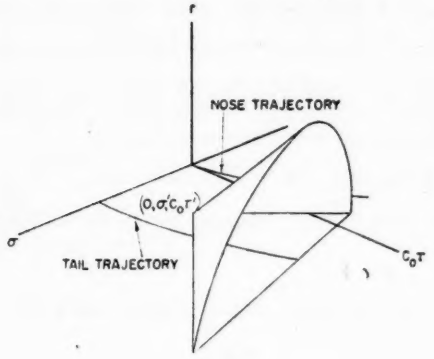

Fig. 1.

5. The Drag Force

The accuracy of the slender-body solution is discussed in the Appendix. As a result of the conclusions drawn there, the following restriction is now applied. The body must be such that the source and multi-source strengths $a_n(s,t)$ are continuous functions of s everywhere, except at the base of the body, $s=l$, in supersonic flow. Discontinuities with respect to time are permitted in the source and multi-source strengths, but it must be understood that the results do not provide an acceptable approximation at instants immediately following such discontinuities. Discontinuities are also permitted in the $\partial a_n/\partial s$; it is shown in the Appendix that these increase the errors of the integrated forces given in what follows by a factor of $O(\log \varepsilon)$ at most.

To calculate the aerodynamic forces, consider the flow of momentum through a surface consisting of the body surface S_b and a circular cylinder moving with velocity $U(t)$ along the x-axis in the negative direction (Fig. 2). The cylinder has a small radius; its curved surface is denoted by S_2, and its plane ends at $s=0$ and $s=l$ are denoted by S_1 and S_3 respectively. The contour of the body at the base is denoted by C_B. For such a surface S, containing a volume V, (the boundary varying with time), the momentum equation may be written

$$\int_{S(t)} (p-p_0)\,\mathbf{n}\,dS = \frac{d}{dt}\int_{V(t)} \rho\,\mathbf{q}\,dV - \int_{S(t)} \rho\,[(\mathbf{q}-\mathbf{w})\,.\,\mathbf{n}]\,\mathbf{q}\,dS, \quad . \quad . \quad (25)$$

where p is the local pressure, ρ the local density, $\mathbf{q}$ the local fluid velocity, $\mathbf{w}$ the velocity of any point on the control surface, and $\mathbf{n}$ is the unit normal drawn inwards to the volume of fluid. Hence, taking the s-component of (25), and ignoring the base drag, we obtain

$$-D + \int_{S_1-S_3} (p-p_0)\,dS = \frac{d}{dt}\int_{V(t)} \rho\,\frac{\partial\phi}{\partial s}\,dV - \int_{S_1-S_3} \rho\left[\frac{\partial\phi}{\partial s} + U(t)\right]\frac{\partial\phi}{\partial s}\,dS + \int_{S_2} \rho\,\frac{\partial\phi}{\partial r}\,\frac{\partial\phi}{\partial s}\,dS +$$

$$+ O(\varepsilon^6 \log^2 \varepsilon). \quad . \quad (26)$$

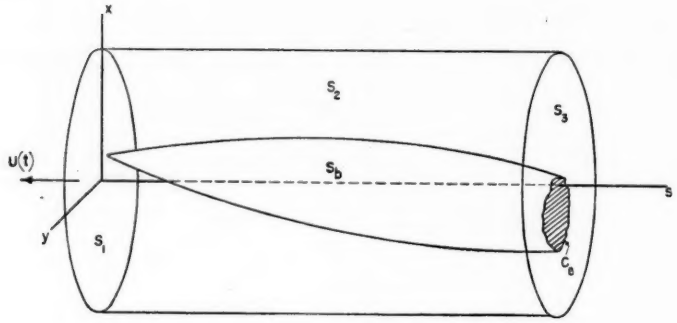

Fig. 2.

From the energy equation we have

$$\left.\begin{aligned} p-p_0 &= -\rho_0\left[U(t)\frac{\partial\phi}{\partial s}+\frac{\partial\phi}{\partial t}+\frac{1}{2}\left(\frac{\partial\phi}{\partial r}\right)^2+\frac{1}{2}\left(\frac{1}{r}\frac{\partial\phi}{\partial\theta}\right)^2\right]+O(\varepsilon^4\log^2\varepsilon),\\ \frac{\rho}{\rho_0} &= 1+O(\varepsilon^2\log\varepsilon). \end{aligned}\right\} \quad (27)$$

Hence, noting that $\partial\phi/\partial r=\partial\phi/r\partial\theta=0$ in S_1, we obtain

$$\frac{D}{\rho_0} = -\int_{S_1-S_3}\frac{\partial\phi}{\partial t}\,dS+\frac{1}{2}\int_{S_3}\left[\left(\frac{\partial\phi}{\partial r}\right)^2+\left(\frac{1}{r}\frac{\partial\phi}{\partial\theta}\right)^2\right]dS-\frac{d}{dt}\int_{V(t)}\frac{\partial\phi}{\partial s}\,dV-$$

$$-\int_{S_3}\frac{\partial\phi}{\partial r}\frac{\partial\phi}{\partial s}\,dS+O(\varepsilon^6\log^2\varepsilon). \quad . \quad (28)$$

Now
$$-\frac{d}{dt}\int_{V(t)}\frac{\partial\phi}{\partial s}\,dV = -\int_{V(t)}\frac{\partial^2\phi}{\partial s\partial t}\,dV+\int_{S_b}\frac{\partial\phi}{\partial s}\frac{\partial n}{\partial t}\,dS,$$

and by Gauss's theorem, writing **k** for the unit vector in the s-direction, we have

$$-\int_{V(t)}\frac{\partial^2\phi}{\partial s\partial t}\,dV=\mathbf{k}.\int_{S(t)}\frac{\partial\phi}{\partial t}\,\mathbf{n}\,dS=\int_{S_1-S_3}\frac{\partial\phi}{\partial t}\,dS-\int_{S_b}\frac{\partial\phi}{\partial t}\frac{\partial n}{\partial s}\,dS.$$

Hence
$$-\frac{d}{dt}\int_{V(t)}\frac{\partial\phi}{\partial s}\,dV=\int_{S_1-S_3}\frac{\partial\phi}{\partial t}\,dS+\int_{S_b}\left(\frac{\partial\phi}{\partial s}\frac{\partial n}{\partial t}-\frac{\partial\phi}{\partial t}\frac{\partial n}{\partial s}\right)dS. \quad . \quad (29)$$

The following result is taken from Ward's analysis (Ref. 1, equations (34) to (36))

$$\frac{1}{2}\int_{S_3}\left[\left(\frac{\partial\phi}{\partial r}\right)^2+\left(\frac{1}{r}\frac{\partial\phi}{\partial\theta}\right)^2\right]dS-\int_{S_2}\frac{\partial\phi}{\partial r}\frac{\partial\phi}{\partial s}\,dS=\pi\int_0^l\left(\frac{\partial a_0}{\partial s}b_0-a_0\frac{\partial b_0}{\partial s}\right)ds-\frac{1}{2}\oint_{C_B}\phi\frac{\partial\phi}{\partial n}\,dm, \quad . \quad . \quad . \quad . \quad (30)$$

where m denotes the circumferential variable. By (29) and (30), (28) now becomes

$$\frac{D}{\rho_0}=\pi\int_0^l\left(\frac{\partial a_0}{\partial s}b_0-a_0\frac{\partial b_0}{\partial s}\right)ds-\frac{1}{2}\oint_{C_B}\phi\frac{\partial\phi}{\partial n}\,dm+\int_{S_b}\left(\frac{\partial\phi}{\partial s}\frac{\partial n}{\partial t}-\frac{\partial\phi}{\partial t}\frac{\partial n}{\partial s}\right)dS+O(\varepsilon^6\log^2\varepsilon). \quad . \quad . \quad . \quad . \quad (31)$$

This result is valid for both subsonic and supersonic speeds, but the body is permitted to have a base only for supersonic speeds.

Finally an identity is derived which will prove useful later. By Gauss's theorem

$$-\frac{d}{dt}\int_{V(t)}\frac{\partial\phi}{\partial s}\,dV=\frac{d}{dt}\left[\int_{S_1-S_2}\phi\,dS-\int_{S_b}\phi\frac{\partial n}{\partial s}\,dS\right]$$

$$=\int_{S_1}\frac{\partial\phi}{\partial t}\,dS-\left[\int_{S_3}\frac{\partial\phi}{\partial t}\,dS-\oint_{C_B}\phi\frac{\partial n}{\partial t}\,dm\right]-\frac{d}{dt}\int_{S_b}\phi\frac{\partial n}{\partial s}\,dS. \quad (32)$$

Comparing (29) and (32) gives

$$\int_{S_b}\left(\frac{\partial\phi}{\partial s}\frac{\partial n}{\partial t}-\frac{\partial\phi}{\partial t}\frac{\partial n}{\partial s}\right)dS=-\frac{d}{dt}\int_{S_b}\phi\frac{\partial n}{\partial s}\,dS+\oint_{C_B}\phi\frac{\partial n}{\partial t}\,dm. \quad . \quad (33)$$

6. The Lateral Forces

The lateral forces may be calculated by following Ward's analysis and by dealing with the unsteady flow terms in a manner analogous to that of the previous section.

The function $$J(s,t)=-i\oint_C\phi\,dz \quad . \quad . \quad . \quad . \quad . \quad . \quad . \quad . \quad . \quad (34)$$

$$=2\pi a_1(s,t)+\left[U(t)\frac{\partial}{\partial s}+\frac{\partial}{\partial t}\right]\left[S(s,t)\,z_g(s,t)\right], \quad . \quad (35)$$

is introduced, where C denotes the body contour in a plane s=constant and z_g is the

complex co-ordinate of the centroid of area of the body cross section. The complex lateral force is then given by

$$\frac{X+iY}{\rho_0} = U(t)\,J(l,t) + \frac{d}{dt}\int_0^l J(s,t)\,ds + O(\varepsilon^5 \log^2 \varepsilon),$$

$$= \int_0^l \left[U(t)\frac{\partial}{\partial s} + \frac{\partial}{\partial t} \right] J(s,t)\,ds + O(\varepsilon^5 \log^2 \varepsilon). \quad . \quad . \quad (36)$$

The complex moment is (M_x and M_y denote the moments about the x- and y-axes in the positive sense for a right-handed system)

$$\frac{M_x+iM_y}{\rho_0} = i\int_0^l s\left[U(t)\frac{\partial}{\partial s} + \frac{\partial}{\partial t} \right] J(s,t)\,ds + O(\varepsilon^5 \log^2 \varepsilon). \quad . \quad . \quad (37)$$

7. The Oscillating Rigid Body

Let (x_1, y_1, s_1, t_1) be variables referred to the axes of a rigid body which is moving with velocity $U(t_1)$ in the direction of the negative σ-axis and is oscillating with angular velocity $-\alpha'(t_1)$ about an axis $x_1=0$, $s_1=s_{1a}(t_1)$, and with angular velocity $\beta'(t_1)$ about an axis $y_1=0$, $s_1=s_{1b}(t_1)$. The angles α and β are taken as positive when the body nose points in the positive x and y directions, respectively. Since it is easier to solve the two-dimensional harmonic problem in terms of these new co-ordinates, we wish to transform our expressions for drag and lift into expressions referred to the new system. For points near the body the new frame is related to the previous one by the transformation

$$\left.\begin{aligned} x_1 &= x + f_a(s,t) + O(\varepsilon^3), & y_1 &= y + f_b(s,t) + O(\varepsilon^3), \\ s_1 &= s + O(\varepsilon^2), & t_1 &= t, \end{aligned}\right\} \quad . \quad . \quad (38)$$

where
$$f_a(s,t) = \int_0^t s_a'(t')\,\alpha(t')\,dt' + \alpha(t)\,[s - s_a(t)],$$

and
$$f_b(s,t) = \int_0^t s_b'(t')\,\beta(t')\,dt' + \beta(t)\,[s - s_b(t)].$$

$$\left.\begin{aligned} &\\ &\end{aligned}\right\} \quad . \quad . \quad . \quad (39)$$

$\partial/\partial t_1$ implies x_1, y_1, s_1 held constant. The potential may be written

$$\phi_1(x_1, y_1, s_1, t_1) = \mathscr{R}\{a_{01}\log z_1 + b_{01} + \sum_{n=1}^{\infty} a_{n1} z_1^{-n}\}, \quad . \quad . \quad (40)$$

where, by expanding $\log z$, z^{-1}, etc., in terms of z_1, and writing $f_a + if_b = f$, we find

$$\left.\begin{aligned} a_{01}(s_1,t_1)&=a_0(s,t), \qquad b_{01}(s_1,t_1)=b_0(s,t),\\ a_{11}(s_1,t_1)&=-a_0(s,t)f(s,t)+a_1(s,t), \text{ etc.}\end{aligned}\right\} \quad . \quad . \quad (41)$$

Let the surface of the body be defined by $g_1(x_1,y_1,s_1)=0$. Then by (14) and (38)

$$\left.\begin{aligned} \frac{\partial n}{\partial s}&=-\left(\frac{\partial g_1}{\partial s_1}+\frac{\partial g_1}{\partial x_1}\frac{\partial f_a}{\partial s}+\frac{\partial g_1}{\partial y_1}\frac{\partial f_b}{\partial s}\right)\left[\left(\frac{\partial g_1}{\partial x_1}\right)^2+\left(\frac{\partial g_1}{\partial y_1}\right)^2\right]^{-\frac{1}{2}}.\\ \frac{\partial n}{\partial t}&=-\left(\frac{\partial g_1}{\partial x_1}\frac{\partial f_a}{\partial t}+\frac{\partial g_1}{\partial y_1}\frac{\partial f_b}{\partial t}\right)\left[\left(\frac{\partial g_1}{\partial x_1}\right)^2+\left(\frac{\partial g_1}{\partial y_1}\right)^2\right]^{-\frac{1}{2}}\end{aligned}\right\} \quad . \quad (42)$$

In the expression for drag we have, using (33),

$$\int_{S_b}\left(\frac{\partial\phi}{\partial s}\frac{\partial n}{\partial t}-\frac{\partial\phi}{\partial t}\frac{\partial n}{\partial s}\right)dS=-\frac{d}{dt}\int_{S_b}\phi\frac{\partial n}{\partial s}dS+\oint_{C_B}\phi\frac{\partial n}{\partial t}dm,$$

$$=-\frac{d}{dt_1}\left[\int_{S_b}\phi_1\frac{\partial n_1}{\partial s_1}dS-\int_0^l ds_1\oint_\sigma\left(\phi_1\frac{\partial f_a}{\partial s}dy_1-\phi_1\frac{\partial f_b}{\partial s}dx_1\right)\right]-$$

$$-\oint_{C_B}\left(\phi_1\frac{\partial f_a}{\partial t}dy_1-\phi_1\frac{\partial f_b}{\partial t}dx_1\right) \quad . \quad (43)$$

where (*cf.* equation (14)) $-\partial n_1/\partial s_1$ is the approximate s_1-component of the unit normal to the body surface, and is independent of the time. Recalling the definitions of the functions J, f_a and f_b (equations (34) and (39)), and writing $\alpha+i\beta=\eta$, we obtain for the expression (43)

$$-\int_{S_b}\frac{\partial\phi_1}{\partial t_1}\frac{\partial n_1}{\partial s_1}dS+\mathscr{R}\left\{\frac{d}{dt_1}\left[\overline{\eta}(t_1)\int_0^l J(s_1,t_1)\,ds_1\right]-\right.$$

$$\left.-\left[\alpha'(t_1)\left(l-s_{1a}(t_1)\right)-i\beta'(t_1)\left(l-s_{1b}(t_1)\right)\right]J(l,t_1)\right\}, \quad (44)$$

and

$$\frac{D}{\rho_0}=\pi\int_0^l\left(\frac{\partial a_{01}}{\partial s_1}b_{01}-a_{01}\frac{\partial b_{01}}{\partial s_1}\right)ds_1-\frac{1}{2}\oint_{C_B}\phi_1\frac{\partial\phi_1}{\partial n_1}dm_1-$$

$$-\int_{S_b}\frac{\partial\phi_1}{\partial t_1}\frac{\partial n_1}{\partial s_1}dS+\mathscr{R}\left\{\frac{d}{dt_1}\left[\overline{\eta}(t_1)\int_0^l J(s_1,t_1)\,ds_1\right]-\right.$$

$$\left.-\left[l\overline{\eta}'(t_1)-\alpha'(t_1)s_{1a}(t_1)+i\beta'(t_1)s_{1b}(t_1)\right]J(l,t_1)\right\}+O(\varepsilon^6\log^2\varepsilon). \quad (45)$$

The expressions for lift and moment are unchanged; (s, t) may be replaced by (s_1, t_1). It remains to express J in terms of a_{11} and $z_{1\theta}$. By equation (35), we have for the present problem, using equations (41), (15) and (38),

$$J(s_1,t_1)=2\pi a_1(s,t)+\left[U(t)\frac{\partial}{\partial s}+\frac{\partial}{\partial t}\right]\left[S(s)z_\theta(s,t)\right]$$

$$=2\pi\left[a_{11}(s_1,t_1)+f(s_1,t_1)\frac{U(t_1)S'(s_1)}{2\pi}\right]+$$

$$+\left[U(t_1)\frac{\partial}{\partial s_1}+\frac{\partial}{\partial t_1}\right]\left[S(s_1)\left(z_{1\theta}(s_1)-f(s_1,t_1)\right)\right]$$

$$=2\pi a_{11}+U\frac{d}{ds_1}(Sz_{1\theta})-US\frac{\partial f}{\partial s_1}-S\frac{\partial f}{\partial t_1}$$

$$=2\pi a_{11}+U\frac{d}{ds_1}(Sz_{1\theta})-S(U\eta+s_1\eta'-\alpha' s_{1a}-i\beta' s_{1b}). \quad . \quad . \quad . \quad . \quad (46)$$

The problem treated in this section is that considered by Phythian[3]. Equation (45) corrects Phythian's expression for drag (*i.e.* his equation (72)), but does not reveal the cause of his error. Phythian used a control surface of constant shape, fixed to the body and rotating with it, and variables corresponding to our (x_1, y_1, s_1, t_1). He took components of momentum in the instantaneous directions of Ox_1, Oy_1, Os_1. In such an approach the volume integral in the momentum equation (25) becomes

$$\int_V\left[\frac{\partial}{\partial t_1}(\rho\mathbf{q})+\boldsymbol{\Omega}\wedge\rho\mathbf{q}\right]dV,$$

where $\boldsymbol{\Omega}$ is the angular velocity of the rotating frame. Phythian omitted the vector product term; if this is added to his analysis the result given here is obtained. In principle the extra term also contributes to the lift, but this contribution proves to be of negligible order, so that Phythian's expression for lift is correct.

8. Laminar Wings of Slender Plan Form

We approach the problem of laminar wings of slender plan form by considering first the ordinary linearised solution for a wing having a span of $O(1)$ and moving forward approximately in the $y\sigma$-plane, its displacements and velocities due to pitching, plunging and rolling being $O(\varepsilon)$. The wing and its wake are represented by a distribution of doublets; from the viewpoint of the ordinary theory it is immaterial whether these are placed in the $y\sigma$-plane or in the instantaneous plane of the wing but, since slender-body theory requires the boundary condition to be satisfied on the body surface, the latter course is chosen. We denote variables referred to the wing axes by (x_1, y_1, s_1, t_1) and define $\sigma_1=s_1-I(t_1)$, $\tau_1=t_1$. $(\partial/\partial\tau_1$ implies x_1, y_1, σ_1 held constant.) The starboard and port edges of the wing are $x_1=0$, $y_1=-b_a(s_1)$ and $y_1=b_b(s_1)$, respectively, the maximum values of b_a and b_b being denoted by B_a and B_b. To keep the slender-wing doublet strength k and the coefficient a_{11} continuous, we specify that the wing be pointed, $b(0)=0$. (*See* equation (54)).

Now
$$\frac{\partial}{\partial \tau} = \frac{\partial}{\partial \tau_1} - (\mathbf{v} + \boldsymbol{\Omega} \wedge \mathbf{r}_1) \cdot \nabla, \quad . \quad . \quad . \quad . \quad (47)$$

where $\mathbf{v}$ is the velocity of the origin of the (x_1, y_1, σ_1) frame, $\boldsymbol{\Omega}$ is the angular velocity of this frame, and $\mathbf{r}_1$ is a position vector with components x_1, y_1, σ_1. $\mathbf{v}$ and $\boldsymbol{\Omega}$ are $O(\varepsilon)$, and the linearised equation may therefore be written

$$\nabla^2 \Phi_1 = \frac{\partial^2 \Phi_1}{\partial x_1^2} + \frac{\partial^2 \Phi_1}{\partial y_1^2} + \frac{\partial^2 \Phi_1}{\partial \sigma_1^2} = \frac{1}{c_0^2} \frac{\partial^2 \Phi_1}{\partial \tau_1^2} + O(\varepsilon^2), \quad . \quad . \quad (48)$$

where the neglected terms are of the same type as those neglected in equation (2). Hence, if ω_1 and p_1 are Fourier and Laplace operators corresponding to σ_1 and τ_1, and $h_1^2 = \omega_1^2 + p_1^2/c_0^2$, our solution is

$$\bar{\Phi}_1 = \int_{-B_a}^{B_b} h_1 \bar{\kappa}(y_1', \omega_1, p_1) K_1 \left[h_1 \sqrt{\{x_1^2 + (y_1 - y_1')^2\}} \right] \frac{x_1}{\sqrt{\{x_1^2 + (y_1 - y_1')^2\}}} \, dy_1' \quad (49)$$

where $\kappa(y_1, \sigma_1, \tau_1) = k(y_1, s_1, t_1)$ is the doublet strength. Near wings of slender plan form, and in the absence of discontinuities in κ, the argument of the Bessel function may be treated as $O(\varepsilon)$; accordingly only the first term in the series expansion of K_1 is retained. The validity of this step is discussed in what follows. There results the approximate potential

$$\bar{\phi}_1 = \int_{-B_a}^{B_b} \bar{\kappa}(y_1', \omega_1, p_1) \frac{x_1}{x_1^2 + (y_1 - y_1')^2} \, dy_1', \quad . \quad . \quad . \quad (50)$$

i.e.
$$\phi_1 = \int_{-b_a(s_1)}^{b_b(s_1)} k(y_1', s_1, t_1) \frac{x_1}{x_1^2 + (y_1 - y_1')^2} \, dy_1', \quad . \quad . \quad . \quad (51)$$

$$= \int_{-b_a(s_1)}^{b_b(s_1)} \frac{\partial k(y_1', s_1, t_1)}{\partial y_1'} \tan^{-1} \frac{y_1 - y_1'}{x_1} \, dy_1'. \quad . \quad . \quad . \quad (52)$$

This potential is again harmonic in (x_1, y_1): the solution of the integral equation which determines k for a given normal velocity on the wing is well known. However, if there are lines $s_1 = \text{constant}$, $x_1 = 0$, which are occupied partly by the wing and partly by the wake, substantial difficulties are introduced. These are avoided by considering only wings whose trailing edges are straight and normal to the direction of motion.

It may be noted in passing that rolling velocities and displacements of $O(1)$ can now be admitted for a wing of slender plan form, since these only cause velocities of $O(\varepsilon)$ normal to the wing surface, and since the solution on the wing is now independent of conditions in the wake.

To illustrate the remarks that follow, consider a wing of slender symmetrical plan form ($b_a = b_b = b$), oscillating in pitch like the body of the previous section, with $\beta(t_1) \equiv 0$. The boundary condition is

$$\frac{\partial \phi_1}{\partial x_1}(0\pm, y_1, s_1, t_1) = -U(t_1)\,\alpha(t_1) - \alpha'(t_1)\,[s_1 - s_{1a}(t_1)] = -F(s_1, t_1), \text{ say.} \qquad (53)$$

$$\left.\begin{aligned} \text{Hence} \quad \phi_1 &= \mathscr{R}\left[F(s_1,t_1)\left(\sqrt{\{z_1^2 + b^2(s_1)\}} - z_1\right)\right], \\ k &= \frac{1}{\pi} F(s_1,t_1)\sqrt{\{b^2(s_1) - y_1^2\}}, \\ a_{11} &= \frac{1}{2} F(s_1,t_1)\, b^2(s_1). \end{aligned}\right\} \qquad (54)$$

It is apparent that $\partial k/\partial s_1$ is not only discontinuous but also infinite at the leading edge (Ward's restriction on the curvature of the body contour has been violated); hence the approximation to (49) is likely to be less accurate than for bodies. The singularity is, however, of the same order as that found in more exact solutions, and the integrated errors are generally assumed to be acceptable. Ward[1] has discussed this point fully.

At subsonic speeds the Kutta-Joukowski condition should be satisfied at the trailing edge, and it is evident that the present solution fails to meet this requirement. This may be attributed to a finite discontinuity in $\partial k/\partial s_1$ and $\partial a_{11}/\partial s_1$ across the trailing edge (k and a_{11} remaining continuous). But it has been seen that this type of discontinuity is admissible on a slender body in spite of the large localised errors it introduces, and there is no reason why the integrated error should be greater in the present case.

The expressions for the aerodynamic forces on the oscillating wing are readily obtained. We have

$$\left.\begin{aligned} a_{01} = b_{01} = 0, \quad J(s_1,t_1) &= 2\pi a_{11} = \pi F(s_1,t_1)\, b^2(s_1), \\ -\frac{1}{2}\oint_{C_B} \phi_1 \frac{\partial \phi_1}{\partial n_1}\, dm_1 = 2\int_0^B F(l,t_1)\sqrt{(B^2 - y_1^2)}\, F(l,t_1)\, dy_1 &= \frac{\pi}{2} F^2(l,t_1)\, B^2. \end{aligned}\right\} \qquad (55)$$

Hence from equations (45), (36) and (37),

$$\frac{D}{\rho_0} = \frac{\pi B^2}{2}\left[U^2\alpha^2 - \alpha'^2(l - s_{1a})^2\right] + V_0 \frac{d}{dt_1}\left[U\alpha^2 - \alpha\alpha' s_{1a}\right] + V_1 \frac{d}{dt_1}\left[\alpha\alpha'\right] \qquad (56)$$

$$\frac{X}{\rho_0} = \pi B^2 U\left[U\alpha + \alpha'(l - s_{1a})\right] + V_0 \frac{d}{dt_1}\left[U\alpha - \alpha' s_{1a}\right] + V_1 \alpha'', \qquad (57)$$

$$\frac{M_y}{\rho_0} = \pi B^2 U l\left[U\alpha + \alpha'(l - s_{1a})\right] - V_0\left[U^2\alpha - U\alpha' s_{1a}\right] + V_1\left[U'\alpha - \frac{d}{dt_1}(\alpha' s_{1a})\right] + V_2\alpha''. \qquad (58)$$

where $$V_m = \pi \int_0^1 s_1^m b^2(s_1)\, ds_1, \quad (m=0, 1, 2). \quad . \quad . \quad . \quad . \quad (59)$$

Because in the present problem we have $a_0=0$, $a_1=a_{11}$, and an anti-symmetric potential, these results would also have been obtained by satisfying the boundary condition in the fixed $y\sigma$-plane. Such a procedure would yield correct pressure differences across the wing, but incorrect pressures (*see* equations (27) and (47)), and it would be inconsistent with the procedure which must be used for bodies with thickness.

The results of this section have been largely given by Miles[9], who used a somewhat different approach and who also questioned the validity of the method for subsonic speeds.

Acknowledgment

The author wishes to express his thanks to Professor W. J. Duncan, under whose general direction this work was done, and to the English Electric Company, whose Research Fellowship at the University of Glasgow he held at the time.

References

1 Ward, G. N. Supersonic Flow past Slender Pointed Bodies. *Quarterly Journal of Mechanics and Applied Mathematics*, Vol. 2, pp. 75-97, March 1949.

2. Miles, J. W. Slender-Body Theory for Supersonic Unsteady Flow. *Journal of the Aeronautical Sciences*, Vol. 19, pp. 280-1, April 1952.

3. Phythian, J. E. Some Unsteady Motions of a Slender Body through an Inviscid Gas. *Quarterly Journal of Mechanics and Applied Mathematics*, Vol. 5, pp. 301-17, September 1952.

4. Fraenkel, L. E. On the Operational Form of the Linearized Equation of Supersonic Flow. *Journal of the Aeronautical Sciences*, Vol. 20, pp. 647-8, September 1953.

5. Watson, G. N. *Theory of Bessel Functions*, 2nd Edition, Cambridge, 1944.

6. Ward, G. N. The Approximate External and Internal Flow past a Quasi-cylindrical Tube Moving at Supersonic Speeds. *Quarterly Journal of Mechanics and Applied Mathematics*, Vol. 1, pp. 225-245, 1948.

7. Lighthill, M. J. Supersonic Flow past Slender Bodies of Revolution, the Slope of whose Meridian Section is Discontinuous. *Quarterly Journal of Mechanics and Applied Mathematics*, Vol. 1, pp. 90-102, 1948.

8. Fraenkel, L. E. Supersonic Flow past Slender Bodies of Elliptic Cross-Section. A.R.C. 15,166 1952 (to be published as an R. & M.).

9. Miles, J. W. On Non-steady Motion of Slender Bodies. *The Aeronautical Quarterly* Vol. II, pp. 183-194, November 1950.

Appendix

The Accuracy of the Slender-Body Solution

(i) *The Accuracy in the Absence of Discontinuities*

If the $a_n(s, t)$ and their first partial derivatives are continuous functions of s and t everywhere, the error of the slender-body potential is uniform, for values of r on and near the body, and can be found by using Ward's technique[1]. In terms of $z=x+iy$, $\bar{z}=x-iy$, σ and τ, we have

$$\frac{\partial}{\partial\tau}+\nabla\Phi.\nabla=\frac{\partial}{\partial\tau}+2\frac{\partial\Phi}{\partial\bar{z}}\frac{\partial}{\partial z}+2\frac{\partial\Phi}{\partial z}\frac{\partial}{\partial\bar{z}}+\frac{\partial\Phi}{\partial\sigma}\frac{\partial}{\partial\sigma}, \quad . \quad . \quad (60)$$

and the exact equation (1) may be written

$$4\frac{\partial^2\Phi}{\partial z\partial\bar{z}}+\frac{\partial^2\Phi}{\partial\sigma^2}-\frac{1}{c_0^2}\frac{\partial^2\Phi}{\partial\tau^2}=\frac{1}{c_0^2}\Big[4\Big(\frac{\partial\Phi}{\partial\bar{z}}\Big)^2\frac{\partial^2\Phi}{\partial z^2}+4\Big(\frac{\partial\Phi}{\partial z}\Big)^2\frac{\partial^2\Phi}{\partial\bar{z}^2}+$$

$$+4\frac{\partial}{\partial\tau}\Big(\frac{\partial\Phi}{\partial z}\frac{\partial\Phi}{\partial\bar{z}}\Big)+8\frac{\partial\Phi}{\partial z}\frac{\partial\Phi}{\partial\bar{z}}\frac{\partial^2\Phi}{\partial z\partial\bar{z}}\Big]+O(\varepsilon^4\log^2\varepsilon). \quad (61)$$

To obtain a second approximation, put

$$\Phi=\varphi+\varphi_I=\tfrac{1}{2}[w(z)+\overline{w}(\bar{z})]+\varphi_I,$$

where w is the complex function of which the slender-body potential is the real part, and φ_I represents the higher order terms to be added. It is assumed that the contribution of φ_I to the right hand side of (61) is negligible compared with the contribution of φ. The right hand side of equation (61) is then known, and an appropriate form of solution is $\varphi_I=\varphi_a+\varphi_b$, where φ_a is a particular integral of the equation

$$4\frac{\partial^2\varphi_I}{\partial z\partial\bar{z}}+\frac{\partial^2\varphi_I}{\partial\sigma^2}-\frac{1}{c_0^2}\frac{\partial^2\varphi_I}{\partial\tau^2}=-\Big(\frac{\partial^2}{\partial\sigma^2}-\frac{1}{c_0^2}\frac{\partial^2}{\partial\tau^2}\Big)\frac{w+\overline{w}}{2}+\frac{1}{c_0^2}\Big[\frac{1}{2}\Big(\frac{\partial\overline{w}}{\partial\bar{z}}\Big)^2\frac{\partial^2 w}{\partial z^2}+$$

$$+\frac{1}{2}\Big(\frac{\partial w}{\partial z}\Big)^2\frac{\partial^2\overline{w}}{\partial\bar{z}^2}+\frac{\partial}{\partial\tau}\Big(\frac{\partial w}{\partial z}\frac{\partial\overline{w}}{\partial\bar{z}}\Big)\Big], \quad . \quad (62)$$

and φ_b is a solution of the linearised equation, having the appropriate properties at infinity and satisfying the boundary condition

$$\frac{\partial\varphi_b}{\partial n}=-\frac{\partial\varphi_a}{\partial n}-\frac{\partial\gamma}{\partial\sigma}\frac{\partial\varphi}{\partial\sigma}\Big[\Big(\frac{\partial\gamma}{\partial x}\Big)^2+\Big(\frac{\partial\gamma}{\partial y}\Big)^2\Big]^{-\frac{1}{2}}. \quad . \quad . \quad (63)$$

Ward's method may be used to show that φ_a, $\partial\varphi_a/\partial\sigma$, $\partial\varphi_a/\partial\tau$, etc., are $O(\varepsilon^4\log^2\varepsilon)$, while $\partial\varphi_a/\partial z$, $\partial^2\varphi_a/\partial z\partial\sigma$, etc., are $O(\varepsilon^3\log\varepsilon)$. It follows that these are also the orders of φ_b and its derivatives. It is worth noting that if terms not appearing in the linearised equation had been omitted from the foregoing analysis, φ_a and φ_b would have been found to be $O(\varepsilon^4\log\varepsilon)$, which is very nearly correct.

(ii) *The Effect of Discontinuities in the $a_n(s, t)$*

To examine the localised errors introduced by discontinuities in the $a_n(s, t)$ and their derivatives, the accuracy of the slender-body potential is considered only as a

solution of the linearised equation. In what follows the slender-body solution is denoted by $\varphi(x, y, \sigma, \tau)$ or $\phi(x, y, s, t)$; the exact solution of the linearised equation with the source and multi-source strengths of the slender-body approximation, (equation (6) with the A_n and B_n defined by equation (8)), is denoted by $\phi+\phi_a$; and the exact solution of the linearised equation which satisfies the boundary condition (13) on the body surface is denoted by $\phi+\phi_a+\phi_b$.

If $a_0(s, t)$ is discontinuous at $s=A$ for all t, (*e.g.* if the body has a rounded or open nose or tail, or a discontinuity in profile slope), then in $\phi+\phi_a$ there are two terms, (by equation (22)),

$$-\frac{1}{2}\left[a_0(A+, t_S')-a_0(A-, t_S')\right]\cosh^{-1}\frac{c_0(t-t_S')}{r} \quad . \quad . \quad . \quad (64)$$

where the t_S' are defined by

$$s \mp \sqrt{\{c_0^2(t-t_S')^2-r^2\}}-I(t)+I(t_S')=A, \qquad t_S'<t-\frac{r}{c_0}. \quad . \quad . \quad (65)$$

In the slender-body approximation ϕ the corresponding terms are, (by equation (23)),

$$-\frac{1}{2}\left[a_0(A+, t_{S_1}')-a_0(A-, t_{S_1}')\right]\log\frac{2c_0(t-t_{S_1}')}{r} \quad . \quad . \quad (66)$$

where

$$s \mp c_0(t-t_{S_1}')-I(t)+I(t_{S_1}')=A, \qquad t_{S_1}'<t. \quad . \quad . \quad . \quad (67)$$

Now it can be shown that in the region $|s-A|>O(\varepsilon)$, $c_0|t_S'-t_{S_1}'|$ is $O\{\varepsilon^2/(s-A)\}$, provided that $U(t')$ is not near sonic speed in the interval between t_S' and t_{S_1}'. (If $U(t')=$constant this restriction is not necessary). Hence in the region $|s-A|>O(\varepsilon)$, ϕ_a is

$$O\left[\frac{\varepsilon^4}{(s-A)^2}+\left|\frac{\varepsilon^4}{s-A}\log\frac{\varepsilon}{|s-A|}\right|\right] \quad . \quad . \quad . \quad . \quad (68)$$

ϕ_b is closely related to ϕ_a. By definition ϕ_b is an exact solution of the linearised equation such that on the body $\partial\phi_b/\partial n=-\partial\phi_a/\partial n$ and such that ϕ_b and its derivatives vanish as $r, s\longrightarrow\infty$. In view of these conditions and of knowledge of the order of ϕ_a, it seems safe to assume that in the range $|s-A|>O(\varepsilon)$, ϕ_b is at most

$$O\left[\frac{\varepsilon^4}{(s-A)^2}\log\frac{\varepsilon}{|s-A|}\right]. \quad . \quad . \quad . \quad . \quad . \quad (69)$$

This assumption is confirmed by such more exact solutions as are available; these being, for the case of a rounded nose at subsonic speed, the classical solution for an ellipsoid of revolution, and for the case of a discontinuity in profile slope at supersonic speed, Ward's quasi-cylinder solution[6].

If $a_0(s, t)$ is discontinuous at $t=B$ for all s on the body, (*e.g.* if the body changes its forward velocity discontinuously or expands discontinuously), the effect is similar. For $c_0(t-B)>O(\varepsilon)$, and for all trajectories, ϕ_a and ϕ_b are of the order given by equations (68) and (69) with $|s-A|$ replaced by $c_0(t-B)$.

These observations must be modified when we consider the potential at points (r, σ, τ) or (r, s, t) lying between the after-cone of the point of intersection of two discontinuity lines $s' = A$, $t' = B$, and the vertical tangent plane of this cone (Fig. 3). The contribution

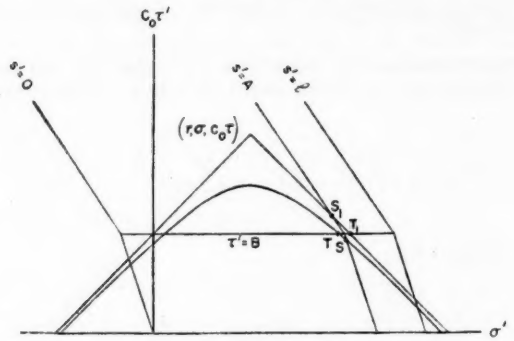

Fig. 3.

of the $s' = A$ discontinuity to $\phi + \phi_a$, which springs from the point S, then differs from the contribution to ϕ, which springs from S_1, by an amount greater than that given, for it is no longer true that

$$a_0(A+, t_{S_1}') = a_0(A+, t_S') + O\left(\varepsilon^2 \frac{\varepsilon^2}{s-A}\right).$$

The same applies to the contributions of the $t' = B$ discontinuity. However, there exist instead relations like

$$a_0(A+, t_{S_1}') = a_0(s_{T_1}', B+) + O\left(\varepsilon^2 \frac{\varepsilon^2}{s-A}\right),$$

so that the combined contribution to $\phi + \phi_a$ of the points S and T is still equal to the contribution to ϕ of the points S_1 and T_1 within the errors given. A similar argument applies when the body changes its velocity discontinuously at $t' = B$ from a substantially subsonic to a substantially supersonic value.

The effect of discontinuities in the multi-source strengths a_n $(n > 1)$ can be studied similarly. It is found that the errors are of the same order as those already quoted, except that no log terms appear.

The expressions (66) may be written

$$\left.\begin{aligned} &-\frac{1}{2}\left[a_0\left(A+, t-\frac{s-A}{\overline{U}\pm c_0}\right) - a_0\left(A-, t-\frac{s-A}{\overline{U}\pm c_0}\right)\right] \log \frac{2c_0(s-A)}{(\overline{U}\pm c_0)r}, \\ &\text{where} \quad \overline{U} = \frac{I(t) - I(t_{S_1}')}{t - t_{S_1}'}. \end{aligned}\right\} \tag{70}$$

It is evident that such terms in ϕ, if used in the region $s - A < O(\varepsilon)$ where they are invalid, lead to a non-integrable singularity in pressure at $s = A$, (of $O\{(s-A)^{-1}\}$), and therefore to infinite drag. Furthermore, it is known that in a more exact solution the region of a body close to a rounded nose or to a discontinuity in profile slope generally makes contributions to the aerodynamic forces which are of the order of these forces

themselves. For supersonic speeds it is possible partially to overcome this difficulty[7, 8], but in the present paper the forces are calculated only for bodies satisfying the restriction mentioned in Section 5.

(iii) *The Effect of Discontinuities in the $\partial a_n/\partial s$ and $\partial a_n/\partial t$*

That part of the source potential $-K_0(hr)\,\bar{\alpha}_0$ which is not the result of discontinuities in α_0 may be written

$$\frac{1}{2}\int_{-\infty}^{\infty} \sinh^{-1}\frac{\sigma'-\sigma}{r}\left[\frac{\partial \alpha_0}{\partial \sigma}\left(\sigma', \tau-\frac{1}{c_0}\sqrt{\{(\sigma'-\sigma)^2+r^2\}}\right)-\right.$$

$$\left.-\frac{1}{c_0}\,\frac{\sigma'-\sigma}{\sqrt{\{(\sigma'-\sigma)^2+r^2\}}}\,\frac{\partial \alpha_0}{\partial \tau}\left(\sigma', \tau-\frac{1}{c_0}\sqrt{\{(\sigma'-\sigma)^2+r^2\}}\right)\right]d\sigma', \qquad (71)$$

where the notation

$$\left.\frac{\partial F(\sigma,\tau)}{\partial \sigma}\right|_{\sigma=M,\ \tau=N} = \frac{\partial F}{\partial \sigma}(M, N)$$

has been introduced.

The expression (71) represents a sum of Riemann integrals taken between the points of discontinuity of the integrand. We can again apply Stieltjes integration by parts to (71), and transform to the variables (s, t), in order to examine the contributions of discontinuities in $\partial a_0/\partial s$ and $\partial a_0/\partial t$. A similar procedure can be applied to the multi-source potentials.

It is found that if $\partial a_n/\partial s$ is discontinuous at $s=A$ for all t, (*e.g.* if the body has a discontinuity in profile curvature at $s=A$), ϕ_a is

$$O\left[\frac{\varepsilon^4}{s-A}\log\frac{\varepsilon}{|s-A|}\right], \quad \text{for } |s-A| \geqslant O(\varepsilon), \qquad (72)$$

and

$$O\left[\varepsilon^2|s-A|+\varepsilon^2|s-A|\left|\log\frac{\varepsilon}{|s-A|}\right|\right], \quad \text{for } |s-A| \leqslant O(\varepsilon), \qquad (73)$$

where the log term appears only for $n=0$. It would be sufficient to write (73) as $O(\varepsilon^3)$; the extended form has been written to indicate the behaviour near $s=A$ of $\phi+\phi_a$, which contributes the first term, and of ϕ, which contributes the second. It is evident that ϕ and ϕ_a are continuous at $s=A$, but that errors in pressure can be $O(\varepsilon^2\log|s-A|)$ and logarithmically infinite. For the reasons already stated, it is assumed that (72) and (73) also give the orders of ϕ_b.

If $\partial a_n/\partial t$ is discontinuous at $t=B$ for all s on the body, the orders of the error are given by (72) and (73) with $|s-A|$ replaced by $c_0(t-B)$.

On the basis of these results it is shown in what follows that, in spite of the substantial localised errors in pressure, discontinuities in the $\partial a_n/\partial s$ only increase the error of the integrated expressions for the aerodynamic forces by a factor of $O(\log\varepsilon)$, provided that the discontinuities are separated by distances of $O(1)$.

The foregoing assumption about the order of ϕ_b is confirmed by the fact that the slender-body approximation for the steady subsonic flow past a body pointed at both ends (the body must be pointed if the a_n are to be continuous functions of s) yields the correct values of zero lift and drag, even though the $\partial a_n/\partial s$ be discontinuous. For supersonic speeds the assumption is again confirmed by the quasi-cylinder solution.

(iv) The Effect on the Aerodynamic Forces of a Discontinuity in the $\partial a_n/\partial s$

Let the $\partial a_n/\partial s$ be discontinuous at $s=0$ and let the body extend from $s=-l_1$ to l_2. Let ϕ_I denote the error of the slender-body solution. Then it follows from the combined results given earlier that there exist positive finite numbers C_1, C_2, C_3 such that

$$\text{for} \qquad |s| \leqslant C_1\varepsilon, \qquad \phi_I < C_2\varepsilon^3, \quad . \quad . \quad . \quad . \quad . \quad . \quad (74)$$

$$\text{and for} \qquad |s| \geqslant C_1\varepsilon, \qquad \phi_I < C_3 \frac{\varepsilon^4}{|s|} \log^2 \frac{\varepsilon}{|s|} \quad . \quad . \quad . \quad (75)$$

The effect of this error on the drag force is given by

$$\frac{D_I}{\rho_0} = -\int_{-l_1}^{l_2} ds \oint_C \left[U(t) \frac{\partial \phi_I}{\partial s} + \frac{\partial \phi_I}{\partial t} + \frac{\partial \phi}{\partial r}\frac{\partial \phi_I}{\partial r} + \frac{1}{2}\left(\frac{\partial \phi_I}{\partial r}\right)^2 + \right.$$

$$\left. + \frac{1}{R^2}\frac{\partial \phi}{\partial \theta}\frac{\partial \phi_I}{\partial \theta} + \frac{1}{2R^2}\left(\frac{\partial \phi_I}{\partial \theta}\right)^2 \right] R \frac{\partial R}{\partial s} \; \theta, \qquad (76)$$

where $r=R(\theta, s, t)$ denotes the body surface. Now

$$\oint_C \frac{\partial \Phi_I}{\partial s}(R, \theta, s, t) R \frac{\partial R}{\partial s} d\theta = \frac{\partial}{\partial s} \oint_C \phi_I (R, \theta, s, t) R \frac{\partial R}{\partial s} d\theta -$$

$$- \oint_C \left[\frac{\partial \phi_I}{\partial r} R \left(\frac{\partial R}{\partial s}\right)^2 + \phi_I \frac{\partial}{\partial s}\left(R \frac{\partial R}{\partial s}\right)\right] \; \theta, \qquad (77)$$

and ϕ_I is a continuous function of s. Hence, we have from the $\partial \phi_I/\partial s$ term in equation (76),

$$-U(t)\left\{ \oint_{C_B} \phi_I R \frac{\partial R}{\partial s} d\theta - \int_{-l_1}^{l_2} ds \oint_C \left[\frac{\partial \phi_I}{\partial r} R \left(\frac{\partial R}{\partial s}\right)^2 + \phi_I \frac{\partial}{\partial s}\left(R \frac{\partial R}{\partial s}\right)\right] d\theta \right\}$$

$$= O\left\{ \varepsilon^6 \log^2 \varepsilon + \int_0^{C_1\varepsilon} \varepsilon^5 ds + \int_{C_1\varepsilon}^{l_2} \frac{\varepsilon^6}{s} \log^2 \frac{s}{\varepsilon} ds \right\}$$

$$= O(\varepsilon^6 \log^3 \varepsilon). \quad . \quad . \quad . \quad . \quad . \quad . \quad (78)$$

The remainder of (76) leads to terms of this order or smaller. The effect upon the lateral forces is similar: for the force X, we merely replace $R(\partial R/\partial s)$ in (76) by $(\partial R/\partial \theta)\sin\theta + R\cos\theta$.